ΕΘΝΙΚΟ ΜΕΤΣΟΒΙΟ ΠΟΛΥΤΕΧΝΕΙΟ
ΣΧΟΛΗ ΗΛΕΚΤΡΟΛΟΓΩΝ ΜΗΧΑΝΙΚΩΝ
ΚΑΙ ΜΗΧΑΝΙΚΩΝ ΥΠΟΛΟΓΙΣΤΩΝ
ΤΟΜΕΑΣ ΗΛΕΚΤΡΙΚΗΣ ΙΣΧΥΟΣ

Μοντελοποίηση Πρότυπων Ανεμογεννητριών και STATCOM για Μελέτες Ευστάθειας ΣΗΕ

ΔΙΠΛΩΜΑΤΙΚΗ ΕΡΓΑΣΙΑ

ΝΙΚΟΛΑΟΣ Γ. ΣΤΥΛΙΑΡΑΣ

Επιβλέπων : Νικόλαος Χατζηαργυρίου

Καθηγητής Ε.Μ.Π.

Αθήνα, Οκτώβριος 2014

ΕΘΝΙΚΟ ΜΕΤΣΟΒΙΟ ΠΟΛΥΤΕΧΝΕΙΟ
ΣΧΟΛΗ ΗΛΕΚΤΡΟΛΟΓΩΝ ΜΗΧΑΝΙΚΩΝ
ΚΑΙ ΜΗΧΑΝΙΚΩΝ ΥΠΟΛΟΓΙΣΤΩΝ
ΤΟΜΕΑΣ ΗΛΕΚΤΡΙΚΗΣ ΙΣΧΥΟΣ

Μοντελοποίηση Πρότυπων Ανεμογεννητριών και STATCOM για Μελέτες Ευστάθειας ΣΗΕ

ΔΙΠΛΩΜΑΤΙΚΗ ΕΡΓΑΣΙΑ

ΝΙΚΟΛΑΟΣ Γ. ΣΤΥΛΙΑΡΑΣ

Επιβλέπων : Νικόλαος Χατζηαργυρίου

Καθηγητής Ε.Μ.Π.

Εγκρίθηκε από την τριμελή εξεταστική επιτροπή την 6η Οκτώβρη 2014.

.....	.....	.....
Νικόλαος Χατζηαργυρίου Καθηγητής Ε.Μ.Π.	Σταύρος Παπαθανασίου Αν. Καθηγητής Ε.Μ.Π.	Παύλος Γεωργιλάκης Επίκουρος Καθηγητής Ε.Μ.Π.

Αθήνα, Οκτώβριος 2014

.....

ΝΙΚΟΛΑΟΣ Γ. ΣΤΥΛΙΑΡΑΣ

Διπλωματούχος Ηλεκτρολόγος Μηχανικός και Μηχανικός Υπολογιστών Ε.Μ.Π.

Ευχαριστίες

Η παρούσα διπλωματική εκπονήθηκε στα πλαίσια του προπτυχιακού Προγράμματος Σπουδών της Σχολής Ηλεκτρολόγων Μηχανικών και Μηχανικών Υπολογιστών του Εθνικού Μετσόβιου Πολυτεχνείου. Θα ήθελα να ευχαριστήσω θερμά τον κ. Νικόλαο Χατζηαργυρίου για την ευκαιρία που μου έδωσε να προσεγγίσω ένα σύγχρονο πρόβλημα της επιστήμης του Ηλεκτρολόγου Μηχανικού, καθώς και για τη διάθεσή του να βοηθήσει και να δώσει τις πολύτιμες συμβουλές του στους φοιτητές.

Ευχαριστώ επίσης ιδιαίτερα τον κ. Ιωάννη Μάργαρη για την βοήθεια που μου προσέφερε στην κατανόηση του θέματος της εργασίας, τις υποδείξεις, τις συμβουλές και την επίλυση όλων των αποριών μου, καθώς και τον κ. Santiago Arnaltes Gómez, καθηγητή του πανεπιστημίου Universidad Carlos III της Μαδρίτης, με τον οποίο συνεργάστηκα κατά τα πρώτα στάδια υλοποίησης αυτής της εργασίας. Ήταν πάντα διαθέσιμος όταν τον χρειαζόμουν και πολύ συνεργάσιμος.

Στη συνέχεια θα ήθελα να ευχαριστήσω την οικογένεια μου, που μου έδωσε την δυνατότητα να μπω σε αυτήν την σχολή και να ολοκληρώσω αυτήν την εργασία. Επίσης, τους φίλους μου όλα αυτά τα χρόνια και ιδιαίτερα τους Γιάννη, Μάριο, Αντρέα, Αντώνη, Θοδωρή, Πολύζο, Ηλία, Στέφανο, Γιώργο, Κοσμά, Λένια και Κατερίνα για τη βοήθεια που μου προσέφεραν, τόσο πρακτική όσο και ψυχολογική, καθώς και για τις ευχάριστες στιγμές που περάσαμε όλα αυτά τα χρόνια.

Τέλος, θα ήθελα να αφιερώσω αυτή τη δουλειά στον παιδικό μου φίλο και συγγενή Αναστάση, που αυτή τη στιγμή δίνει τη μάχη για τη ζωή του κατά του καρκίνου, με αξιέπαινο θάρρος και υπομονή. Εύχομαι ταχεία ανάρρωση.

Περίληψη

Η αυξημένη διείσδυση αιολικής παραγωγής στα συστήματα ηλεκτρικής ενέργειας (ΣΗΕ) δείχνει πως οι διαχειριστές των συστημάτων μεταφοράς και διανομής ηλεκτρικής ενέργειας έχουν ανάγκη τη χρήση δυναμικών μοντέλων αιολικής παραγωγής για μελέτες ευστάθειας ΣΗΕ. Μέχρι τώρα, για την ανάπτυξη τέτοιων παγκοσμίως αποδεκτών μοντέλων, σημαντική δουλειά έχει πραγματοποιηθεί, κυρίως από το Western Electricity Coordinated Council (WECC), το Dynamic Performance of Wind Power Generation (DPWG) working group της IEEE και την International Electrotechnical Commission (IEC). Πρότυπα μοντέλα έχουν αναπτυχθεί για τις τέσσερις κύριες διαμορφώσεις ανεμογεννητριών, μοντέλα τα οποία επανεξετάζονται κι ανανεώνονται συνεχώς.

Αυτή η εργασία μελετά τη δυναμική συμπεριφορά ενός αιολικού πάρκου, αποτελούμενο από ανεμογεννήτριες σταθερών στροφών, απ' ευθείας συνδεδεμένες με το δίκτυο. Το σύστημα, το οποίο αναπτύχθηκε στο περιβάλλον Simulink του λογισμικού MATLAB, υπόκειται σε διαφορετικά πιθανά δυναμικά φαινόμενα ή μεταβολές της ταχύτητας του ανέμου, ενώ παράλληλα εξετάζονται τα αποτελέσματα που θα έχει η μεταβολή διάφορων παραμέτρων, όπως ο χρόνος εκκαθάρισης του σφάλματος, το σημείο στο οποίο συμβαίνει, το μήκος της γραμμής μεταφοράς που συνδέει το πάρκο με το δίκτυο ή η αναπαράσταση του μηχανικού μέρους της ανεμογεννήτριας, στην ευστάθεια του συστήματος. Επίσης, μοντελοποιείται και προσομοιώνεται ένα STATCOM με σκοπό την αύξηση της δυνατότητας παραμονής του αιολικού πάρκου σε λειτουργία υπό συνθήκες χαμηλής τάσης. Τέλος, προσομοιώνεται το πρότυπο μοντέλο για την αντίστοιχη διαμόρφωση ανεμογεννήτριας (Τύπου 1) και οι αποκρίσεις για κάθε κατάσταση λειτουργίας που εξετάζεται συγκρίνονται με τις αντοίστιχες αποκρίσεις του προτύπου, για να αξιολογηθούν.

Τα αποτελέσματα παρέχουν μία πλήρη εικόνα σχετικά με την μεταβατική συμπεριφορά του συστήματος, ενώ η γενικά πιστή αναπαράσταση του εξεταζόμενου μοντέλου από το πρότυπο επαληθεύει τα αποτελέσματα κι ενισχύει την ιδέα ότι ίσως σύντομα τα πρότυπα μοντέλα θα χρησιμοποιούνται παγκοσμίως για μελέτες μεταβατικής ευστάθειας ΣΗΕ.

Λέξεις κλειδιά: ανεμογεννήτρια σταθερών στροφών, πρότυπα μοντέλα, STATCOM, μετατροπέας πηγής τάσης, μετασχηματισμός dq, MATLAB/SIMULINK, μεταβατική ευστάθεια, δυναμική συμπεριφορά, έλεγχος γωνίας βήματος πτερυγίων, αδιάλειπτη λειτουργία υπό χαμηλή τάση, κρίσιμος χρόνος εκκαθάρισης

Abstract

The increasing wind energy penetration in power systems implies that Transmission System Operators (TSOs) and Distribution System Operators (DSOs) need to use dynamic models of wind power generation for power system stability studies. Until now, a significant amount of work has been performed towards the development of such universally accepted models, primarily by the Western Electricity Coordinated Council (WECC), the IEEE Working Group on Dynamic Performance of Wind Power Generation (DPWG) and the International Electrotechnical Commission (IEC). Generic models have been developed for four of the major wind turbine generator configurations and are constantly reviewed and updated.

This thesis investigates the dynamic behavior of a wind farm comprising fixed-speed wind turbine generators directly connected to the grid. The system, simulated at the Simulink environment of MATLAB software, is subjected to a variety of possible dynamic phenomena or wind speed variations, also examining the effects on the system stability of several parameters, such as the fault clearing time, fault terminal, connection line length or wind turbine mechanical representation. A STATCOM is also modeled and simulated in order to enhance the wind farm Fault-Ride-Through (FRT) capability and its impact on the system stability is illustrated. Finally, the generic model for the corresponding wind turbine generator configuration (Type 1) was simulated and the responses of each case examined were compared with the generic model responses in order to be evaluated.

The results form a complete picture regarding the system's transient behavior, while the examined model's overall faithful representation of the generic model validates the results and reinforces the view that shortly generic model may be universally used for power system stability analyses.

Index Terms: fixed-speed wind turbine generator, generic models, STATCOM, voltage-sourced converter, dq transformation, MATLAB/SIMULINK, transient stability, dynamic behavior, pitch control, low voltage ride-through, critical clearing time

Contents

1. Introduction

1.1. Conventional Electric Power Production

Electric power is primarily produced in large-scale systems that base their operation on conventional technologies. Their operation relies on the combustion of a fundamental energy source, most commonly fossil fuels (e.g. natural gas, coal, oil, lignite, etc.) and can generally be described by the Rankine cycle: water is heated, the fossil fuel combustion takes place in a boiler and the produced steam spins the steam turbine, which drives the electrical generator. After it passes through the turbine, the steam is condensed in a condenser and recycled to where it was heated. Additionally, another type of fossil fuel power plants uses a gas turbine in conjunction with a heat recovery steam generator (HRSG). It is referred to as a combined cycle power plant because it combines the Brayton cycle of the gas turbine with the Rankine cycle of the HRSG. These conventional large-scale systems have capacities of some hundreds of MWs, operate at high loads (operation at a range of 50% to 100% of their capacity), having high capacity factors (operation of many hours annually), and covering the base load needs of the electricity grid.

However, one of the most important downsides of the fossil-fuel based electric power production is the unfavorable environmental effects. The combustion of fossil fuels leads to the inevitable production of carbon dioxide (CO_2), while most of the times harmful emissions are produced, such as carbon monoxide (CO), nitrogen oxides (NO_X), sulfur oxides (SO_X), unburned hydrocarbons (HC) and solid particles [1]. Such emissions contribute the most to acid rain and air pollution, while they also have been associated with global warming. CO_2 emissions, in particular are considered responsible for 50% of the overheating of the atmosphere. Modern power plants have developed filtering technologies for the exhaust air in the smoke stacks but the chemical composition of the coal makes it very difficult to remove impurities from the solid fuel prior to its combustion. These technologies have restricted the power plant pollution, comparing to that of older technologies, but still the emission levels are still on average several times greater than natural gas power plants.

Figure 1 depicts the CO_2 emissions from fossil fuel use and cement production in the top 6 emitting countries and the European Union from 1990 until today.

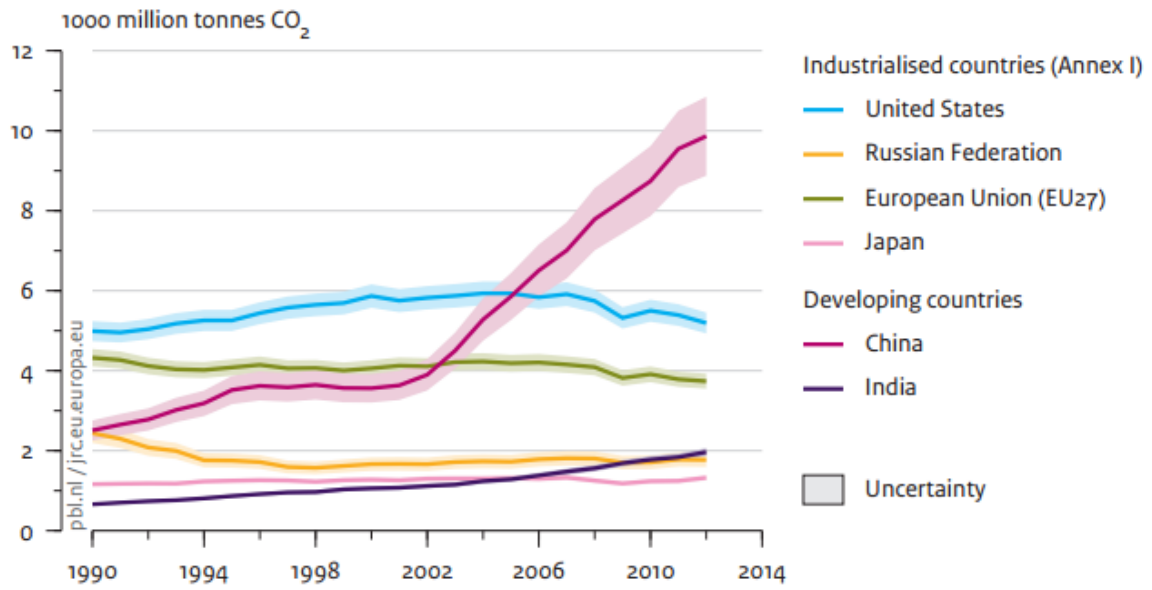

Figure 1: CO_2 Emissions from fossil fuel use and cement production in the top 6 emitting countries and the EU [2]

The other major issue regarding electric power production from conventional sources is the requirement of continuous fuel supply in order to operate, which contributes to the operating cost. This cost depends on various local and global parameters, such as fuel availability and type, fuel purity, world economic conditions, etc [1]. Furthermore, the finiteness of the fossil fuel reserves constitutes an alarming factor. According to the energy report of the International Energy Outlook for 2013, world energy consumption will grow by 56 percent between 2010 and 2040 [3]. Taken into account this and also the prediction that fossil fuels will continue to supply almost 80 percent of world energy use through 2040 [3], it is clear that fossil fuel depletion is only a matter of time.

1.2. Renewable Energy Sources

The previously mentioned issues, regarding the conventional electric power production has led to research and development of alternative energy resources in the latest years, collectively named as renewable energy sources.

As their name implies, the main characteristic of renewable energy sources is that they can be extracted in a “renewable” way, meaning that their resource availability is hardly varied. The most common renewable energy sources include solar energy, wind power, hydropower, biomass, biofuel and geothermal energy, while some new technologies, like marine energy (kinetic energy created by the movement of water in the world’s oceans) or cellulosic ethanol (processed biomass turned into ethanol in refineries) are on the rise, although yet not widely demonstrated or have limited commercialization.

On the whole, it was not until recently that renewables began to contribute significantly in the power demand. This stems from the relatively high electricity price compared to the conventional electricity prices and also from the fact that power production from renewables is not easily and in most cases only partially controlled, contrary to conventional production, which is fully controllable.

Despite these disadvantages, renewables today play a major role in the energy mix in many countries around the world and a lot of new policies have been adapted from the European Union and several individual countries (e.g. the Kyoto protocol) during the latest years, regarding renewable energy sources use, as they constitute the basis of the economic development model of green economy. In 2013, prices for renewable energy technologies, primary wind and solar, continued to fall, rendering them increasingly mainstream and competitive with conventional energy sources. However, in the absence of a level playing field, high penetration of renewables is still dependent on a robust policy environment. Overall, the rate of policy adoption has slowed relatively to the early-to-mid 2000s. Revisions to existing policies are occurring at an increasing rate and new types of policies are becoming to emerge to address changing conditions. Integrated policy approaches that conjoin energy efficiency measures with the implementation of renewable energy technologies, for example, are becoming more common. [4]

In the pie chart below, the power mix in the European Union is depicted.

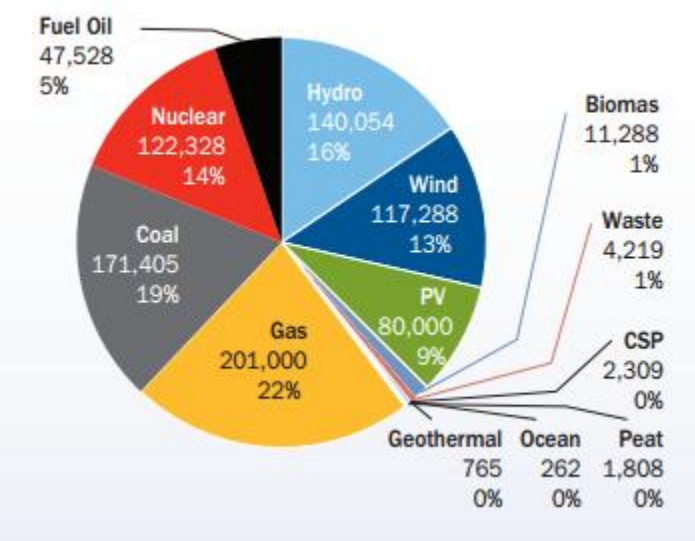

Figure 2: European Union Power Mix 2013 [5]

1.3. Wind Power

Wind power constitutes the cornerstone of power production from renewable sources and is a relatively new form of energy. It is considered as the fastest growing technology in the renewable energy forms field and, in comparison with other renewable resources, as for example solar energy technologies, it is relatively cheap. Wind is an inexhaustible primary energy source, with limited negative environmental effects. While wind turbines visually, as well as noisily, affect the environment, the consequences are small and the ecosystems are affected in a very small way. In addition, once they are removed, the noise and the visual effect immediately disappear and no permanent environmental changes are observed.

As it is shown in figure 3, the total recorded installed wind power capacity by the end of 2013 was 318 GW, growing by 35 GW over the preceding year. Wind power installations continue to increase worldwide and the estimated capacity by 2015 is 500 GW. The penetration of wind power in the electrical grids increases steadily in many European countries and thus wind power generation is expected to contribute to European Union's 2020 targets for reduction of carbon dioxide emissions by more than 30% and to supply at least 14-16% of Europe's electricity. Denmark leads wind penetration participation in Europe (28% in 2011), a country that has recently set the ambitious target to produce 50% of its electricity from wind turbines by the end of 2020 [5].

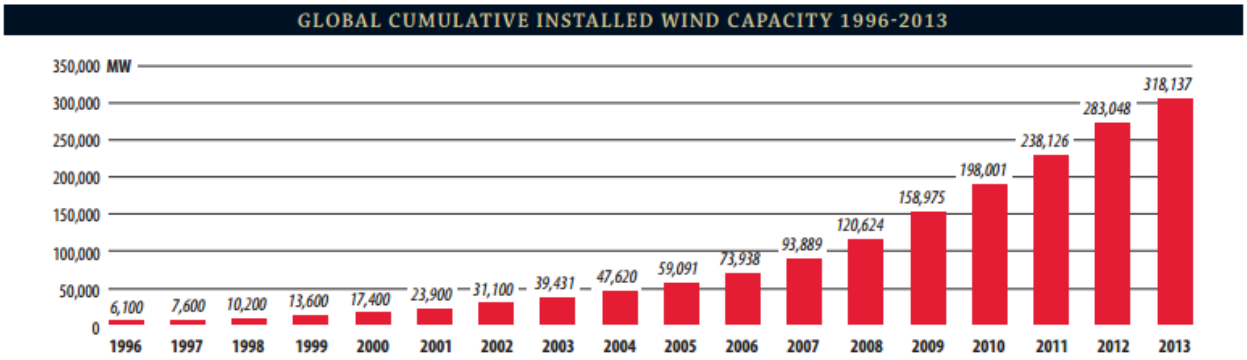

Figure 3: Global Cumulative Installed Wind Capacity 1996-2013 [6]

This increasing wind power penetration results in a necessity to further study the influence on the grids and particularly, on the power system stability. Each country has its own grid requirements and specific guidelines regarding wind power generation should and have been imposed. In addition, it is of paramount importance for wind turbine models that efficiently depict the system dynamic behavior to be developed, so as the grid operators will have a clear picture of the high wind energy penetration effects.

1.4. Basic Thesis Outline

This thesis comprises eight chapters and is structured as follows:

In chapter 2, an overview of the current wind turbine technologies is presented. Evolutions in the wind turbine design as well as the four major configurations for wind turbines are discussed. Furthermore, regarding the individual wind turbine technology, the parts that comprises a wind turbine are explained, i.e. the aerodynamic part with its control and the mechanical part, and different representations of the latter are shown.

In chapter 3, the grid code requirements that have been imposed for wind power integration, focusing on European countries, are discussed. These requirements include frequency and voltage operating range, active power control, reactive power control and voltage regulation and most importantly low voltage ride-through capabilities.

Chapter 4 is dedicated to the wind turbine generator (WTG) generic models. The issues that stem from the lack of non-specific, non-proprietary WTG models are addressed, the work towards the generic model development that has been carried out until now is documented and the generic models for the four major wind turbine topologies are described. Finally, the model specifications, as well as the process of their validation, are highlighted.

Chapter 5 explains the operating principle of the static synchronous compensator (STATCOM) and of the Flexible AC Transmission Systems (FACTS) in general. The voltage-sourced converter operation is also elaborated, as a STATCOM component, in addition to the STATCOM control system and a bibliography review regarding modifications in the STATCOM's control system for wind power applications is carried out.

In chapter 6, the case system studied is described, as well as all the system components. The mathematical representation, the exact development process and the parameters for each model are presented.

Chapter 7 includes all the cases of operation simulated and the results are analytically described.

In chapter 8, conclusions are extracted based on the simulation results and recommendations for further research are posed.

2. Wind Turbine Technologies

2.1. Current Trends in Wind Turbine Technology

The operation of a wind turbine relies in two energy conversion systems:

- The mechanical system, which converts the kinetic energy of the wind to mechanical torque in the turbine rotor
- The electrical system, in which the generator converts the rotor mechanical torque in electric energy

Although the wind turbine operation principle is relatively simple, nonetheless, it remains a quite complex system, which combines knowledge from various fields. The design and optimization of the blades requires complex aerodynamic knowledge: the driving axis structure, as well as the wind turbine tower requires advanced mechanical engineering knowledge, while the control and protection systems require electrical engineering and automatic control system knowledge.

Two important technological advances have recently been attained in wind power production. First of all, there has been a significant increase in size, aiming at a further increase of the production cost. The wind generator rotor, as well as the typical size of the construction have became way larger than they used to be. The world's biggest world turbine is currently the SeaTitan 10MW turbine, designed by the American energy technologies company AMSC [7]. In figure 4, the evolution of the wind turbine sizes, introduced in the market, is presented.

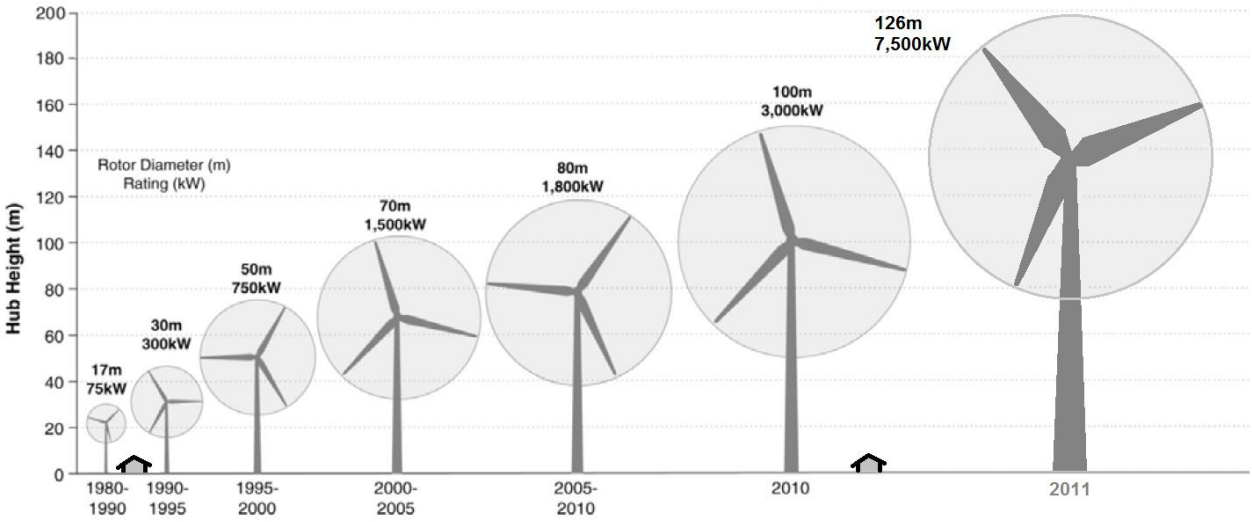

Figure 4: Evolution of Wind Turbine Sizes

As far as the whole construction size is concerned, large wind farms, which are composed of tens to hundreds wind turbines are tended to be constructed instead of individual or small groups of wind turbines. In addition, offshore wind farm construction is on the rise. The reason why wind turbines are organized in wind farms is mainly because in that way, locations with favorable wind behavior are largely used, while at the same time the visual disturbance, caused by the turbines, is restricted in these areas.

The second important advance in wind turbine technology is the transition from fixed speed wind turbine generators to variable speed. The difference, as their name implies, is that at a fixed speed WTG, the rotor's speed is constant, while at a variable speed WTG, rotational speed can be varied and controlled within the design limits. Variable speed systems are technically more complex than fixed speed, as they include more parts and require more complex control systems, a fact that renders them more expensive. Despite their complexity and cost, they have a lot of advantages compared to fixed speed technologies, such as increased power efficiency, noise and mechanical load reduction and better active and reactive power control. For that reason, in the last years most constructors have switched to variable speed systems. Nevertheless, fixed speed WTG, which are the study purpose of this thesis, are still an important part of all wind power installations.

2.2. Wind Turbine Types

There are several characteristics, based on which wind turbines can be categorized. These characteristics include, among others, the rotational speed as mentioned previously (fixed-speed or variable-speed), the generator type or the control method. In spite of the differences among the several types, there are some common details that describe the existing wind turbines and their grid interconnection. This allows their classification and systematization, a fact that is necessary in order for more realistic WTG models to be developed for voltage stability studies, such as the generic models that are discussed in a later chapter.

Based on these details, currently four types of wind turbines have been formed. In the future, new wind turbine types may become available.

2.2.1. Type 1: Fixed-Speed Wind Turbine Induction Generator

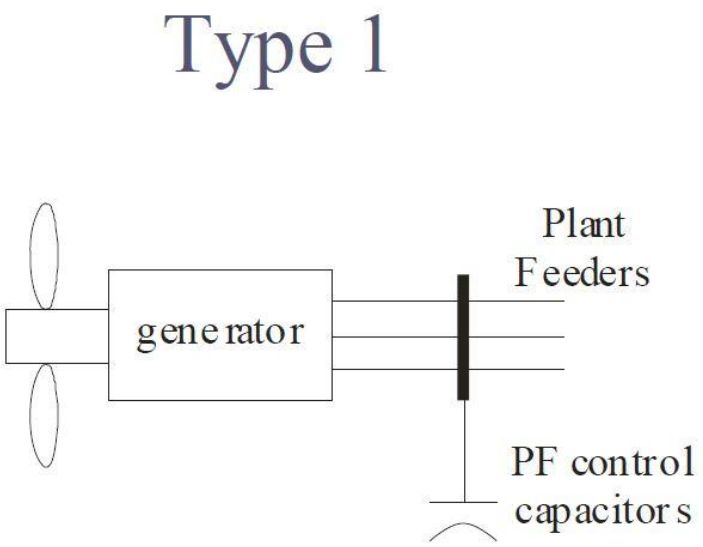

Figure 5: WTG Type 1 configuration

Wind turbine Type 1 is one of the oldest technologies used in wind turbine generators. It consists of an induction generator connected to the rotor blades via a gearbox. This type of turbine is very rugged and simple in its construction. The induction generator used in most of the turbines is usually the squirrel cage generator, operating in a low slip range between 0-1%. Many turbines use dual-speed induction generators, where two sets of windings are used within the same stator frame. The first set is designed to operate in a low rotational speed (corresponds to low wind speed operation), while the second is designed to operate in a high rotational speed (high wind speed operation). Since the start-up current is high, many wind turbines of this type employ a phase-controlled soft-starter to limit start-up currents. This soft-starter consists of back-to-back thyristors in series with each phase of the induction generator.

The natural characteristic of an induction generator is that it absorbs reactive power from the utility supply. Thus, this type of turbine requires reactive power support implemented in the form of switched capacitors connected in parallel with each phase of the winding. Operation without switched capacitors can lead to excessive reactive power drawn from the utility, creating a significant voltage drop across the transmission line and resulting in low voltage at the terminals of the induction generators.

The size of the capacitors switched in and out is automatically adjusted according to the operating point of the induction generator. At higher wind speeds, the generated power and the operating slip of the generator increase and, as a result, the reactive power

required is also larger. For such high reactive support demands, other means, such as a STATCOM, can be used. It is customary to keep the operation of the induction generator at close to the unity power factor.

Aerodynamic control is usually performed with the use of stall or active stall control. In wind turbines with rated power of equal or less than 1 MW, more commonly the stall control is used, while for turbines with higher ratings the active stall control is preferred. That is because the high power levels require the adjustment of the pitch angle of the blades, in order for the strain in the mechanical parts of the turbine to be avoided.

2.2.2. Type 2: Wound Rotor Induction Generator with Adjustable External Rotor Resistance

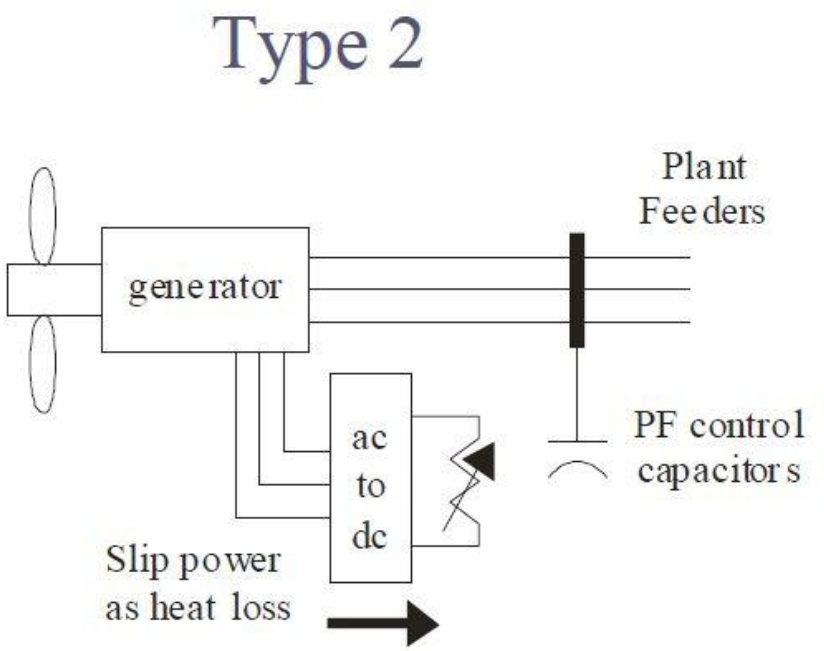

Figure 6: WTG Type 2 configuration

Wind Turbine Type 2 is a wound rotor induction generator with adjustable external resistors. The adjustable external resistor is implemented by a combination of external three-phase resistors, connected in parallel with a power electronics circuit (diode-bridge and DC chopper). Both the resistors and the power electronics circuit are connected to the rotor winding. By adjusting the duty ratio of the DC chopper, the effective value of the external resistor is determined.

The wind turbine starts to generate when the rotor speed is above the synchronous speed. An increase in the wind speed is accompanied by an increase in the input

aerodynamic power, the rotor slip, as well as the electric output power. As long as $P<P_{rated}$, the external rotor resistors are short-circuited (duty ratio=1). Once the output power reaches its rated output, the external rotor resistance is adjusted to maintain the turbine output constant. This is achieved by keeping the effective total rotor resistance constant at the value of $\frac{R_2}{slip_{rated}}$.

$$R_{2,tot} = R_2 + R_{2,ext} \tag{2.1}$$

$$\frac{R_{2,tot}}{slip} = \frac{R_2}{slip_{rated}} \tag{2.2}$$

To prevent the rotor speed from reaching run-away conditions and to reduce the mechanical loads on the blades and the turbine structures, the aerodynamic power is also controlled by controlling the pitch angle of the blades in the high wind speed regions. The blade pitch is controlled accordingly, in a way that the rotor speed ranges from 0 up to 10 % above the synchronous speed.

2.2.3. Type 3: Variable-Speed Wind Turbine with Doubly Fed Induction Generator

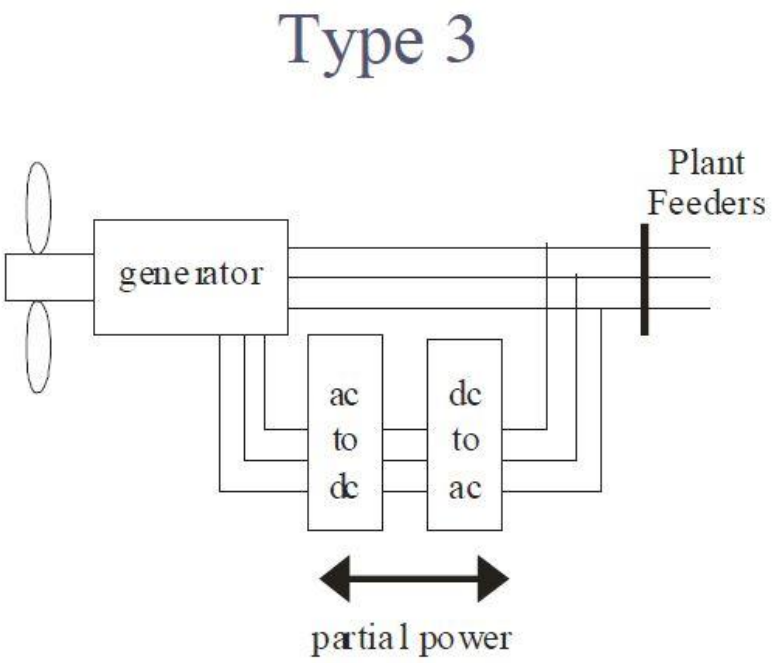

Figure 7: WTG Type 3 configuration

This structure includes a rotor with pitch angle blade control, connected via a gearbox to a wound rotor induction generator and a variable frequency power converter. As the converter delivers only the rotor power to the grid, it is designed to have a rated power of only the 30 % of the generator rated power. Furthermore, being connected to the rotor circuit, it allows reactive power compensation and control and a safe grid interconnection. The wind turbine generator has a speed range of ±30% around the synchronous speed, while the relatively small size of the power converter renders this topology particularly attractive.

The wide range of wind speeds in which the energy efficiency of the wind turbine is maximized, significantly increases the energy efficiency of the whole configuration, a fact that is considered its main advantage compared to the type 1 and 2 configurations. The generator torque remains almost constant, in contrast with the fixed-speed wind turbine generator, as the rapid wind's speed variations are absorbed by the generator's speed variations. This is rendered possible by the operation of the power converter, which, at the same time, reduces the mechanical strain in the wind turbine generator parts. In addition, type-3 WTGs are equipped with a number of functions that allow their contribution in the grid parameters' adjustment, as required by the grid operators, in reference to active and reactive power control, quick reaction in transient and dynamic events, contribution to the power system stability and increased power quality.

However, the use of slip rings in the generator rotor for the converter connection, the requirement for a protection system during grid faults, reliability issues and increased cost related to the power converter use are some of the basic disadvantages of this configuration.

2.2.4. Type 4: Variable-Speed Wind Turbine Generator with Full Scale Power Converter

In this variable-speed WTG configuration, the rotor, which includes a blade pitch angle control, is connected via an asynchronous or synchronous generator and a full scale power converter to the grid. In the case of the asynchronous generator, a gearbox is also used. The full scale converter, apart from allowing reactive power control and a safe grid interconnection, also allows variable-speed operation through the generator's entire speed range.

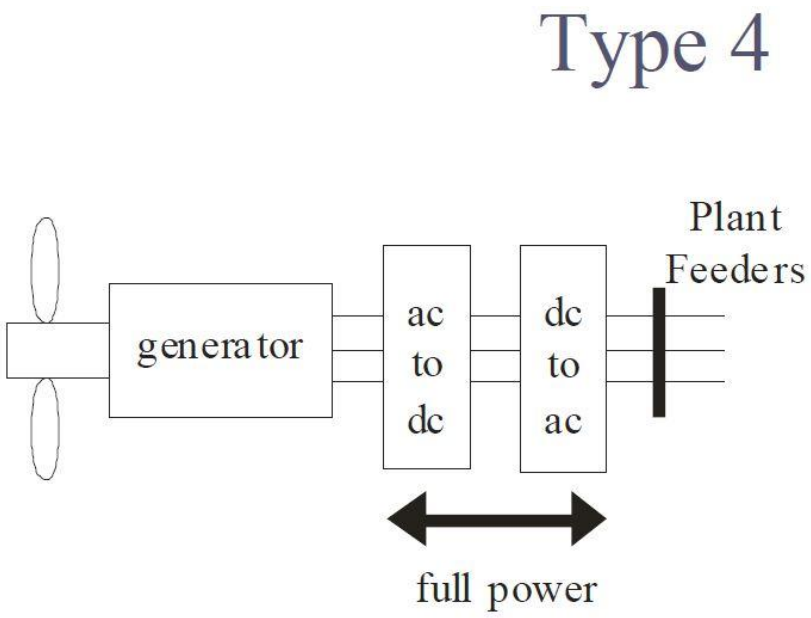

Figure 8: WTG Type 4 configuration

The advantages and disadvantages of this WTG type are generally similar to that of type 3 and are related to the power converter use. Variable-speed operation in type 4 is obviously expanded compared to type 3, as there isn't any type of connection between the generator and the system frequency. Furthermore, the protection against transients in type 4 is significantly increased because of the intermission of the converter, while the direct connection of the stator to the grid in type 3 makes it susceptible to transient currents. Finally, type 4 exhibits important advantages compared to type 3, regarding the energy efficiency, reliability and maintenance issues.

2.3. Wind Turbine Aerodynamic Power

The kinetic energy in a parcel of air of mass, m, flowing at speed v_w, in the x direction is:

$$U = \frac{1}{2} m v_w^2 = \frac{1}{2} (\rho A x) v_w^2 \tag{2.3}$$

where U is the kinetic energy in Joule, A is the cross-sectional area in m^2, ρ is the air density in kg/m^3 and x is the thickness of the parcel in m. If we visualize the parcel with side x, moving at speed v_w (m/sec) and the opposite side fixed at the origin, we see the kinetic energy increasing uniformly with x, because the mass is increasing uniformly [8].

The power in the wind P_w, is the time derivative of the kinetic energy:

$$P_w = \frac{dU}{dt} = \frac{1}{2}\rho A v_w^2 \frac{dx}{dt} = \frac{1}{2}\rho A v_w^3 \tag{2.4}$$

The fraction of power extracted from the power in the wind by a practical wind turbine is usually given by the factor C_p, standing for the coefficient of performance or power coefficient. Using this notation, the actual mechanical power output can be written as:

$$P_m = c_p\left(\frac{1}{2}\rho A v_w^3\right) = \frac{1}{2}\rho \pi R^2 v_w^3 c_p(\lambda, \beta) \tag{2.5}$$

where R is the blade radius of the wind turbine (m). The coefficient of performance is not constant, but varies with the wind speed, the rotational speed of the turbine and turbine blade parameters, such as angle of attack and pitch angle. Generally, it is accepted that the power coefficient C_p is a function of the tip speed ratio λ and blade pitch angle β (deg). The tip speed ratio is defined as

$$\lambda = \frac{\omega_R R}{v_w} \tag{2.6}$$

where ω_R is the mechanical angular velocity of the turbine rotor in rad/s an v_w is the wind speed in m/s. The angular velocity ω_R is determined from the rotational speed n (r/min) by the equation

$$\omega_R = \frac{2\pi n}{60} \tag{2.7}$$

The value of the coefficient of performance is limited by the Betz's law. In 1919, the physicist Albert Betz showed that for a hypothetical ideal wind-energy extraction machine, the fundamental laws of conservation of mass and energy allowed no more than 16/27 (59.3%) of the kinetic energy of the wind to be captured. This limit can be approached by modern wind turbine designs which may reach 70 to 80% of this theoretical limit.

2.4. Wind Turbine Mechanical Part

A typical wind energy conversion system is shown in figure 9. The components the mechanical system comprises are the wind turbine, the low-speed shaft, the gearbox, the high-speed shaft and the wind generator rotor. The common approach adopted for the analysis of the dynamic motion of a mechanical system (i.e. windmill drive train system) is

that the wind turbine, the gearbox and the generator rotor can be modeled as masses, while the windmill shafts can be modeled as spring elements. Obviously, accurate results are obtained by increasing the number of masses, springs and damper, which are used to represent the physical characteristics of the actual wind system (i.e. increasing the degree of freedoms). Thus, the more faithful representation of the actual system is the three-mass mechanical model, as depicted in figure 10.

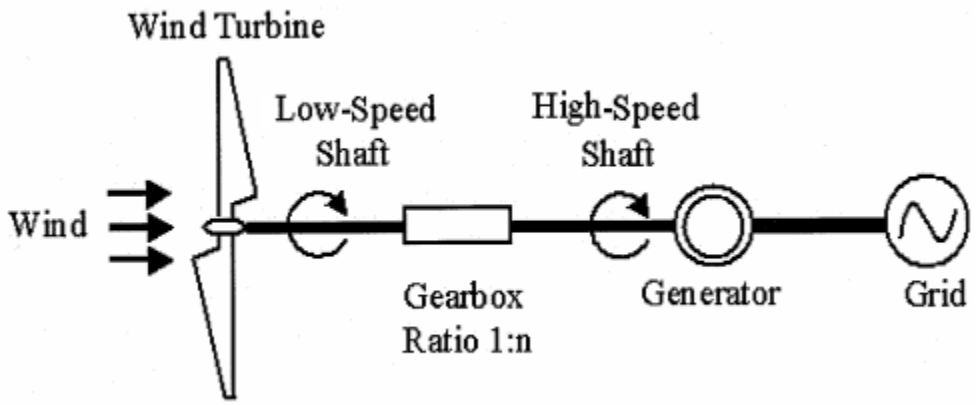

Figure 9: Schematic diagram of a typical wind energy conversion system

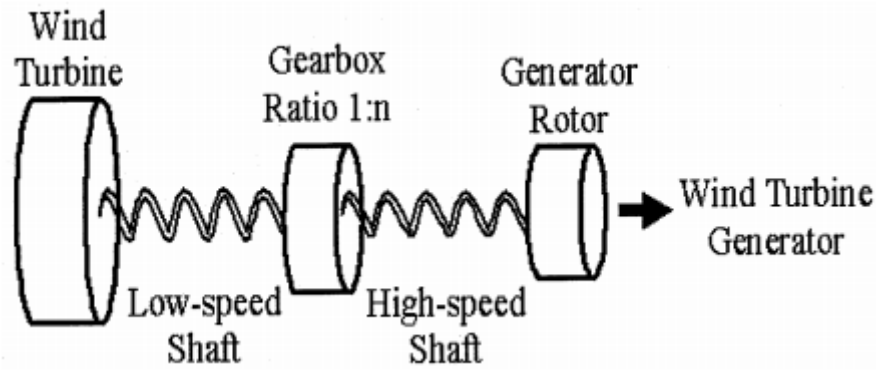

Figure 10: Three-mass mechanical model

The parameters used to describe the mechanical components are the shaft stiffness, the inertia of each component and the damping coefficient.

The three-mass mechanical model can be simplified to the two-mass system shown in figure 11 by converting the wind turbine inertia and the low-speed shaft masses and shaft stiffness to the generator (high-speed) side. This is performed as follows:

$$K_H = \frac{K_L}{n^2} \tag{2.8}$$

$$J_H = \frac{J_L}{n^2} \tag{2.9}$$

$$n = \frac{n_H}{n_L} \tag{2.10}$$

where:

n the transmission ratio of the gearbox

n_H, n_L numbers of high-speed and low-speed gears

K_H, K_L high-speed and low-speed shaft stiffness

J_H, J_L mass moment of inertia of high-speed and low-speed masses

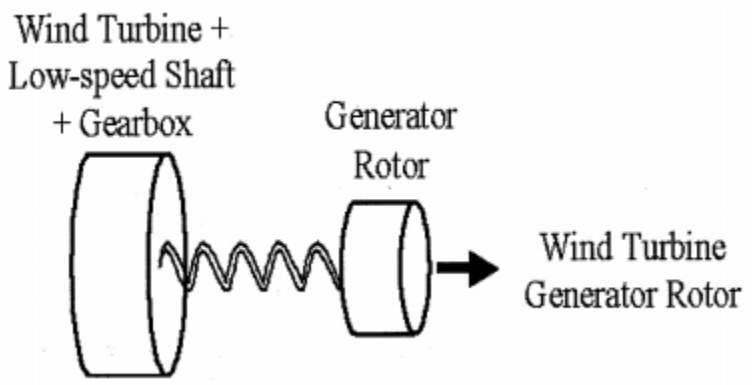

Figure 11: Two-mass mechanical model

Finally, when all the mechanical components are lumped together and modeled as a single rotating mass (figure 12), the one-mass mechanical model is extracted. The one-mass mechanical model is the most simplified representation of the mechanical components and their interaction. Its dynamic behavior is described by the following differential equation:

$$\frac{d\omega}{dt} = \frac{T_m - T_e}{J} \tag{2.11}$$

where:

J moment of inertia of the rotating mass

ω rotor speed

T_m input mechanical torque applied on the wind turbine rotor

T_e electromagnetic torque developed inside an induction machine

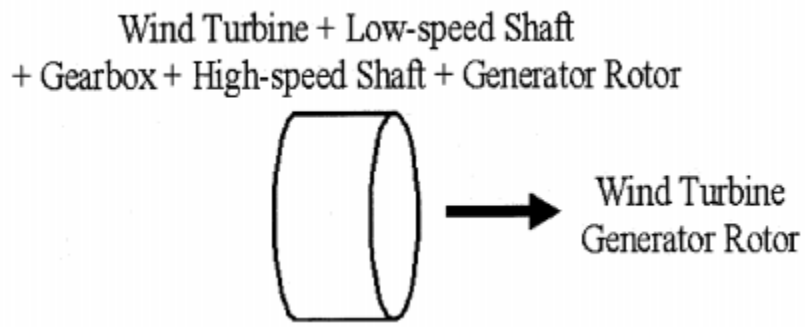

Figure 12: One-mass mechanical model

2.5. Wind Turbine Aerodynamic Control

Wind turbines are designed to withstand extreme winds statically. This means that they can survive a storm, but only when they are not spinning. They are not designed for extreme rotational torques or speeds. At very large aerodynamic torques or rotational speeds, the forces on the blades and other parts of the turbine are enormous and will literally tear the turbine apart. This is why turbines are always designed with a cut-out speed, above which brakes will slow the turbine to a halt. However, there is a range of wind speeds before the cut-out speed where turbines employ various active and passive control strategies to deal with high wind speeds that would otherwise pose a threat to the turbines. These control strategies can broadly be classified as pitch control and stall control, respectively.

A pitch-regulated wind turbine has an active control system that can vary the pitch angle (turn the blade around its own axis) of the turbine blades to decrease the torque produced by the blades in a fixed-speed turbine and to decrease the rotational speed in variable-speed turbines. This type of control is usually employed for high wind speeds only (usually above the rated speed), when high rotational speeds and aerodynamic torques can damage the equipment. When wind speeds get very high (above rated power), the blades will pitch so that there is less lift and more drag due to increasing flow separation along the blade length (the blades are pitched into stall). This will decrease the turbine's rotational speed or the torque transferred to the shaft, so that the rotational speed or the torque is kept constant below a set threshold. Pitch-regulated turbines see increasing power up until the rated wind speed, beyond which power is maintained constant until a cut-out speed when the pitch control is no longer able to limit the

rotational speed/aerodynamic torque or where other forces like structural vibrations, turbulence or gusts pose a threat to a rotating turbine. In figure 42, the pitch-regulated turbine is represented by the red curve:

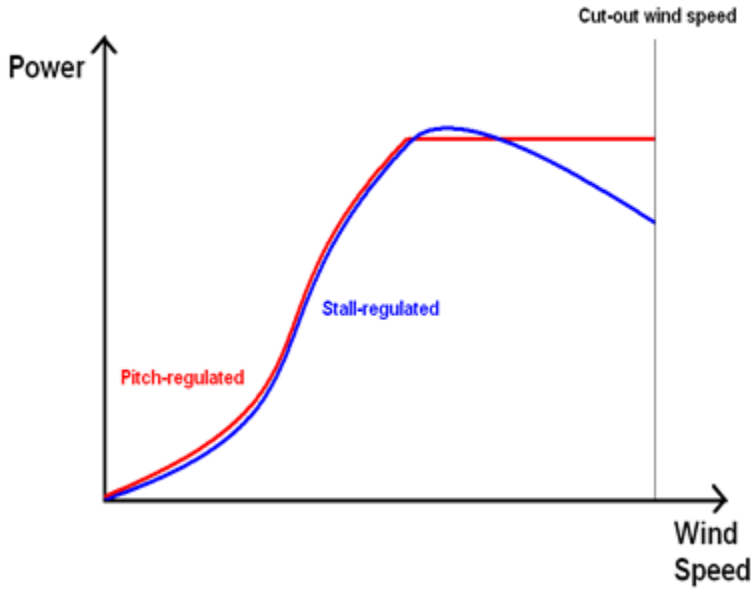

Figure 13: Wind turbine aerodynamic control

Stall-regulated wind turbines, on the other hand, have their blades designed so that when wind speeds are high, the rotational speed or the aerodynamic torque, and thus the power production, decreases with increasing wind speed above a certain value (usually not the same as the rated wind speed). This behavior is illustrated in figure 13, where a typical stall-regulated turbine is represented by the blue curve. The decrease in power with increasing wind speeds is due to aerodynamic effects on the turbine blades (regions of the blade are stalled, propagating from the hub and outwards with increasing wind speeds). The blades are designed so that they will perform worse (in terms of energy extraction) in high wind speeds to protect the wind turbine without the need for active controls. The benefit of stall-regulation over pitch-regulation is limited in the capital cost of the turbine, as well as lower maintenance associated with more moving parts. Like pitch-regulated wind turbines, stall-regulated wind turbines also have brakes to bring the turbine to a halt in extreme wind speeds.

The difference then, between pitch-regulated and stall-regulated wind turbine, is mostly noticeable in high wind speeds. While the stall-regulated systems rely on the aerodynamic design of the blades to control the aerodynamic torque or the rotational speed of the turbine in high wind speeds, the pitch-regulated systems use an active pitch control for the blades. This allows the pitch-regulated systems to have a constant power

output above the rated wind speed, while the stall-regulated systems are not able to keep a constant power output in high winds.

3. Grid Code Requirements

3.1. Introduction

In order to maintain reliable grid performance in response to the increasing wind penetration, transmission system operators (TSOs) update their grid connection codes with specific requirements regarding the operation of wind generators and wind farms. In general, wind farms are expected to support the grid and to provide ancillary services much like conventional power plants (e.g. active power control, frequency regulation and dynamic voltage control and low voltage ride-through (LVRT)).

Power system stability and the quality of the power provided to customers, are frequently threatened by faults. Voltage dips, following faults, can expand to greater parts of the grid and the transient duration depends from a variety of factors, with the most vital the time response of the protection system, which ensures that the fault is cleared, isolating the parts that transients are occurring. In relatively weak systems, the danger of voltage collapse is particularly intense. The time scale of these phenomena ranges from some tens tenths of seconds to some seconds [9].

In addition, apart from the previous reasons, the wind turbine disconnection may be deemed necessary in order to avoid the case of islanding. Islanding refers to the condition in which a distributed generator, after its disconnection caused by a fault, continues to power a location, even though electrical grid power from the electric utility is no longer present. This situation is particularly undesirable, as the voltage and frequency levels in that autonomous part are no longer controllable, jeopardizing the other grid components. Also, islanding can be dangerous to utility workers, who may not realize that a circuit is still powered, and it may prevent automatic re-connection of devices.

For these reasons, the establishment of grid code requirements is of paramount importance. The requirements vary between countries and their severity usually depends on the wind power penetration level, as well as on the robustness of the national or regional power network. Grid code requirements have been a drive for the development of wind turbine technology. Manufacturers in the wind energy sector are constantly trying to improve wind turbines, mainly in the area of wind turbine control and electrical system design, in order to meet the new grid code requirements. This can often imply higher costs, as more advanced power electronic designs and more complex controls

have to be utilized. Grid code requirements can be divided based on the restricted variable in the following categories.

3.2. Frequency and Voltage Operating Range

The problem of adapting power production to power demand is fundamental in power conversion systems. Frequency control in an electric power system is performed by adjusting continuously the power production from the system generators to match consumption as effectively as possible, securing that frequency maintains its nominal value. Any deviation from the planned production or consumption moves the system frequency away of its nominal value. In the case of a sudden load increase, the produced voltage frequency decreases and has to be restored back to nominal by increasing power production through primary control. Under-frequency can also occur as a result of an unexpected generation loss. On the other hand, over-frequency occurs with a sudden load decrease or an unexpected generation increase (e.g. wind gusts).

Grid codes require that wind farms must be capable of operating continuously within the voltage and frequency variation limits encountered in normal operating conditions. In addition, they should remain in operation in case of frequency deviations outside normal operating limits for a specific time interval and in some cases with a specific active power output. By having the ability to remain connected to the grid for a wider frequency range, wind farms support the system during abnormal operating conditions and allow a fast system frequency restoration. Consequently, wind farms must be designed appropriately, as abnormal frequencies can overheat the generator windings, degrade insulation material and damage power electronic devices.

Frequency ranges required by various European countries' grid codes are presented in figure 14. In the green frequency ranges, wind turbines must remain connected and operate continuously at full power output. In the white ranges, they must remain connected at least for the minimum time specified, usually at a lower power output in order to support the grid during frequency restoration. In many cases, the active power reduction must be controlled proportionally with the frequency deviation from the nominal value. In the extreme grey frequency ranges, wind turbines are allowed to disconnect from the grid. Active power requirements at different frequencies, if specified by the grid code, are also shown in figure 14.

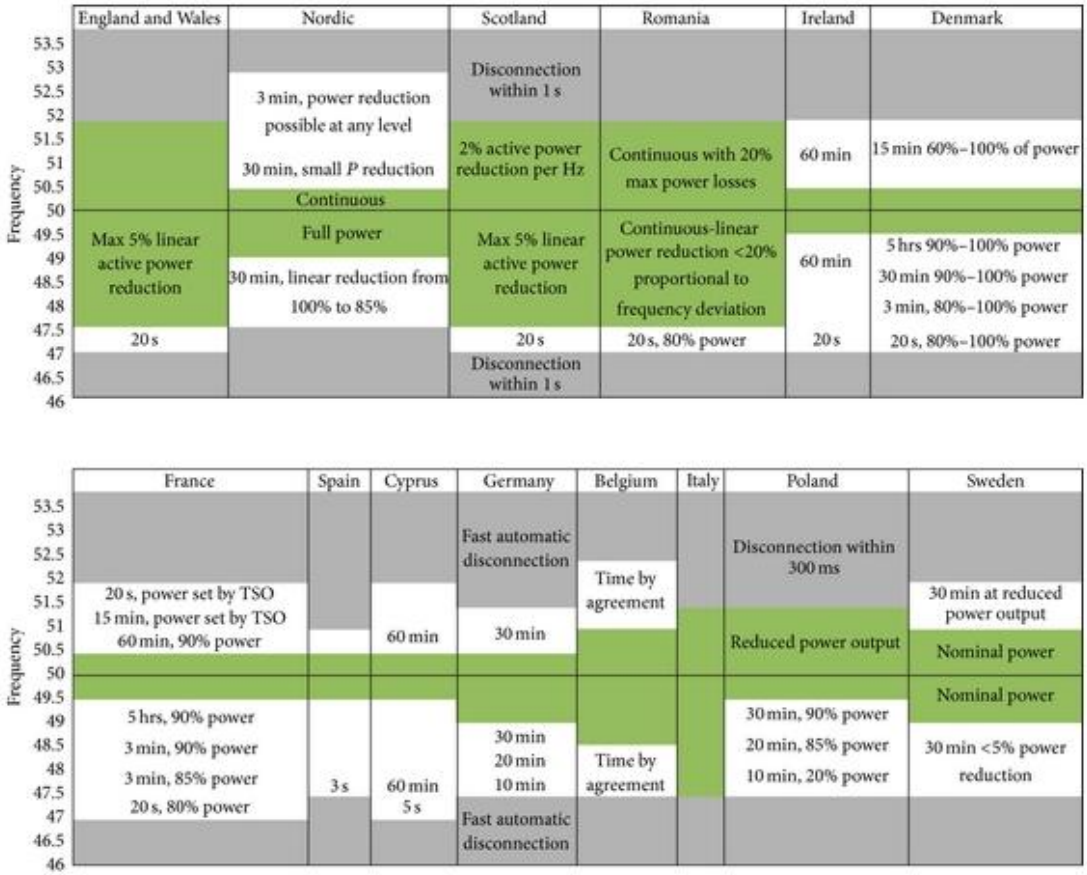

Figure 14: Required frequency range of operation in different grid codes [10]

Overall, in today's wind power systems, wind turbines are required to remain connected in the case of large frequency deviations, with the most extreme frequencies being 47 Hz and 53 Hz. As frequency deviation increases, the minimum connection time and minimum active power conditions are loosened. As it can also be observed, in the case of under-frequencies, wind turbines have to remain connected to the grid for longer periods before they are allowed to trip. The largest frequency ranges of mandatory continuous operation, in which wind turbines must not trip, are observed for the United Kingdom, Romania (47.5 Hz – 52 Hz) and Italy (47.5 Hz – 51.5 Hz). Wider frequency ranges are expected in isolated systems with weak interconnections, where system stability is more vulnerable to disturbances compared to large interconnected systems.

3.3. Active Power Control

The ability of wind power plants to regulate their active power output to a defined level and at a defined ramp rate (e.g. in the case of active power curtailment requested by the

TSO) constitutes the active power control. These requirements aim to ensure a stable frequency in the system, to prevent overloading of transmission lines and to minimize the effects of dynamic operation of wind turbines on the grid (e.g. during extreme wind conditions, at startup/shutdown).

The ability of wind turbines to control their active power is also important for transient stability during faults. If power can be efficiently controlled as soon as the fault occurs, the turbine can be prevented from overspeeding. Hence, the reactive power needed for the re-magnetization of the generators is less after the fault is cleared, a fact that helps the grid voltage to be re-established. Often, active power generation is reduced temporarily by the control system during the low voltage period. This allows an increase of reactive power generation without exceeding the rated current of the converters. After the fault period, a fast return to normal active power generation is essential to ensure power balance and grid stability.

In practice, most grid codes demand active power curtailment upon request from the network operator, at a specified set-point. This is achieved either by disconnecting wind turbines or by controlling the pitch angle of the blades in order to limit the power extracted from the wind. Some grid codes also impose limitations on the rate of change of active power, with maximum and minimum ramp-up and ramp-down rates. These limitations aim to suppress large frequency fluctuations caused by extreme wind conditions and to avoid large voltage steps and in-rush currents during wind farm startup and shutdown.

3.4. Reactive Power Control and Voltage Regulation

Voltage levels in a power system must be maintained constant (within a very narrow range) because equipment of the utility and consumers are designed to operate at specific voltage levels. Recent grid codes demand from wind farms to provide reactive output regulation to the same extent as conventional power plants do. They should be able to generate or absorb reactive power in order to influence the voltage level at the point of common coupling (PCC). Under normal operation the voltage at the PCC can be increased by injecting reactive power to the grid and can be decreased by absorbing reacting power. Wind farms should have reactive power capabilities in order to support the PCC voltage during voltage fluctuations and to assist in balancing the reactive power demand in the grid. The reactive power control requirements are related to the characteristics of each network, since the influence of reactive power injection to the voltage level is dependent on the network short-circuit capacity and impedance. Some

codes prescribe that the TSO may define a set-point value for voltage or power factor or reactive power at the wind farm's connection point. [11]

Voltage and reactive power control constitute determining factors in the power system stability. A factor that renders this type of control vital is that voltage control should be performed in a local level, in contrast with frequency and active power control. Reactive power cannot be transferred over long distances and therefore, control should be performed in all grid parts, including production, consumption flow of reactive power among all voltage levels in a power system. A basic control component are the synchronous generators of conventional production units, using the automatic voltage regulators and the excitation field that ensure that voltage remains between the default levels on their terminal bus. In the rest grid parts, additional control is executed by:

- Reactive power production or consumption elements, such as switching capacitors and inductors, FACTS (Flexible AC Transmission Systems) and synchronous compensators (STATCOM, SVC)
- Line Compensation Element, such as series capacitors
- On load Tap-Changing Transformers

These methods are divided in active and passive compensation. In the first case, the reactive power consumed or produced, is automatically changed according to the voltage of the bus they are connected to, while in the second case, contribution to voltage control is achieved by adjusting the grid characteristics, since the equipment is fixed or switch-connected to the transmission or distribution system.

3.5. Low Voltage Ride-Through (LVRT)

In the past, during grid disturbances and low grid voltages the wind turbines and farms were allowed to disconnect from the grid. However, the large increase in the installed wind capacity in transmission systems necessitates that wind generation remain in operation in the event of network disturbances. For this reason, grid codes issued during the last years invariably demand that wind farms (especially those connected to HV grids) must withstand voltage dips to a certain percentage of the nominal voltage (down to 0% in some cases) and for a specified duration. Such requirements are known as Low Voltage Ride-Through (LVRT) or Fault Ride-Through (FRT) and they are described by a voltage-versus-time characteristic, denoting the minimum required immunity of the wind power station. The LVRT requirements also include fast active and reactive power restoration to the pre-fault values, after the system voltage returns to normal operation levels. Some codes impose increased reactive power generation by the wind turbines during the

disturbance, in order to provide voltage support, a requirement that resembles the behavior of conventional synchronous generators in over-excited operation. In addition, it is worth mentioning that LVRT-related codes do not allow wind turbine disconnection because of power oscillations. Consequently, a special damping system is probably required. Several LVRT voltage-time profiles are presented in figure 15.

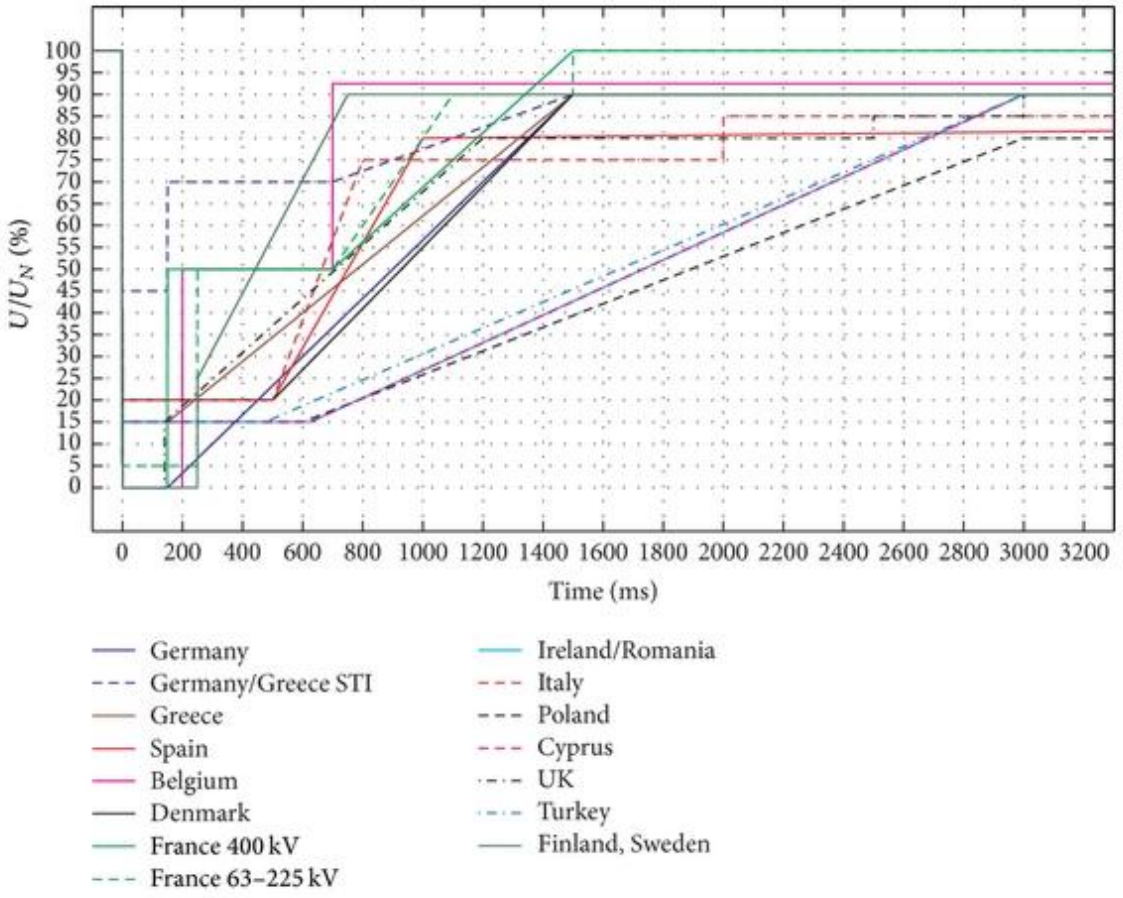

Figure 15: LVRT requirements in various grid codes [10]

These characteristics denote that wind turbines should remain connected for any voltage dip that is described by the area above the limit line. For voltage dips that cover the area under the limit line, disconnection of the wind turbine is allowed. In some cases, there is also an intervening situation between the acceptable and unacceptable disconnection that is known as short term interruption (STI). In this area, temporary disconnection is allowed, but re-synchronization with the grid must be completed in the next two seconds. A STI characteristic for German and Greek codes is presented in figure 15.

The diversification of the LVRT requirements among different countries is obvious. That is reasonable, as the characteristics depend on the necessities and strength of each grid, a fact that is highly varying between different countries.

Furthermore, in some countries voltage control is required during the low voltage faults as shown in figure 16. Wind farms must supply reactive current to the grid based on the depth of the voltage dip, in order to support the local voltage and thus limit the geographical low voltage area caused by the grid fault. During this low voltage period the active current can be decreased and priority should be given to the reactive current in order to back up the grid voltage. The German grid code asks for a constant of proportionality k between the voltage deviation and the required reactive current that can be set in the range k=0-10 after an agreement with the network operator, with a default value k=2.

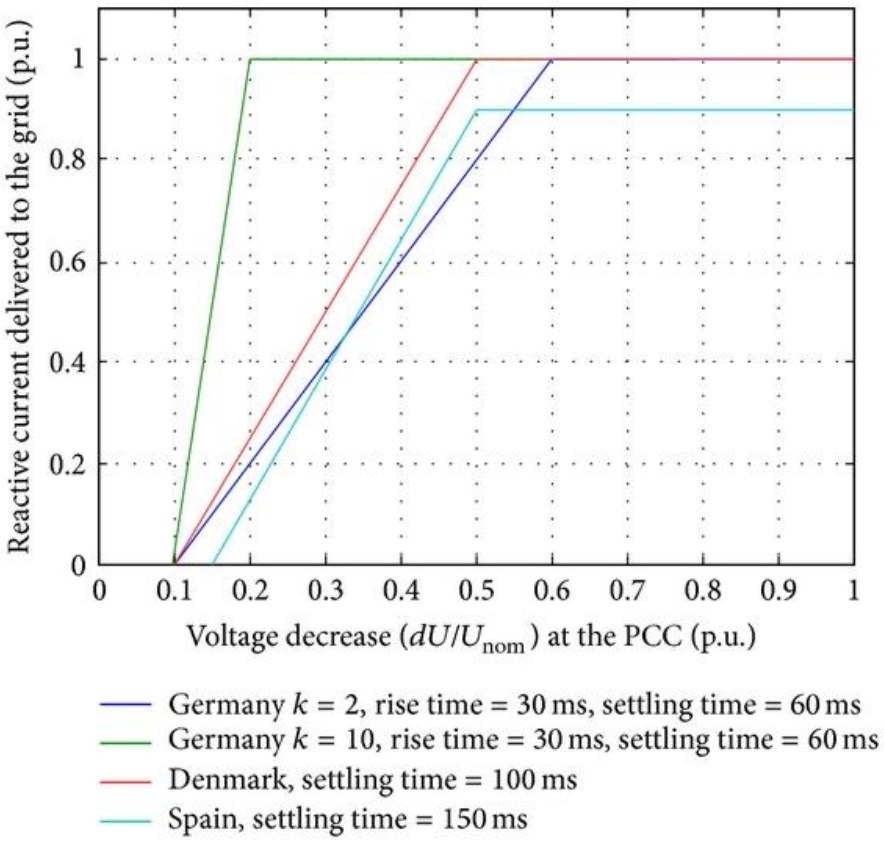

Figure 16: Reactive current requirements with grid voltage decrease [10]

3.6. Conclusion

All of the above requirements determine the limits and the specifications regarding the integration of large wind farms in the electric power systems. The differences between codes imposed to each country by the TSO depend on the inherent characteristics of the corresponding grid, the production and consumption dispersion, the technology involved in the production process, the total system inertia, the protection system and the fault-clearing times and various other technical factors. Systems that are not interconnected and therefore, weaker, are more susceptible of fault and voltage dips spreads.

4. Generic Models

4.1. Introduction and Early Development

With the increasing installed capacity of wind power in power systems, the validated dynamic wind turbine generator models are of particular interest for grid operators to investigate the impact of high wind power penetration on the stability of the power system. Most of the existing dynamic WTG are proprietary user defined models, developed by manufacturers or consultants. These vendor-specific models reproduce the behavior of their WTGs with a great level of accuracy and detail. However, major obstacles are created when used for efficiently performing stability studies with wind power. Firstly, many of the inputs required for the models are proprietary and consequently cannot be publicly shared or distributed. Secondly, these vendor-specific models are user-written and need to be compiled and implemented in different simulation programs. It takes a lot of time for the user to incorporate a large number of these models into power system network models. Thirdly, the simulation time would be quite long and would not be suitable for power system stability analyses. [12]

The absence of WTG generic models is also a significant problem from the system operator's perspective. The system operators are the end users of wind turbine models and due to the general lack of power system analysis expertise on the part of wind turbine manufacturers, the wind turbine model development process has proved cumbersome. Models are developed on behalf of manufacturers by third parties and supplied to system operators for use. As many of the turbine models are not yet mature, system operators have acted as model testers reporting model bugs, irregularities and errors and often advising manufacturers on appropriate action [13].

This is in sharp contrast with other commonly used power system equipment, such as synchronous generators and excitation systems, for which widely accepted, easily

accessible and well-documented models are available in the public domain. Furthermore, maintenance of numerous vendor-specific models is unmanageable for regional reliability organizations and grid operators, who are responsible for conducting system studies and/or maintaining a master dynamic database for large electrical systems. The current situation is untenable and underlines the need to develop publicly available WTG generic models.

Of particular interest to the industry are positive-sequence dynamic models of the type routinely used for simulation of large-scale power system networks. These models are required for demonstrating compliance with power system reliability criteria and for planning system expansions. With increased installed capacity and larger nameplate ratings, it is imperative that wind power plants be properly represented in power system dynamic simulations.

In principle, generic WTG models should exhibit the following characteristics:

- Allow an easy exchange of model data between interested parties
- Facilitate comparisons of system dynamic performance between different simulation programs
- Allow the implementation of WTG models in different simulation programs
- Provide a mechanism by which manufacturers can tune the model parameters to best represent their equipment without having to reveal proprietary information

Based on the IEEE definition, there are four wind turbine types which are commercially available:

- Type 1: Fixed-speed wind turbine with asynchronous generator directly connected to the grid, i.e. without power converter. Type 1A refers to wind turbines without fault-ride through capability while type 1B wind turbines are equipped with blade angle FRT control.
- Type 2: Partially variable-speed wind turbine with wound rotor asynchronous generator, blade angle control and variable rotor resistance (VRR).
- Type 3: Variable-speed wind turbine with wound rotor asynchronous generator, direct connection of the stator to the grid and rotor connection through a back-to-back power converter. This type is usually referred to as doubly-fed induction generator (DFIG) wind turbine.
- Type 4: Variable-speed wind turbines with synchronous or asynchronous generators connected to the grid though a full scale power converter. There are two different models

of type four WTGs: type 4A, where the aerodynamic and mechanical parts are neglected and type 4B, which includes a two-mass mechanical model assuming constant aerodynamic torque.

According to the definition given in [14], the term generic model refers to non-proprietary dynamic models that can be used to represent wind turbine generators with similar physical and control topology, regardless of the manufacturer. Recognizing the need for generic wind turbine generator models, Western Electricity Coordinating Council (WECC) through its Wind Generation Modeling Group (WGMG) has led a comprehensive effort to develop generic positive-sequence WTG dynamic models, suitable for grid planning studies. [15] These models have now been implemented and validated in at least two widely used commercial transient stability simulation programs, Power System Simulation for Engineering (PSSE) and Positive Sequence Load Flow (PSLF). The level of detail and the amount of input data required for such models is under continuous revision due to changes in the relevant power system technologies. The response of the generic models applied in power system stability studies and the applicability of these models in various cases have to be carefully assessed in order to ensure reliable evaluation of the critical operating scenarios of the power [16].

The International Electrotechnical Commission (IEC) is a non-profit, non-governmental international standards organization that prepares and publishes international standards for all electrical, electronic and related technologies – collectively known as "electrotechnology". IEC standards cover a vast range of technologies from power generation, transmission and distribution to home appliances and office equipment, semiconductors, fiber optics, batteries, solar energy, nanotechnology and marine energy, as well as many others. It also manages three global conformity assessment systems that certify whether equipment, system or components conform to its International Standards.

IEC, through its Working Group 27 started the standardization work – IEC 61400-27: Electrical simulation models for wind power generation (Committee Draft) to define standard, public dynamic simulation models for wind turbines and wind power plants. The 42 members of Working Group 27 represent all types of companies and organizations with a potentially high interest in the development and the use of the standard [17]. The group is composed of both modeling and validation subgroups. These models should be applicable for dynamic simulations of power system events, such as short circuits (low voltage ride through), loss of generation or loads and typical switching events. The modeling part of the standard draft has a substantial overlap with WECC WGMG. However, it also considers input from other sources, including the publications from

European researchers and vendors. The aim is that the generic models have a reasonable coverage of the actual wind turbines.

4.2. Overall Structure

The overall process for developing the WTG generic models is illustrated in figure 17.

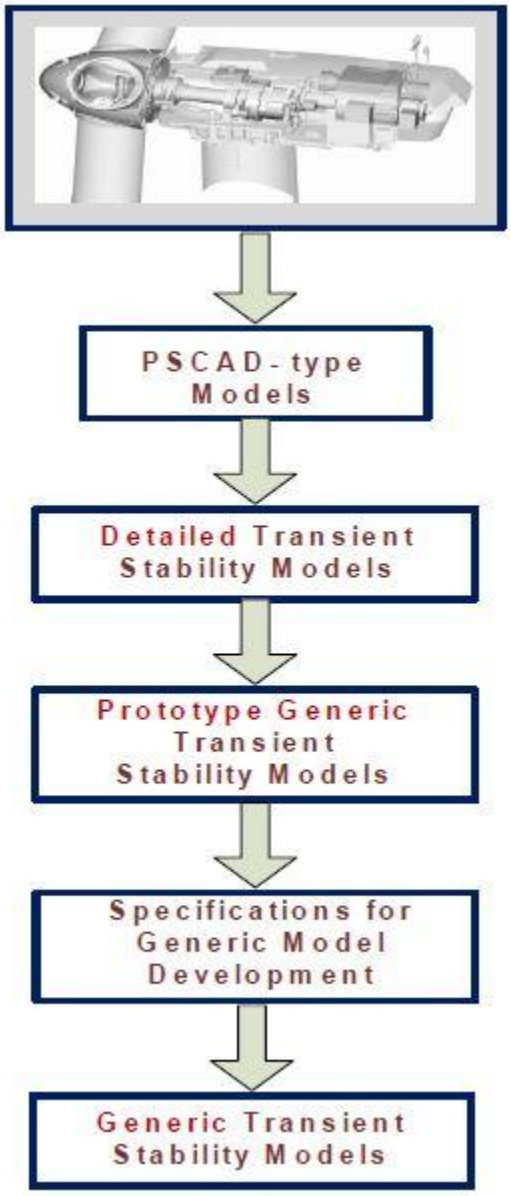

Figure 17: Overall process for developing the generic WTG models [15]

Typically, it initiates from a sophisticated three-phase, PSCAD-type model, with detailed representation of the very fast dynamics associated with the electronic components. This

type of model is needed by manufacturers for detailed analysis and design. These models often need to be proprietary and vendor-specific, and include features not required for bulk power system analyses. From these PSCAD-type models, positive-sequence detailed transient stability models are derived by manufacturers to perform dynamic analyses. These detailed models also contain features that are not needed for typical transient stability studies; furthermore, the availability of these models is also often restricted. In order to circumvent the limitations associated with the general accessibility of WTG models, four prototype generic WTG models were developed by simplifying a detailed transient stability model. For instance, GE's WTG models were used as the basis to develop the generic Type 3 and Type 4 WTGs. To accomplish this, essential features likely to be common to different WTGs were retained, e.g. pitch controller, whereas others that are more proprietary in nature were simplified, e.g. the power coefficient curve [15].

Preceding their development, several overall design guidelines and modeling assumptions were established for the generic models. These include:

- The models are intended for the simulation of events in a time associated with typical transient stability simulations, i.e. ten to twenty seconds.
- It is assumed that in the simulation time frame the wind speed remains constant.
- The models are not designed for use in simulations that involve severe frequency excursions.
- The models allow for the use of a single mass (equivalent to the generator and turbine inertias) or two separate masses.
- The models are suitable for representing individual WTGs or the equivalent of a wind power plant.
- The main model components do not include protective functions. These functions are to be modeled externally.

In addition, for the generic WTG models of Types 1, 2 and 3, the dynamics associated with the turbine and generator inertias are included within the Wind Turbine Model. This was done to facilitate the per unit representation of a two-mass inertial model and the computation of the shaft stiffness. This representation is in contrast with the transient stability models of synchronous generators which typically include the inertia of the machine.

The description of the WTG generic model of each turbine type, according to the work performed by WECC Wind Generation Modeling Group and the IEEE Working Group on Dynamic Performance of Wind Power Generation, is presented in the next section. It is

highlighted that these models were developed so as to simulate the response of each WTG, rather than the exact component itself.

4.3. Generic Wind Turbine Model Description

4.3.1. Generic WTG Type 1

The generic model Type 1 was developed to simulate the performance of a wind turbine, employing a conventional induction generator directly connected to the grid. It is represented by three subsystems, as depicted in figure 18.

The generator model includes the generator dynamics. It represents a standard induction generator; however, unlike a conventional generator model, it contains no mechanical state variables for the machine rotor – these are included in the wind turbine subsystem. However, proper modifications of the model can permit the use of an induction generator model that includes its inertia equation. Such a modified model is discussed in [12].

The wind turbine subsystem may use either the one-mass or the two-mass mechanical model, with a block diagram representation of each is shown in figures 19 and 20 respectively.

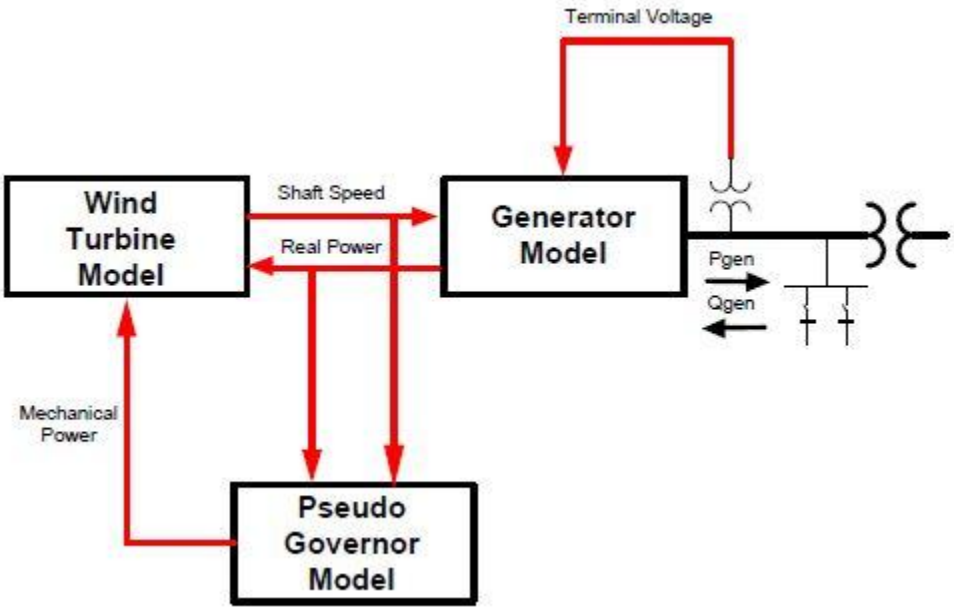

Figure 18: WTG of Type 1 [15]

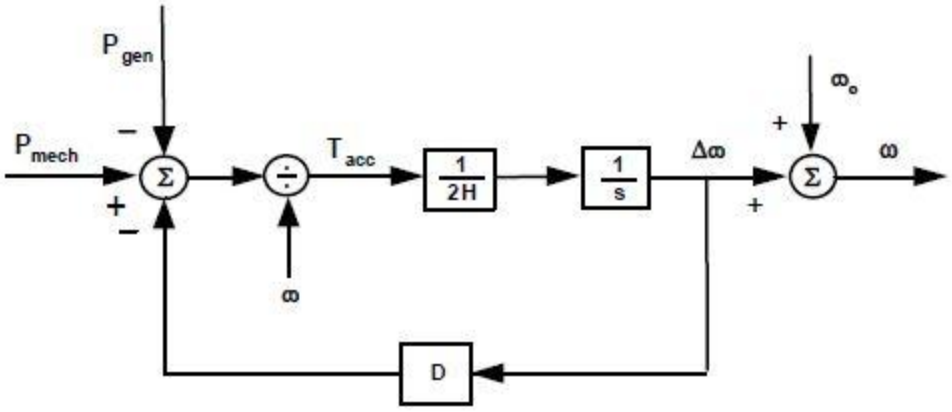

Figure 19: Turbine model - One mass model [15]

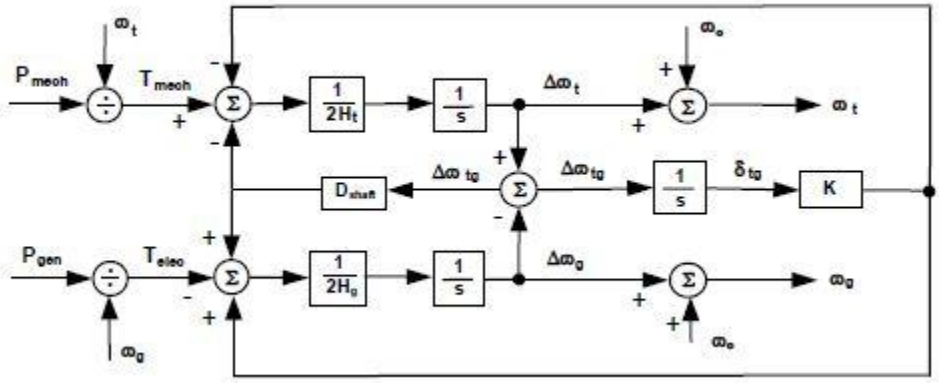

Figure 20: Turbine model - Two mass model [15]

The inertia constant in the single mass representation, H, is equal to the sum of the inertia constants of the generator and the turbine ($H_g + H_t$). The stiffness constant, K, is a function of the first shaft torsional resonant frequency. The damping factor, D_{shaft} represents the natural damping, which acts to resist the speed difference. In [18], it is shown that a proper selection of the value of this factor can lead to an efficient representation of the damping torque component, generated by the power electronics in WTG type 3. Therefore, these mechanical models are also used for the Types 2 and 3 generic WTG models.

Finally, the mechanical power is generated by the pseudo governor model shown in figure 21. This model was designed and developed following a thorough investigation of the

aero-dynamic characteristics and pitch control of several vendor-specific WTG models. The model uses two inputs: rotor speed deviation and generator electrical power. The output is the mechanical power on the rotor blade side. The filters are used to smooth the outputs. The pseudo governor model is used for the Types 1 and 2 generic WTG models and it represents an attempt to simplify the computation of the aero-torque.

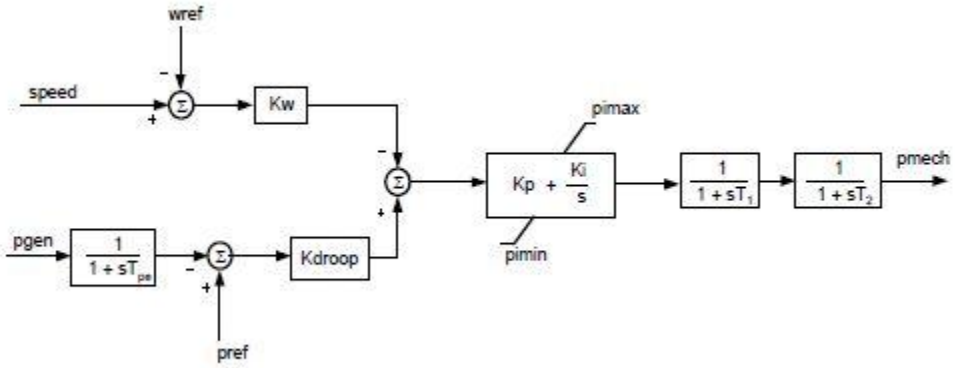

Figure 21: Type 1 & 2 Pseudo Governor Model [15]

4.3.2. Generic WTG Type 2

The configuration of the Generic WTG Type 2 model is quite similar to that of Type 1, with an additional module for the Rotor Resistance Control. It is depicted in figure 22.

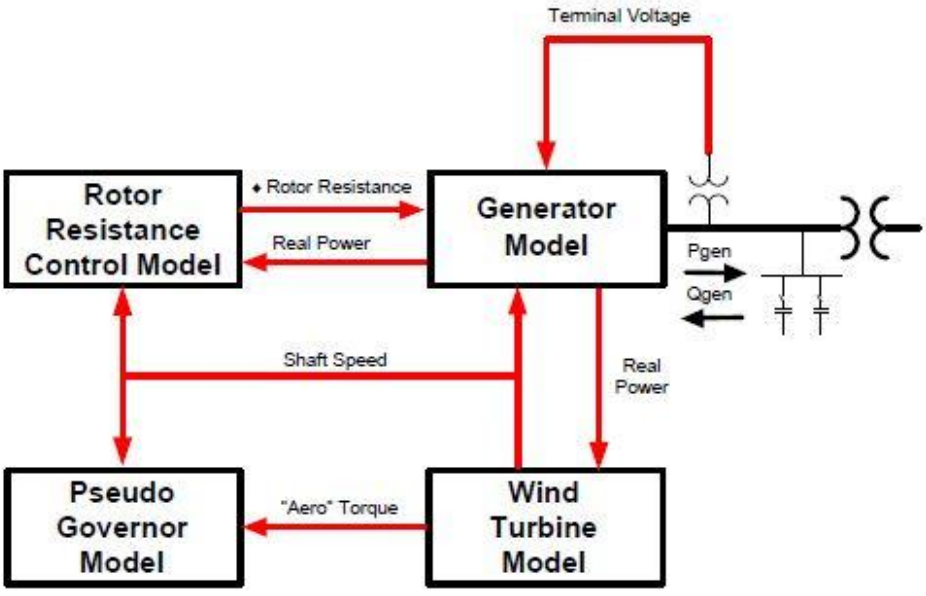

Figure 22: WTG of type 2 [15]

The generator is an induction generator with provisions for adjusting its rotor resistance via the rotor resistance controller. This controller has as inputs the rotor speed and the generator electrical power (figure 23). The model calculates the portion of the available rotor resistance to be added to the rotor resistance included in the generator module via a PI controller and based on the Power vs. Slip Curve that has to be provided.

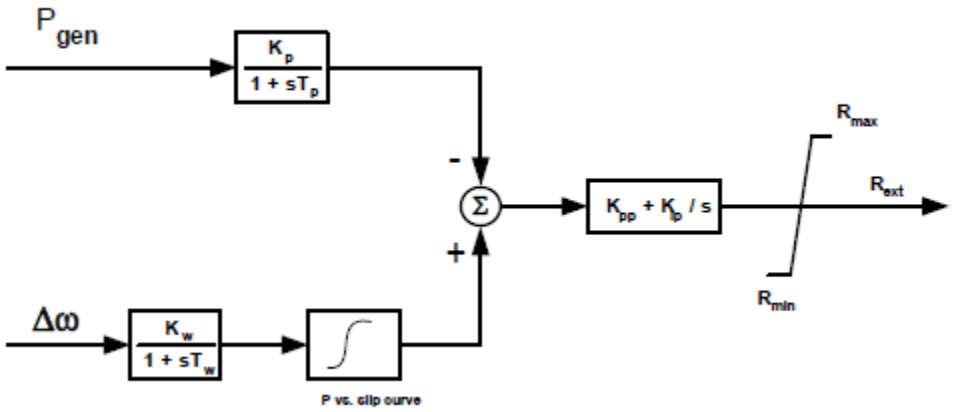

Figure 23: Type 2 WTG Rotor Resistance Controller [15]

4.3.3. Generic WTG Type 3

The generic model Type 3 was developed to simulate the performance of a wind turbine, employing a doubly-fed induction generator with the active control by a power converter connected to the rotor terminals. The general structure is presented in figure 24.

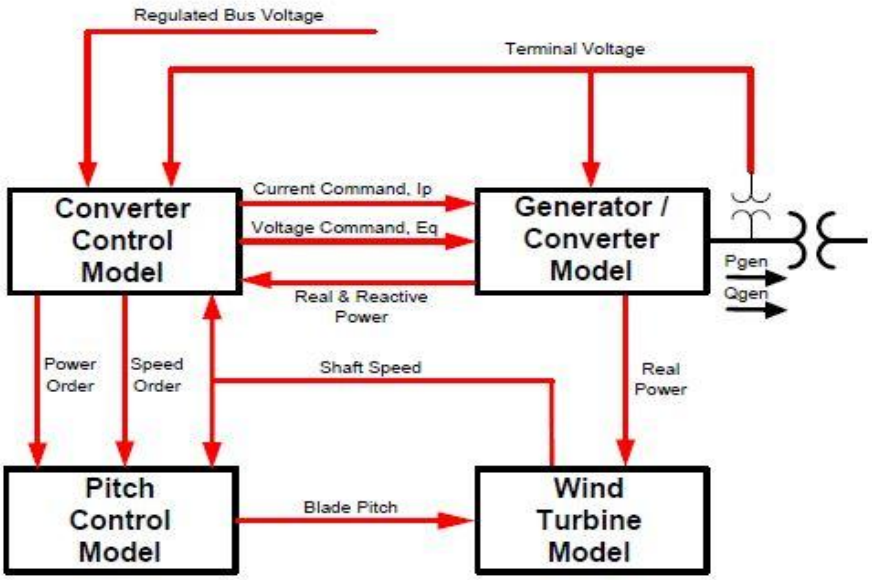

Figure 24: WTG of Type 3 [15]

This model is derived from simplifications of the detailed GE's wind turbine models. Such simplifications include the elimination of the active power control and the GE's WindINERTIA control. The model consists of four main components: generator/converter, converter control, wind turbine and pitch control.

An additional simplification has been made in the construction of the generator/converter model, which is depicted in figure 25. The flux dynamics have been eliminated to reflect the rapid response of the converter to the higher level commands from the electrical controls. This model also includes a Low Voltage Power Logic (which can be bypassed), in order to limit the real current command during and immediately following sustained faults. It also accepts two signals from the converter control, I_{pcmd} and E_{qcmd}, which dictate the active and reactive power to be delivered to the system respectively.

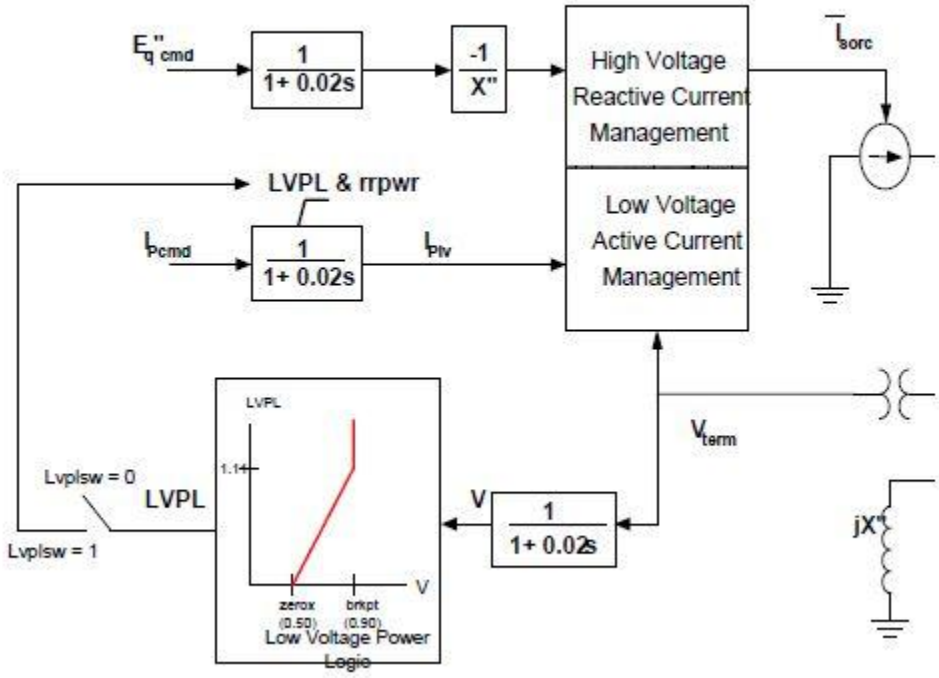

Figure 25: Type 3 WTG Generator/Converter Model [15]

The converter control model, shown in figures 26 and 27, consists of two components: the reactive and active power control modules, each of which generates the signals E_{qcmd} and I_{pcmd}, mentioned above. There are three choices for the reactive power order, Q_{ord}: It can be maintained constant, or be computed by either the Wind Plant Reactive Power Control Emulator or the power factor regulator. The Wind Plant Reactive Power Control Emulation represents a simplified equivalent of the supervisory VAR controller portion of

the entire wind farm management system. The active power order is derived from the generator power and speed. The speed reference, ω_{ref}, is obtained from a turbine speed setpoint versus power output $f(P_{gen})$ curve.

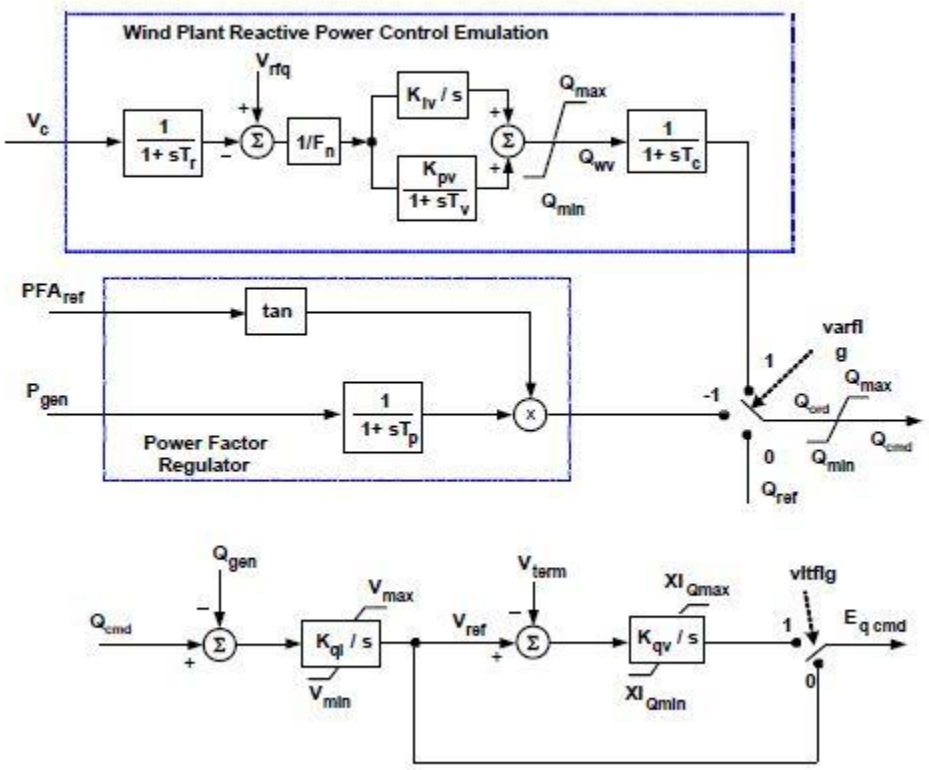

Figure 26: Type 3 WTG Reactive Power Control Model [15]

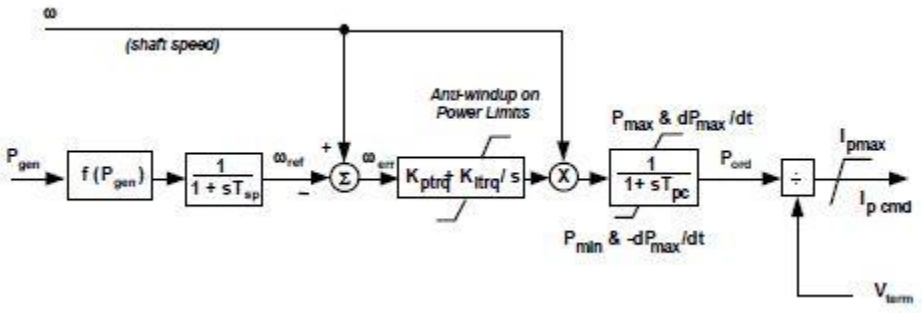

Figure 27: Type 3 WTG Active Power (Torque) Control Model [15]

For the calculation of the aerodynamic power, a very simplified model is used (figure 28). This model does not require representation of the power coefficient curve and is based on the results of the investigation reported in [19].

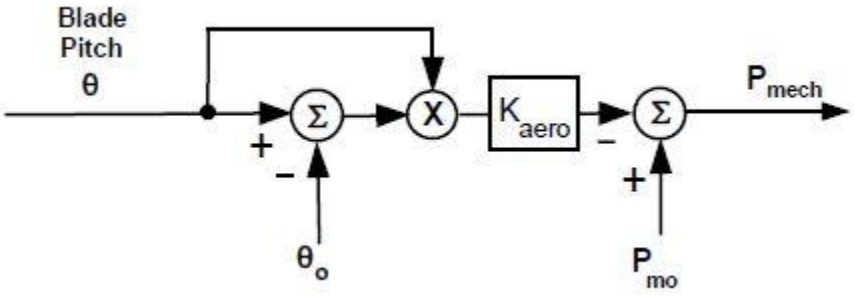

Figure 28: Simplified Aerodynamic Model [15]

Finally, the pitch controller is shown in figure 29. In this model, the blade position actuators are rate-limited and there is a time constant associated with the translation of blade angle to mechanical output. The pitch control consists of two PI controllers that act on the speed and power errors.

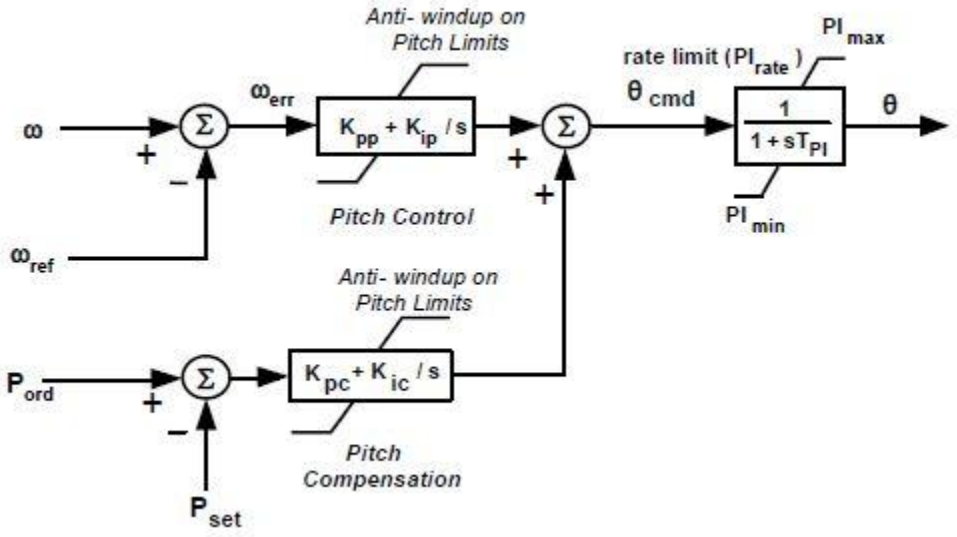

Figure 29: Type 3 WTG Pitch Controller Model [15]

4.3.4. Generic WTG Type 4

The generic WTG model Type 4 simulates the performance of a wind turbine employing a generator connected to the grid via a power converter. It consists of three basic components: generator/converter, converter control and wind turbine. They are presented, along with their connectivity, in figure 30. The model is based on GE's wind turbine model documented in [20].

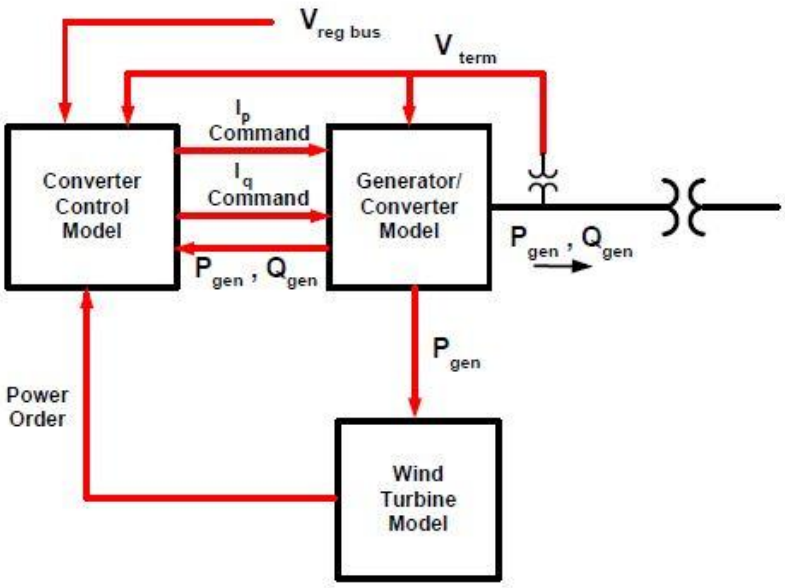

Figure 30: WTG of Type 4 [15]

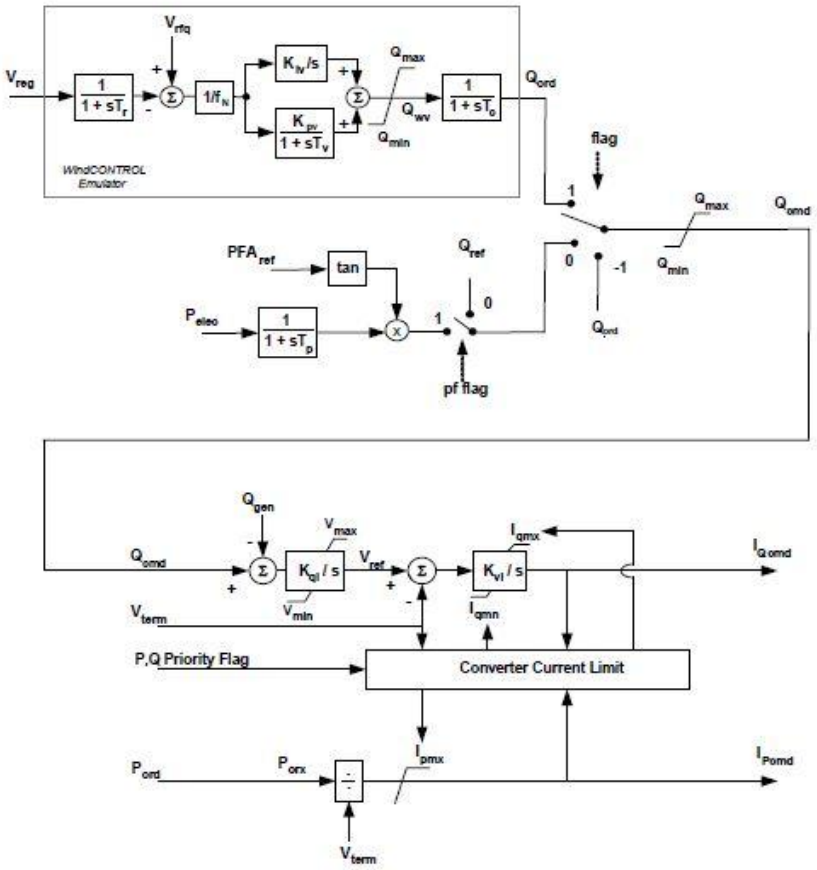

Figure 31: Type 4 WTG Converter Control Model [15]

The generator model is very similar to the Type 3 generator model shown in figure 25. The main difference is that the model takes as inputs both reactive and active current commands. These signals are generated by the converter control model, shown in figure 31. The overall structure of the controller is somewhat similar to the Type 3 WTG reactive power control model, but in includes logic to determine the current limits.

The model used to calculate the current limit is shown in figure 32. The objective of this limit is to protect the converter by preventing the combination of the real and reactive currents from exceeding the converter capability. As it can be observed, it is possible to give priority to either real or reactive power, depending upon the value of a user-specified P, Q priority flag. This flag is determined, based on the equipment features selected and is normally dictated by the host system grid code.

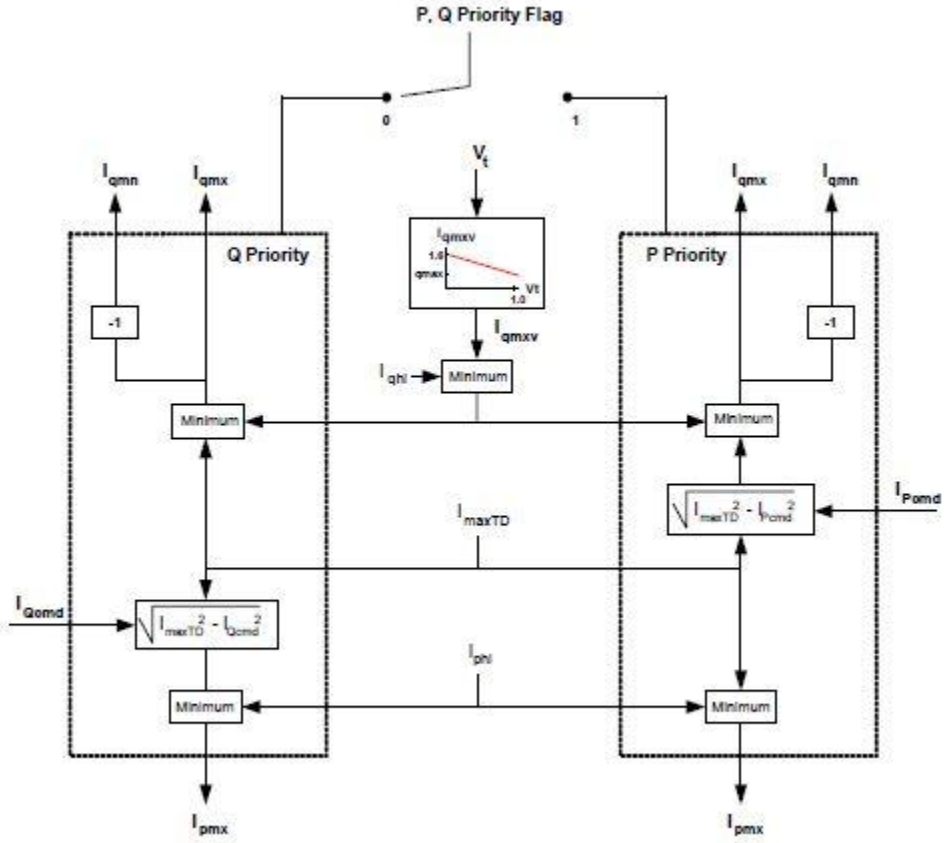

Figure 32: Type 4 WTG Converter Current Limit Model [15]

The Type 4 generic WTG includes the simplified turbine model shown in figure 33.

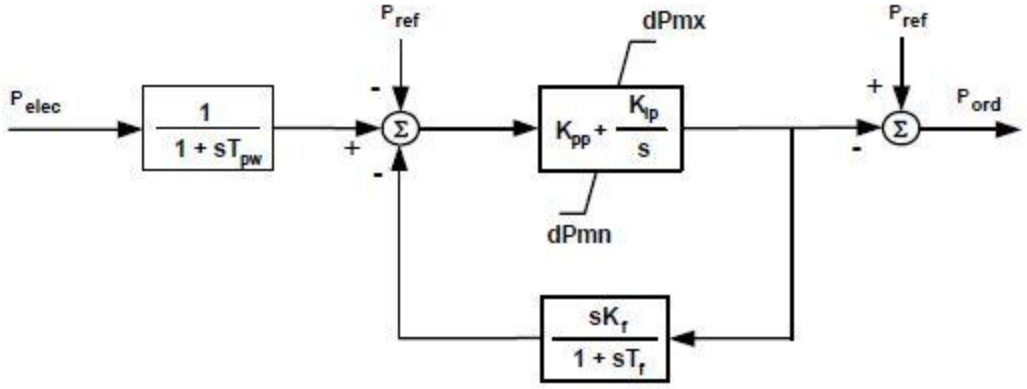

Figure 33: Type 4 WTG Wind Turbine Model [15]

4.4. Generic Model Specifications

In order to facilitate the implementation of the generic WTG models in different simulation programs, the Working Group on Dynamic Performance of Wind Power Generation has written a set of modeling specifications. In principle, with these specifications in place, the implementation of WTG models that are consistent in their functionality in different simulation programs becomes possible. Furthermore, by defining specifications agreed upon by interested parties, a more open dialog is possible regarding upgrades to the models.

The specifications are divided into two categories: functional specifications and model description. The former category defines the functional characteristics of the models, while the latter specifies the manner in which the models should be described. These specifications are fully documented in [15].

4.5. Generic Model Validation

Apart from developing the generic models, a lot of effort had to be put on choosing how to validate their efficiency. Model validation is a key requirement if wind turbine models are to be used with confidence in power system stability studies. We can broadly define the goal of model validation as to establish that a model and its chosen parameters adequately represent the dynamic performance of the "as-installed" device being modeled for the purpose of power system studies [21].

Validation involves two distinct processes: measurement and comparison. Wind turbine measurement for the purpose of model validation may be carried out in numerous ways, but the requirement of validation during severe transient disturbances makes this process difficult. Three approaches have been proposed [13]:

1. Staged generator testing
2. Staged full-scale turbine testing
3. Opportunistic wind farm testing

Staged generator testing may be carried out using the turbine generator and controls alone, without the turbine blades. This measurement setup allows validation measurements to be carried out during the turbine manufacture or at a dedicated test facility. The lack of turbine blade structure makes this type of test feasible, but it will not enable relevant interactions with the wind turbine blade structure or the tower to be observed.

Staged full-scale turbine testing may be carried out at dedicated test facilities, where a full-scale turbine may be installed and subjected to electrical disturbances for the purpose of model validation. This process is expensive however, and the requirements of different grid codes may mean that multiple tests need to be carried out for different jurisdictions.

Probably even more importantly, staged tests are designed such that the unit is isolated from the power system. The response of the unit to an open-circuit step test or following a load rejection is only a function of the unit and its controls. The dynamics of the power system comprising many units and a complex connecting system are not involved.

Opportunistic testing at the wind farm site has been suggested as the solution to the model validation problem. Here measurement equipment is installed at the wind farm site. The equipment records naturally occurring power system disturbances, which are then used to validate wind turbine models. There are various issues associated with this approach; however, these are primarily related to the likelihood of occurrence of a balanced three-phase fault of sufficient magnitude to validate a wind turbine model. Most naturally occurring power system disturbances are complex in nature [13].

A more detailed account of the approaches that have been implemented for wind turbine model validation and more specifically to the generic models can be found in [21].

4.6. Conclusion

The development of wind turbine and wind farm models is vital for the investigation of the effects of large penetrations of wind energy on the stability of power systems. Although a significant amount of effort has been invested in developing and implementing the prototype generic WTG models, the models are not in the final form and a significant amount of work remains to be done. In fact, wind power system modeling constitutes one of the major fields of research in our days.

Nevertheless, the evidence to-date indicates that relatively simple models that exclude proprietary information can be used successfully in bulk power system studies. In needs to be emphasized that to further refine and expand the existing prototype models, it is critical to have the active participation by all parties involved in the development of wind power. Particularly, WTG manufacturers need to be engaged, as they alone possess an intimate knowledge of the dynamic models used to represent their WTGs. Only with their involvement and cooperation can the generic models be developed [15].

5. Static Synchronous Compensator (STATCOM)

5.1. Introduction

Power flow is a function of transmission line impedance, the magnitude of the sending and receiving end voltages, and the phase angle between the voltages. By controlling one or a combination of the power flow arguments, it is possible to control the active, as well as the reactive power flow in the transmission line. In the past, power systems were simple and designed to be self-sufficient. Active power exchange of nearby power systems was rare as AC transmission systems could not be controlled fast enough to handle dynamic changes in the system and, therefore, dynamic problems were usually solved by having generous stability margins so that the system could recover from anticipated operating contingencies.

Today, it is possible to increase the system loadability and hence security by using a number of different approaches. It is a usual practice in power systems to install shunt capacitors to support the system voltages at satisfactory levels. Series capacitors are used to reduce transmission line reactance and thereby increase power transfer capability of lines. Phase shifting transformers are applied to control power flows in transmission lines by introducing an additional phase shift between the sending and receiving end voltages.

In past days, all these devices were controlled mechanically and were, therefore, relatively slow. They are very useful in a steady state operation of power systems but

from a dynamical point of view, their time response is too slow to effectively damp transient oscillations. If mechanically controlled systems were made to respond faster, power system security would be significantly improved, allowing the full utilization of system capability while maintaining adequate levels of stability. This concept and advances in the field of power electronics led to a new approach introduced by the Electric Power Research Institute (EPRI) in the late 1980s. Called Flexible AC Transmission Systems or simply FACTS, it was an answer to a call for a more efficient use of already existing resources in present power systems while maintaining and even improving power system security [22].

5.2. Basic Principles of Active and Reactive Power Control

Active (real) and reactive power in a transmission line depend on the voltage magnitudes and phase angles at the sending and receiving ends, as well as the line impedance. To facilitate the understanding of the basic issues in power flow control and to introduce the basic ideas behind voltage-sourced converter (VSC)-based FACTS controllers, the simple model shown in figure 25 is used. The sending and receiving end voltages are assumed to be fixed and can be interpreted as points in large power systems where voltages are "stiff". The sending and receiving ends are connected by an equivalent reactance, assuming that the resistance of high voltage transmission lines is very small. The receiving end is modeled as an infinite bus with a fixed angle of 0^0.

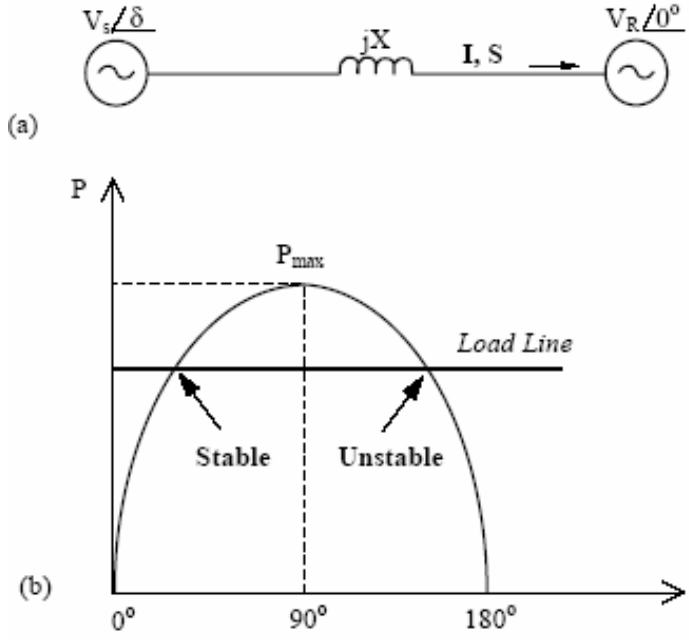

Figure 34: (a) Model for calculation of real and reactive power, (b) Power angle curve for (a) [22]

Complex, active and reactive power flows in this transmission system are defined, respectively, as follows:

$$\boldsymbol{S_R} = P_R + jQ_R = \boldsymbol{V_R} \cdot \boldsymbol{I}^* \tag{5.1}$$

$$P_R = \frac{V_S V_R}{X} \sin \delta \tag{5.2}$$

$$Q_R = \frac{V_S V_R \cos \delta - V_R^2}{X} \tag{5.3}$$

Similarly, for the sending end:

$$P_S = \frac{V_S V_R}{X} \sin \delta = P_{max} \sin \delta \tag{5.4}$$

$$Q_R = \frac{V_S^2 - V_S V_R \cos \delta}{X} \tag{5.5}$$

where V_S and V_R are the magnitudes (in RMS values) of sending and receiving end voltages, respectively, while δ is the phase-shift between sending and receiving end voltages.

The equations for sending and receiving active power flows, P_S and P_R, are equal because the system is assumed to be a lossless system. As it can be seen in Figure 34(b), the maximum active power transfer occurs, for the given system, at a power or load angle δ equal to 90^0. Maximum power occurs at a different angle if the transmission losses are included. The system is stable or unstable depending on whether the derivative $\frac{dP}{d\delta}$ is positive or negative. The steady state limit is reached when the derivative is zero.

In practice, a transmission system is never allowed to operate close to its steady state limit, as certain margin must be left in power transfer in order for the system to be able to handle disturbances such as load changes, faults, and switching operations. As can be seen in Figure 34(b), the intersection between a load line representing sending end mechanical (turbine) power and the electric load demand line defines the steady state value of δ; a small increase in mechanical power at the sending end increases the angle.

For an angle above 90^0, increased demand results in less power transfer, which accelerates the generator, and further increases the angle, making the system unstable; on the left side intersection, however, the increased angle δ increases the electric power

to match the increased mechanical power. In determining an appropriate margin for the load angle δ, the concepts of dynamic or small signal stability and transient or large signal stability are often used. By the IEEE definition, dynamic stability is the ability of the power system to maintain synchronism under small disturbance, whereas transient stability is the ability of a power system to maintain synchronism when subjected to a severe transient disturbance such as a fault or loss of generation. Typical power transfers correspond to power angles below 30^0; to ensure steady state rotor angle stability, the angles across the transmission system are usually kept below 45^0.

Closer inspection of equations (5.2) and (5.4) shows that the real or active power transfer depends mainly on the power angle; inspection of equations (5.3) and (5.5) shows that the reactive power requirements of the sending and receiving ends are excessive at high angles and high power transfers. It is also possible to conclude that reactive power transfer depends mainly on voltage magnitudes, with flows from the highest voltage to the lowest voltage, while the direction of active power flows depends on the sign of the power angle.

Equations (5.2) to (5.5) show that the power flow in the transmission line depends on the transmission line reactance, the magnitudes of sending and receiving end voltages and the phase angle between the voltages. The concept behind FACTS controllers is to enable control of these parameters in real-time and, thus, vary the transmitted power according to system conditions. The ability to control power rapidly, within appropriately defined boundaries, can increase transient and dynamic stability, as well as the damping of the system. For example, an increase or decrease of the value of transmission line reactance X, as can be seen from equations (5.2) and (5.4), increases or decreases the value of maximum power transfer P_{max}. For a given power flow, a change of X also changes the angle between the two ends. Regulating the magnitudes of sending and receiving ends voltages, V_S and V_R, respectively, can also control power flow in a transmission line. However, these values are subject to tight control due to load requirements that limit the voltage variations to a range between 0.95 and 1.05 per unit, and hence cannot influence the power flows in a desired range. From the equations of reactive power flow, (5.3) and (5.5), it can be concluded that the regulation of voltage magnitude has much more influence over the reactive power flow than the active power flow [22].

5.3. STATCOM Basic Operating Principles

5.3.1. Basic Configuration

The Static Synchronous Compensator (STATCOM) is a shunt device of the FACTS family using power electronics to control power flow and improve transient stability on power grids. The fundamental concept behind its operation is the control of the amount of reactive power injected into or absorbed from the power system as a mean of voltage regulation. When the system voltage is low, the STATCOM generates reactive power (STATCOM capacitive), while when the voltage is high, it absorbs reactive power (STATCOM inductive).

The variation of reactive power is performed by means of a Voltage-Sourced Converter (VSC), connected on the secondary side of a coupling transformer. The VSC uses forced-commutated power electronic devices (such as GTOs, IGBTs or IGCTs) to synthesize a voltage from a DC voltage source. The STATCOM uses this voltage as a reference in order to determine whether it will perform in capacitive or inductive operation.

In its simplest form, the STATCOM is made up of a coupling transformer, a VSC and a DC energy storage device. The energy storage device is a relatively small DC capacitor and hence the STATCOM is capable of only reactive power exchange with the transmission system. If a DC storage battery or other DC voltage source were used to replace the DC capacitor, the controller could exchange real and reactive power with the transmission system, extending its region of operation from two to four quadrants. A functional model of a STATCOM is shown in figure 35.

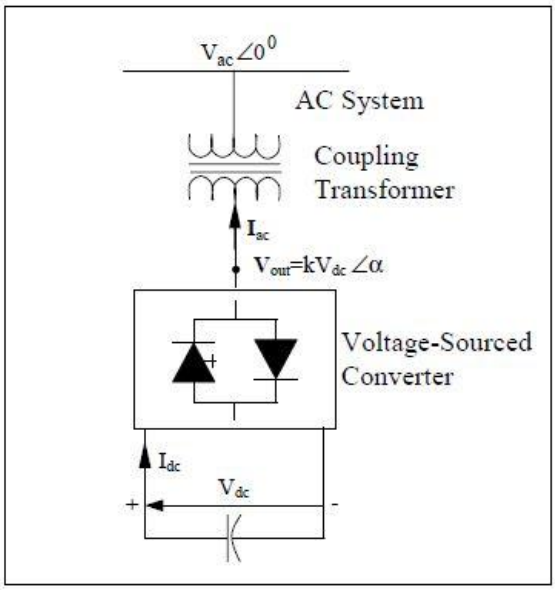

Figure 35: Functional model of a STATCOM

The STATCOM's output voltage magnitude and phase can be varied. By changing the phase angle α of the operation of the converter switches relatively to the phase of the AC system bus voltage, the voltage across the DC capacitor can be controlled, thus controlling the magnitude of the fundamental component of the converter AC output voltage, as $V_{out} = kV_{dc}$. Note that the coefficient k in this equation depends on the converter configuration, number of switching pulses and the converter controls. The difference between the converter output voltage and the AC system bus voltage basically determines the flow of reactive power through the coupling transformer to or from the system.

The real power flowing into the converter supplies the converter losses due to switching and charges the DC capacitor to a satisfactory voltage level. The capacitor is charged and discharged during the course of each switching cycle, but in steady state, the average capacitor voltage remains constant. If that were not the case, there would be real power flowing into or out of the converter, and the capacitor would gain or lose charge each cycle. In steady state, all of the power from the AC system is used to replenish the losses due to switching. The ability of the STATCOM to absorb/supply real power depends on the size of DC capacitor and the real power losses due to switching. Since the DC capacitor and the losses are relatively small, the amount of real power transfer is also relatively small. This implies that the STATCOM's output AC current $\mathbf{I_{ac}}$ has to be approximately $\pm 90^{o}$ with respect to AC system voltage at its line terminals.

Varying the amplitude of the converter three-phase output voltage $\mathbf{V_{out}}$ controls the reactive power generation/absorption of the STATCOM. If the amplitude of the converter output voltage $\mathbf{V_{out}}$ is increased above the magnitude of the AC system bus voltage $\mathbf{V_{ac}}$, then the AC current $\mathbf{I_{ac}}$ flows through the transformer reactance from the converter to the AC system, generating reactive power. In this case, the AC system draws capacitive current that leads by an angle of 90^{o} the AC system bus voltage, assuming that the converter losses are equal to zero. The AC current flows from the AC system to the VSC if the amplitude of the converter output voltage is decreased below that of the AC system and consequently the converter absorbs reactive power. For an inductive operation, the current lags the AC voltage by an angle of 90^{o}, assuming again that the converter losses are neglected. If the amplitudes of the AC system and converter output voltages are equal, there will be no AC current flow in/out of the converter and hence there will be no reactive power generation/absorption.

The current magnitude can be calculated using the following equation:

$$I_{ac} = \frac{V_{out} - V_{ac}}{X} \tag{5.6}$$

assuming that the AC current flows from the converter to the AC system. V_{out} and V_{ac} are the magnitudes of the converter output voltage and AC system voltage respectively, while X represents the coupling transformer leakage reactance. The corresponding reactive power exchanged can be expressed as follows:

$$Q = \frac{V_{out}^2 - V_{out}V_{ac}\cos a}{X} \tag{5.7}$$

where the angle α is the angle between the AC system bus voltage $\mathbf{V_{ac}}$ and the converter output voltage $\mathbf{V_{out}}$.

The STATCOM V-I characteristic is shown in figure 36. This characteristic shows the ability of the STATCOM to support a very low system voltage; down to about 0.15 per unit, which is the value associated with the coupling transformer reactance. This is in strong contrast with the corresponding thyristor-based FACTS controller, the Static VAR Compensator (SVC), which at full capacitive output becomes an uncontrolled capacitor bank. A STATCOM can support system voltage at extremely low voltage conditions as long as the DC capacitor can retain enough energy to supply losses.

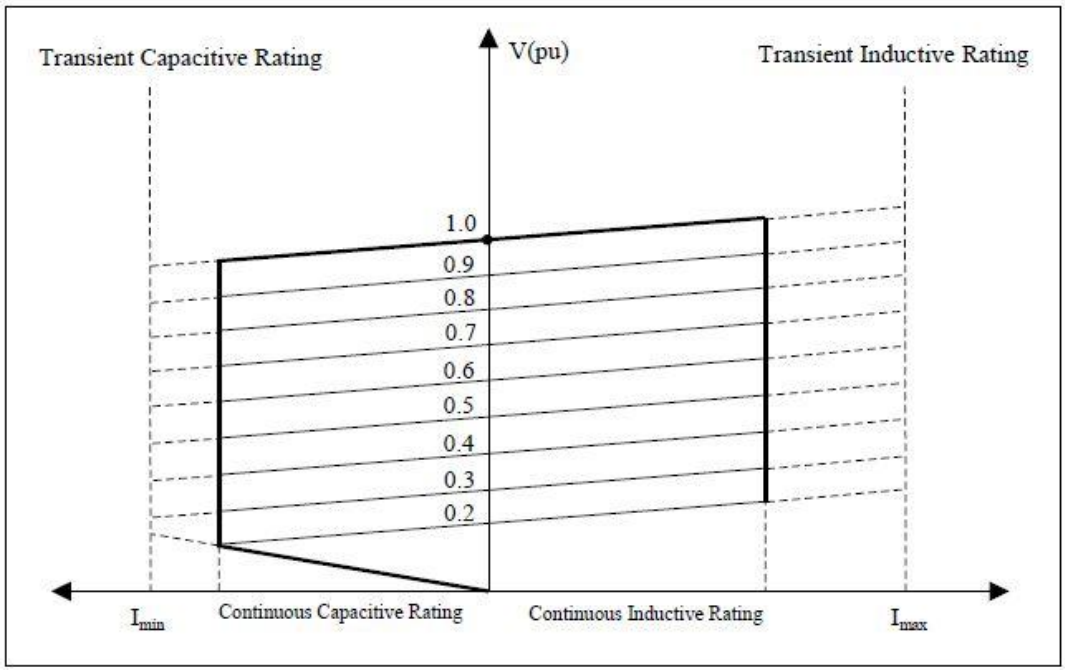

Figure 36: STATCOM V-I characteristic [22]

5.3.2. Voltage-Sourced Converter

Historically, power electronic converters have been predominantly employed in domestic, industrial and information technology applications. However, due to advancements in power semiconductor and microelectronics technologies, their application in power systems has gained considerably more attention in the past two decades. Thus, power electronic converters are increasingly utilized in power conditioning, compensation and power filtering applications [23].

A power electronic converter consists of a power circuit – which can be realized through a variety of configurations of power switches and passive components – and a control/protection system. The link between the two is established through gating signals issued for semiconductor switches and also through feedback signals. Therefore, the transfer of energy in a converter system is accomplished through appropriate switching of the semiconductor switches by the control scheme, based on the overall design performance, the supervisory commands and the feedback from a multitude of system variables.

A VSC is a specific class of converter systems that transforms, through appropriate switching sequence, a DC voltage at its DC terminals into an AC voltage of controllable frequency, magnitude and phase angle at its AC terminals. The output voltage could be fixed or variable, at a fixed or variable frequency. For FACTS application purposes, it is always assumed that the output voltage waveform has a fixed frequency, equal to the fundamental frequency of the power system to which the converter is connected, as high voltage and power harmonics could create many problems.

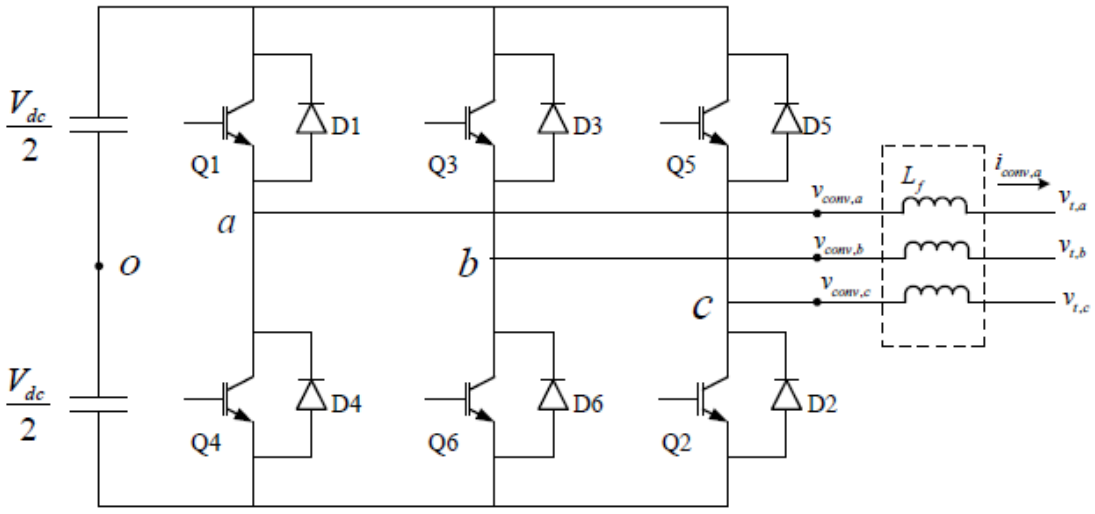

Figure 37: Configuration of a DC/AC Voltage-Sourced Converter

The typical configuration of a VSC is shown in figure 37. By sending the appropriate switching commands to the switches, we are able to produce the DC voltage V_{DC} for the desired time intervals at the converter output. Consequently, it is possible to adjust the the frequency and the rms value of the converter output voltage, by selecting the appropriate switching logic.

The connection between the AC-side terminal and the AC-side voltage source is established through an interface reactor (coupling transformer). The AC-side terminal voltage is a switched waveform and contains voltage ripple. Thus, the interface reactor acts as a filter and ensures a low-ripple AC-side current.

There are various ways to produce the switching pulses, some of which use a high-frequency carrier signal f_C, while other perform the modulation without a carrier signal. Pulse-Width-Modulation (PWM) methods with a carrier signal are the most common practice. Their common characteristic is that whether the switches conduct or not is determined based on the result of the comparison between a modulating signal and the carrier signal. Thus, given the carrier signal, the required switching frequency is also known. The use of a carrier signal has the advantage of switching the harmonic distortion of the produced signal to the carrier frequency and to its multiples, reducing the need of filters.

The most typical case of modulation is the sinusoidal pulse-width modulation (SPWM). In this technique, three sinusoidal modulating signals are used, one for each half-bridge, and also a triangular waveform as a carrier. Each of the modulating signals, which are sinusoidal with a frequency equal to the frequency of the desired produced voltage, is compared with the carrier signal, and the result determines the range of the pulses.

The ratio of the amplitude of control signal to the amplitude of the carrier signal is called modulating factor.

$$m = \frac{A_{control}}{A_{carrier}} \tag{5.8}$$

The modulating factor determines the amplitude of the fundamental component of the converter output voltage. Depending on its value, we can define the following operating conditions of the converter:

- If $0 \leq m \leq 1$, then we are in the linear operation of the SPWM

- If $1 < m \leq 3$, we have over-modulation, a situation where the relation between the amplitude of the fundamental component of the output voltage and the modulating factor is no longer linear
- If $m > 3$, we have square-pulse operation

In the applications examined in this thesis, we always assume linear converter operation. That means that the maximum value of the output voltage is extracted for $m = 1$. The rms value of the output voltage is calculated as:

$$V_{1,rms} = \frac{\sqrt{3}}{2\sqrt{2}} \cdot m \cdot V_{DC} \tag{5.9}$$

5.3.3. STATCOM Control

The design of VSC controllers for purposes that they are connected to power systems, requiring tracking of a sinusoidal voltage, such as the case of a STATCOM, is almost invariably performed using the dq0 frame transformation. As explained in [23], if the STATCOM terminal voltage was a DC voltage, then its control could be sufficiently performed by means of a proportional-integral (PI) compensator. However, since that in a three-phase VSC system we are invariably interested in tracking sinusoidal voltage or current commands, the compensator design task would face a lot of hardships. By using the dq0 transformation, an easy and decoupled control of the active and reactive components of the current is achieved. This transformation is explained in more detail in Appendix A.2.

Let us consider a STATCOM connected to a three-phase power system. Figure 38 depicts two vectors, one to represent the transmission line voltage at the point of connection and the other to describe the current in the STATCOM lines.

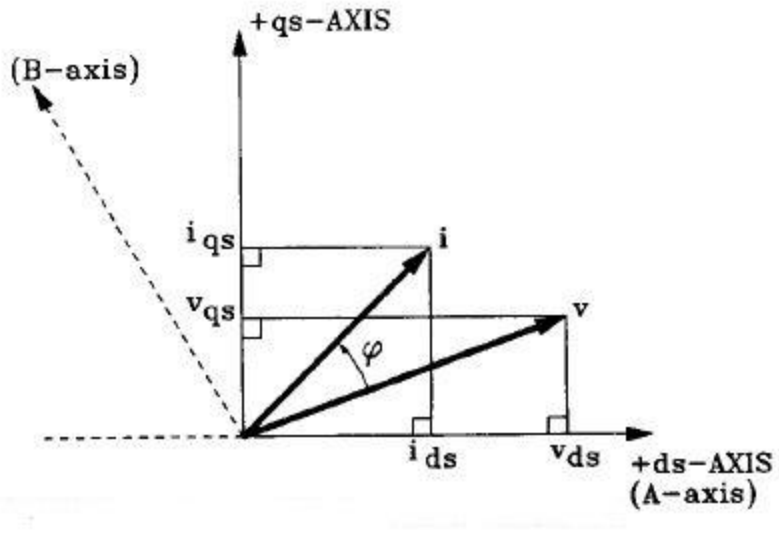

Figure 38: Voltage and current vector in the stationary reference frame [24]

As discussed in Appendix A.3, the real and reactive power components in the dq coordinate system are:

$$P = \frac{3}{2}\left(v_d i_d + v_q i_q\right) \tag{5.10}$$

$$Q = \frac{3}{2}\left(v_q i_d + v_d i_q\right) \tag{5.11}$$

Equations (5.10) and (5.11) suggest that if v_q=0, the real and reactive power components are proportional to i_d and i_q, respectively. To take advantage of this property, the angle Θ of the dq0 transformation, is chosen so that the d-axis is always coincident with the instantaneous voltage vector and the q-axis in quadrature with it (so that by default v_q=0). This is illustrated in figure 39. The dq coordinates within this synchronously-rotating reference frame are obtained by the following time-varying transformation:

$$[T] = \frac{2}{3}\begin{bmatrix} \cos\Theta & \cos\left(\Theta - \frac{2\pi}{3}\right) & \cos\left(\Theta + \frac{2\pi}{3}\right) \\ -\sin\Theta & -sin\left(\Theta - \frac{2\pi}{3}\right) & -sin\left(\Theta + \frac{2\pi}{3}\right) \\ \frac{1}{\sqrt{2}} & \frac{1}{\sqrt{2}} & \frac{1}{\sqrt{2}} \end{bmatrix} \tag{5.12}$$

$$[T]^{-1} = \frac{3}{2}[T]_t \qquad \Theta = \tan^{-1}\left(\frac{v_{qs}}{v_{ds}}\right)$$

$$\begin{bmatrix} i_a \\ i_b \\ i_c \end{bmatrix} = [T]^{-1} \begin{bmatrix} i_d \\ i_q \\ 0 \end{bmatrix} \qquad \begin{bmatrix} v_a \\ v_b \\ v_c \end{bmatrix} = [T]^{-1} \begin{bmatrix} |v| \\ 0 \\ 0 \end{bmatrix}$$

and substituting in (5.11), we get:

$$P = \frac{3}{2}|v| i_d \tag{5.13}$$

$$Q = \frac{3}{2}|v| i_q \tag{5.14}$$

Equations (5.13) and (5.14) show that under balanced steady state conditions, the coordinates of the voltage and current vectors in the rotating reference frame are constant quantities. This feature is useful for analysis of the two current components and is widely employed for decoupled control of grid-connected VSC systems.

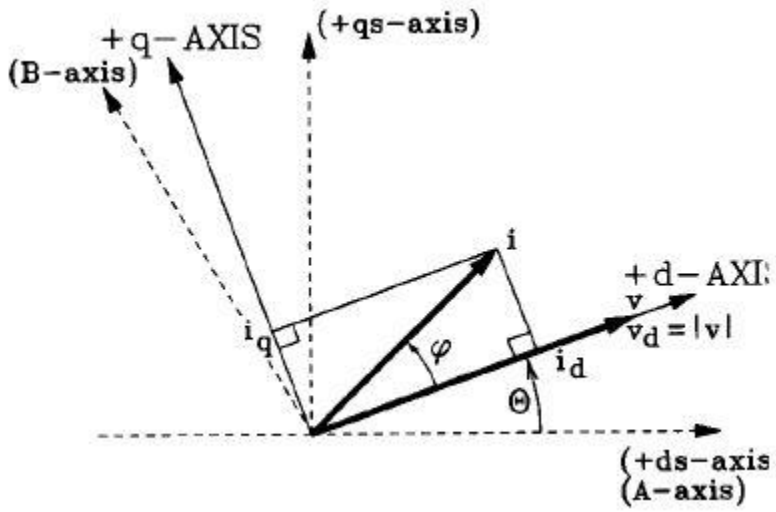

Figure 39: Voltage and current vector in the rotating reference frame [24]

A typical STATCOM control system structure is that depicted in figure 40.

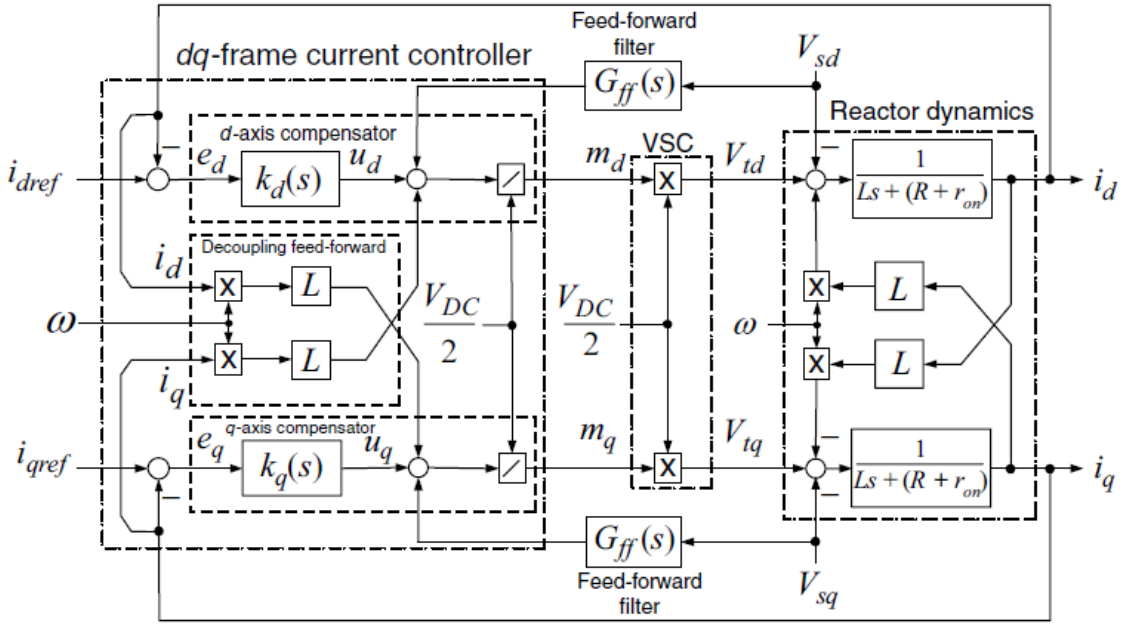

Figure 40: Control block diagram of a current-controlled VSC system [23]

We see that control is performed independently for the d- and q-axes current components. Given the reference signals i_{dref} and i_{qref}, two PI controllers perform their error regulation, outputting the control variables u_d and u_q respectively. Then a feed-forward filter is used to "predict" the output values. In practice, it adds the current STATCOM output voltage to the control variables. The result is the new STATCOM output voltage, which, after it passes through the filter reactor transfer function, produces the new i_{dq} currents.

5.3.4. Applications for Wind Power Topologies

The growing penetration of the produced wind power (size growth of wind farms) forced the TSO and DSO to develop stricter and more detailed grid codes for wind turbines. The new grid codes specify new requirements for wind power plants regarding issues such as frequency control, voltage control and fault-ride through behavior. Reactive power compensation, which in practice influences the voltage control, is STATCOM's main function. Besides of that, STATCOM's applications include the following:

- Stabilization of weak system voltage
- Reduce transmission losses
- Enhance transmission capacity
- Power oscillation damping

- Improve power factor
- Reduce harmonics
- Flicker mitigation
- Assist voltage after grid faults

STATCOM can also be widely used for retrofitting old wind turbines or wind power plants which are no longer able to comply with new strict codes. Such a case is described in [25]. This can be done by adding STATCOM alone or with a battery storage. In [26], it is shown how a STATCOM with a battery energy storage system can improve the produced power quality.

Among the FACTS family, STATCOM has the best capability for providing reactive power compensation for wind power systems. The SVC has also been used, but, as validated in [27] and [28], the result is poorer.

In order to meet the new strict requirements imposed by the TSOs and the DSOs, a variety of modifications of the STATCOM control system have been implemented. Some of them with their bibliographic citations are listed below:

- In [29] a modified STATCOM controller with two additional auxiliary damping loops is proposed to prevent the sub-synchronous resonance (SSR) phenomenon in a series-compensated wind farm, as well as to mitigate the system oscillations
- In [30], a modified control, based on the series combination of a power factor control loop and a voltage regulation loop is demonstrated, in an attempt to enhance the LVRT capability of fixed-speed wind turbines.
- The need for the torsional torques to be mitigated in fixed-speed wind turbines, directly connected to the grid is recognized in [31] and a STATCOM control technique, labeled Indirect Torque Control is suggested. The basic concept to take advantage of the STATCOM reactive current absorption/injection, in order to smooth the generator electromagnetic torque, when the machine is decelerated through the maximum torque region.
- In [32], the behavior of a fixed-speed-turbine wind farm during asymmetrical faults is examined, highlighting the detrimental effects the negative-sequence voltage component has on the system torsional oscillations. The STATCOM control system is expanded with the capability to coordinate the control between the positive and the negative sequence of the grid voltage. The results clarify the effects of the positive- and the negative-sequence voltage compensation by the STATCOM on the wind farm operation.
- An addition attempt to configure the STATCOM control so as to be able to handle asymmetrical grid faults is performed in [33]. The modified controller adapts a

negative reactive current control strategy, which reduces the electromagnetic torque oscillations and therefore, the mechanical strain.

- In [34], an inverse system sliding mode controller, based on non-linear feedback linearization technology for system decoupling, is proposed. The results are compared with the PI controller of inversed system and it is verified that the proposed controller is more efficient and assists in the wind farm LVRT capability.
- In [35], a method based on Particle Swarm Optimization algorithm is presented for tuning the STATCOM parameters. The main purpose of this approach is to maintain the wind farm PCC voltage in reference value and to minimize the voltage deviations immediately after a heavy loaded line outage, which is connected the wind farm.
- An advanced STATCOM control strategy design, called Smart-STATCOM, is presented in [36]. The proposed system's capability of self-controlling reactive power and harmonic voltages at the same time accounts for its name.
- In [37], a fuzzy logic controller is used as the STATCOM control methodology and the results are compared with the conventional PI controller.
- In [38], an alternative representation of the fixed-speed wind turbine leads to a novel, robust STATCOM control design. Specifically, the wind generator (which is a highly non-linear system), is modeled as a linear part plus a non-linear part, the non-linear term being the Cauchy remainder term in the Taylor Series expansion and of the equations used to model the wind farm. The controller resulting from this robust design provides an acceptable performance over a wide range of conditions needed to operate the wind farm during severe faults.
- Finally, [39] and [40] are overviews and comparisons of different STATCOM control techniques, among them the Bang-Bang current controller, the fuzzy logic controller, a control based on Resonant Regulators and a DFT Synchronization Algorithm.

6. Models Developed For Simulation Purposes

6.1. Case System Study

The line diagram of the power system simulated is presented in figure 41. It consists of the 4.5 MW wind farm under study and its grid connection. The wind farm comprises three fixed-speed induction generators, driven by variable-pitch wind turbines. The generators used are squirrel-cage induction generators with their stators directly connected to the 60 Hz grid. Between each WTG and the PCC are interposed the necessary capacitor banks for the safe operation of the induction generators, a step-up

transformer to connect the WTG with the 25 kV distribution network and a 1-km feeder. Then, grid connection is achieved by a 25 kV, 25 km feeder and another step-up transformer.

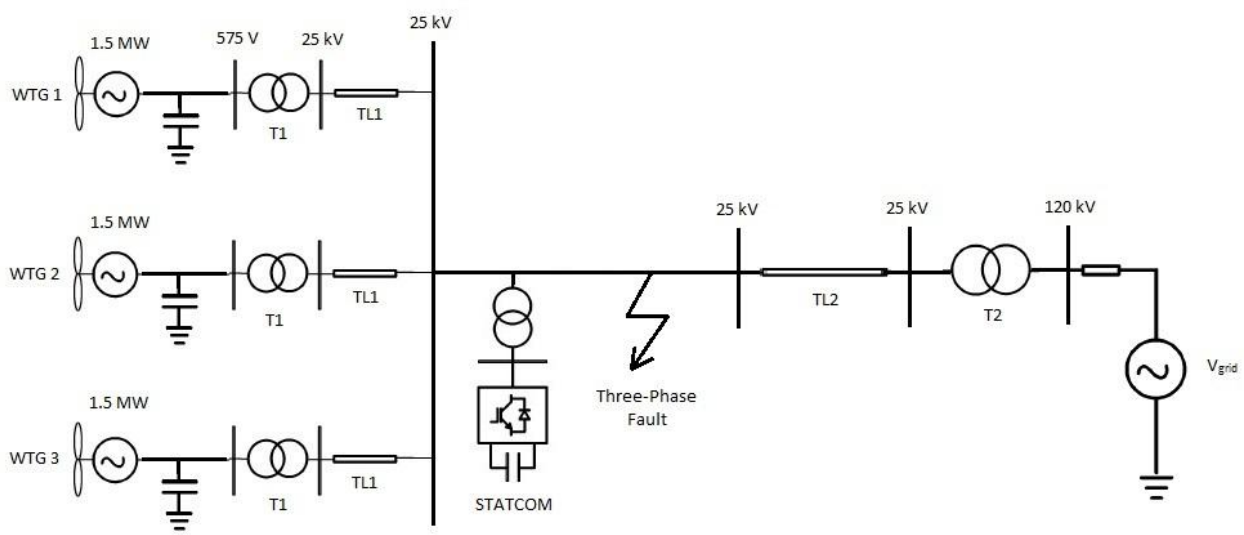

Figure 41: Case system study

In order to generate power, the induction generators' speed must be slightly above the synchronous speed. Speed varies at approximately between 1 pu at no load and 1.005 pu at full load. Also, to bolster the reactive power compensation provided by the capacitor banks, a 3-MVA STATCOM is connected at the PCC. Different durations of three-phase faults at the PCC and wind speed variations are examined and the impact of STATCOM is illustrated.

6.2. Wind Turbine

The wind turbine modeled had the following characteristics:

Table 1: Simulated Wind Turbine Parameters

Wind Turbine Characteristic	Value
Rated Power	1.5 MW
Blade Radius	47 m
Turbine Swept Area	6940 m^2
Cut-in Wind Speed	4 m/s
Rated Wind Speed	9 m/s
Cut-out Wind Speed	Depends on the pitch controller configuration
Nominal Value of Tip Speed Ratio	8.1

Nominal Value of Coefficient of Performance	0.48
Gearbox Ratio	1:100

6.2.1. Test Model

6.2.1.1. Aerodynamic Part

The wind turbine model structure is shown in figure 42. Its inputs are the wind speed in m/s, the generation rotational speed in per unit and the blade pitch angle in degrees. Its output is the mechanical torque applied to the generator in per unit.

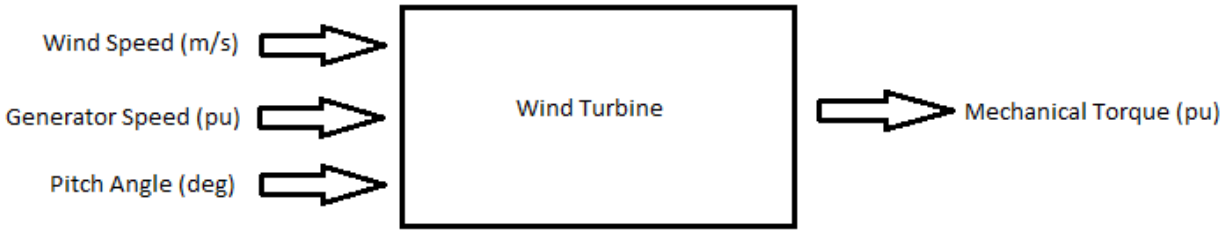

Figure 42: Wind turbine model

The power output was calculated by the equation $P_m = \frac{1}{2}\rho\pi R^2 v_w^3 c_p(\lambda,\beta)$. In the per-unit system, it is written as:

$$P_{m,pu} = c_{p,pu} v_{w,pu}^3 \tag{6.1}$$

where $P_{m,pu}$ is the power in pu of nominal power for particular values of ρ and A, $c_{p,pu}$ is the coefficient of performance in pu of the maximum value of c_p and $v_{w,pu}$ is the wind speed in pu of the base wind speed. The power is then divided by the generator rotational speed in order to extract the mechanical torque, since the turbine is represented with the one-mass lumped mechanical model.

A generic equation was used to model c_p (λ,β), based on the modeling turbine characteristics of [41]. Specifically,

$$c_p(\lambda,\beta) = c_1\left(\frac{c_2}{\lambda_i} - c_3\beta - c_4\right)e^{-\frac{c_5}{\lambda_i}} + c_6\lambda \tag{6.2}$$

with

$$\frac{1}{\lambda_i} = \frac{1}{\lambda + 0.008\beta} - \frac{0.035}{\beta^3 + 1} \tag{6.3}$$

The coefficients c_1 to c_6 are: c_1=0.5176, c_2=116, c_3=0.4, c_4=5, c_5=21 and c_6=0.0068. In the following figure, the c_p-λ characteristics, for different values of the pitch angle β, are illustrated. The maximum value of c_p (c_{pmax}=0.48) is achieved for β=0 degree and for λ=8.1. This particular value of λ is defined as the nominal value (λ_{nom}).

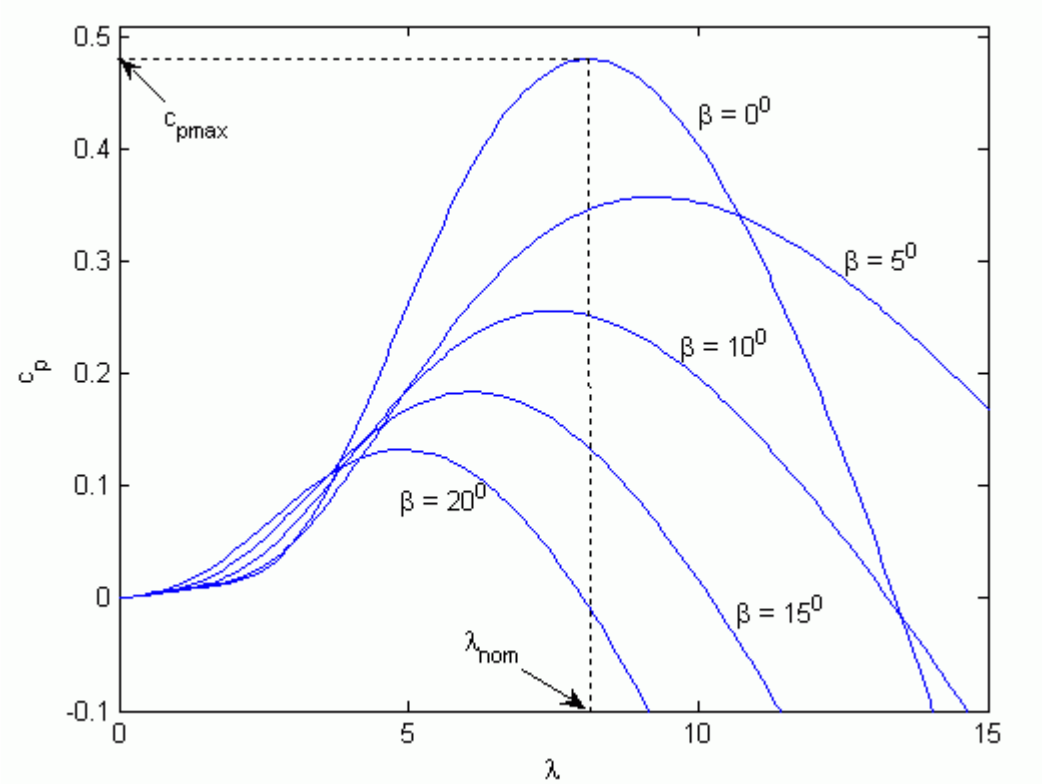

Figure 43: Cp-λ characteristics for different values of the pitch angle β

Finally, the wind turbine power curve for different wind speeds is illustrated in the figure 44 below.

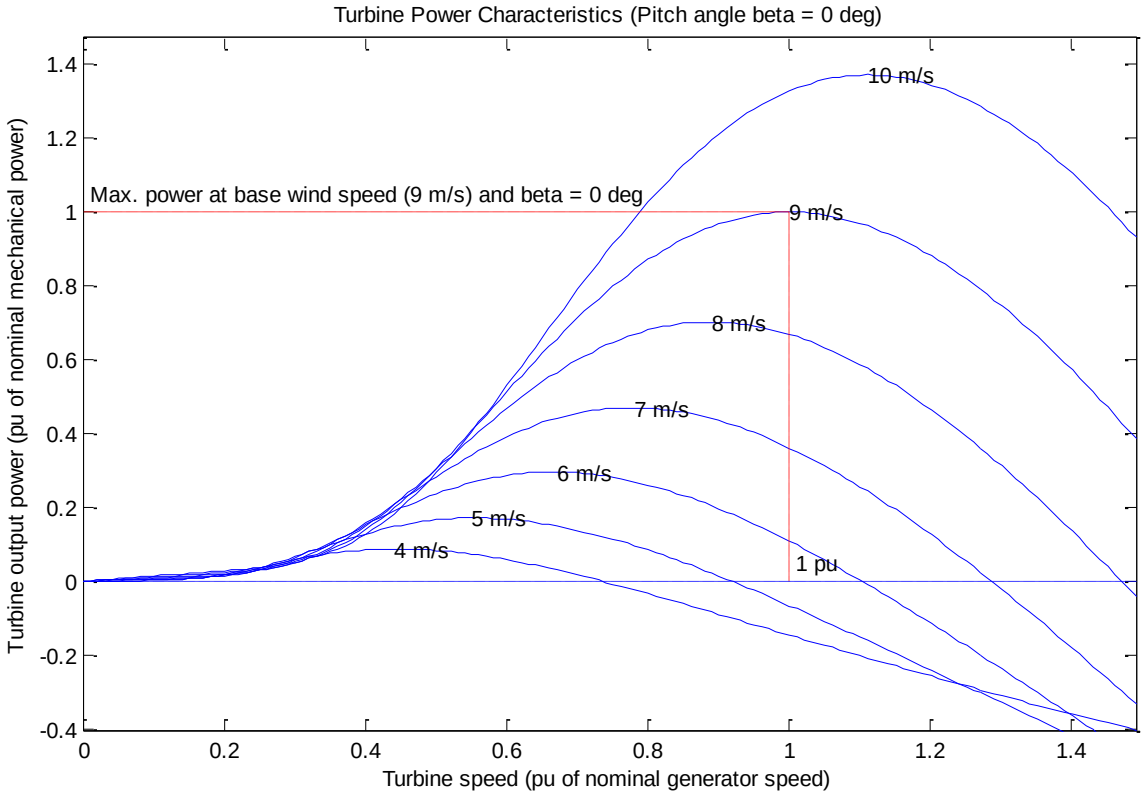

Figure 44: Wind Turbine Power Curve

6.2.1.2. Mechanical Part

In this model, a simplified one-mass mechanical part representation was implemented. Specifically, that means that the stiffness of the drive train is infinite and the friction factor and the inertia of the turbine are included in those of the generator that is coupled with the turbine. The generator input is extracted directly by the power calculated by equation (2.5).

6.2.1.3. Aerodynamic Control

Aerodynamic control is performed by controlling the blade pitch angle of each turbine. The objective is that the electric output maintains its nominal value for wind speeds higher than the nominal. This is accomplished by means of a Proportional-Integral (PI) controller, as depicted in figure 45. The pitch angle is kept constant at zero degree when the measured electric output power is under its nominal value. On the other hand, when it increases above the nominal value, the PI controller increases the pitch angle to bring back the measured power to its nominal value. A maximum angle of 45 degrees has been set, as well as a rate limiter, in order for the simulation to be more realistic. That is

because, in real cases, there is a delay before the control can act and set the pitch angle at its desired value. In the simulations of this thesis, the pitch angle rate limiter has been set to 2 degrees / second. The PI controller gains were chosen so as to limit the speed and torque variations and consequently the mechanical strain. The gain values were K_P=5 and K_I=20.

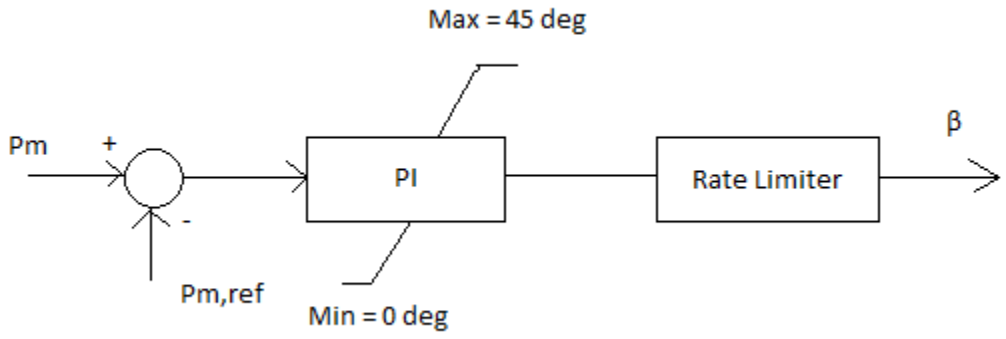

Figure 45: Wind Turbine Pitch Controller

6.2.2. Generic Model Wind Turbine Implementation

6.2.2.1. Aerodynamic Part

The implementation of the generic type 1 wind turbine in Simulink was performed in accordance with [42] and generally follows the procedure described in section 4.3.1. The main difference is spotted in the aerodynamic part, where, instead of the pseudo governor model described in section 4.3.1, a constant aerodynamic torque is assumed. This assumption is acceptable if the study of a dynamic event, such as a three-phase fault, is the objective, as during the short-time period, the aerodynamic torque can be considered constant. The block diagram of the aerodynamic model is shown in figure 46.

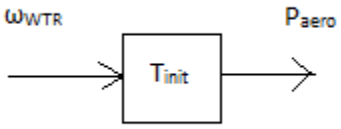

Figure 46: Block diagram for constant aerodynamic torque model

6.2.2.2. Mechanical Part

The mechanical part is modeled by the two-mass mechanical model. In this model, the generator block does not include its inertia equation, in contrast with the test model,

where the generator is coupled with the wind turbine. Therefore, the generator inertia has to be included in the mechanical model. The block diagram of the mechanical model is presented in figure 47. The separate masses represent the low-speed turbine and the high-speed generator. The connecting resilient shaft is modeled as a spring and a damper.

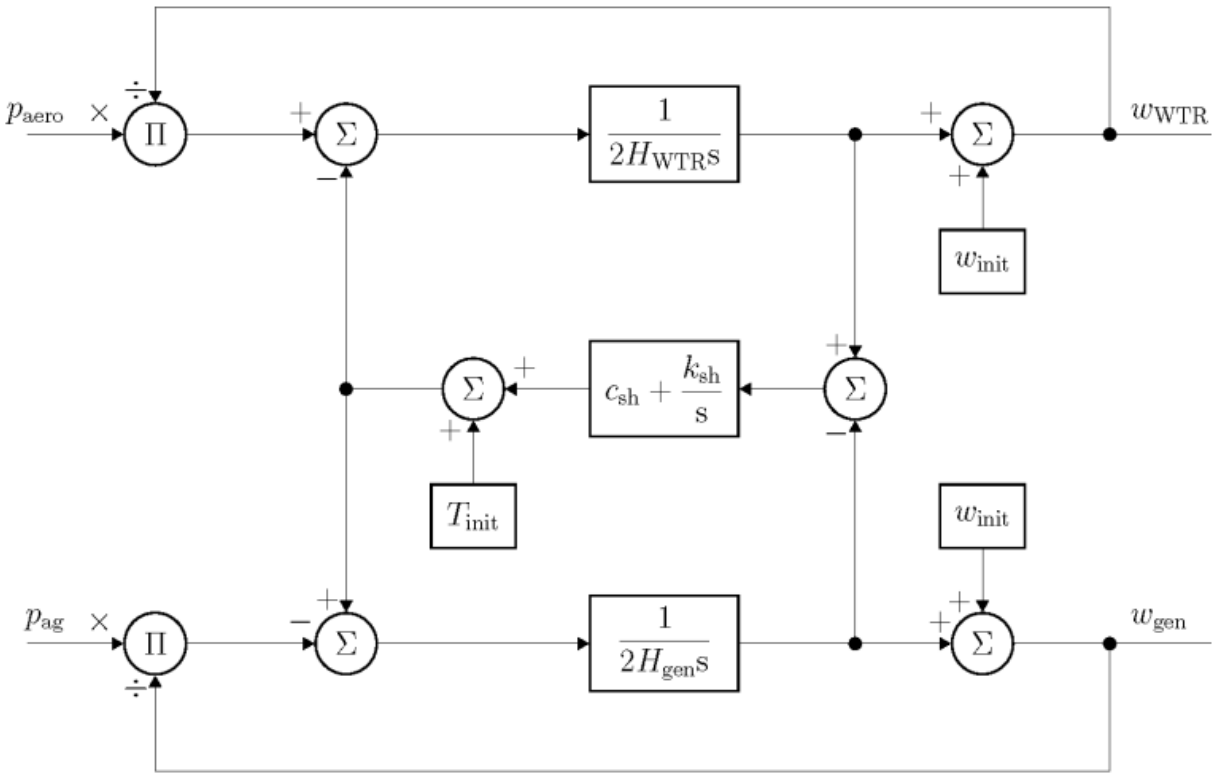

Figure 47: Block diagram for two-mass mechanical model in IEC standard (Simulink) [42]

Having determined the value of the lumped inertia constant H (= H_{WTR} + H_{gen}), the other two-mass mechanical model parameters are calculated as follows:

$$H_{WTR} = H_{WTFfrac} \cdot H \tag{6.4}$$

$$H_{gen} = H - H_{WTR} \tag{6.5}$$

$$k_{sh} = 2 \cdot (2\pi f_1)^2 \cdot H_{WTR} \cdot \frac{H_{gen}}{H} \tag{6.6}$$

where $H_{WTFfrac}$ is the turbine inertia fraction (H_{WTR}/H) and f_1 the first shaft torsional resonant frequency. If we set $H_{WTFfrac} = 0$, the model is switched to the one-mass mechanical model.

Default generic model values were used for the calculation, i.e.:

Table 2: Default values for the generic mechanical model

Variable	Default Value
Lumped Inertia Constant H	5.3 sec
Turbine inertia fraction $H_{WTFfrac}$ (H_{WTR}/H)	0.92
First Shaft Torsional Frequency f_1	5 Hz
Shaft Damping Factor (pu P/pu speed)	1

The parameters used in the simulation are shown in table 3.

Table 3: Two-mass mechanical model parameters

Symbol	Description	Value
H_{WTR}	Inertia Constant of Wind Turbine Rotor	4.876 sec
H_{gen}	Inertia Constant of Generator	0.424 sec
k_{sh}	Shaft Stiffness	446.74 pu
c_{sh}	Shaft Damping	1 pu
w_{init}	Initial Steady State Shaft Rotor Speed	1.005
T_{init}	Initial Steady State Shaft Torque	-1

The initialization parameters are extracted assuming nominal operating initial conditions.

6.3. Asynchronous Machine

6.3.1. Electrical Part

In all simulations in this thesis, the asynchronous machine block of the powerlib library of Simulink was used. The squirrel-cage induction generator was selected. The electrical part of the machine is represented by a fourth-order state-space model and the mechanical by a second-order system. All electrical variables and parameters are referred to the stator, as indicated by the prime signs, while all stator and rotor quantities are in the arbitrary two-axis reference frame (dq frame, see appendix A.2). The subscripts used are defined as follows:

Table 4: Asynchronous machine variables' subscripts definition

Subscript	Definition
d	d axis quantity
q	q axis quantity
r	Rotor quantity
s	Stator quantity
l	Leakage inductance
m	Magnetizing inductance

The fourth-order dynamic equations are commonly used for the induction generator representation for wind power applications, as they are tested and well-established. A second-order model can also be obtained by neglecting the stator flux transients and constitutes a relevantly good compromise. The differences between these two models and their impact on the system stability are examined in [43].

The equivalent electrical circuit of the machine is shown in figure 48.

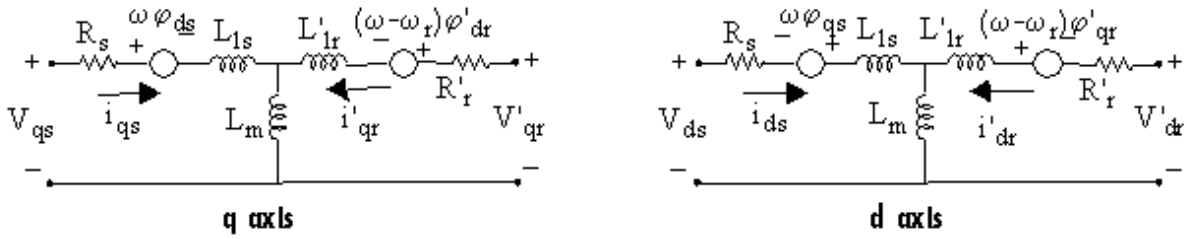

Figure 48: Asynchronous machine equivalent circuit

It is described by the following equations:

$$
\begin{aligned}
V_{qs} &= R_s i_{qs} + \frac{d\varphi_{qs}}{dt} + \omega\varphi_{ds} \\
V_{ds} &= R_s i_{ds} + \frac{d\varphi_{ds}}{dt} - \omega\varphi_{qs} \\
V'_{qr} &= R'_r i'_{qr} + \frac{d\varphi'_{qr}}{dt} + (\omega - \omega_r)\varphi'_{dr} \\
V'_{dr} &= R'_r i'_{dr} + \frac{d\varphi'_{dr}}{dt} - (\omega - \omega_r)\varphi'_{qr} \\
T_e &= 1.5p\left(\varphi_{ds} i_{qs} - \varphi_{qs} i_{ds}\right)
\end{aligned}
\tag{6.7}
$$

where

$$\varphi_{qs} = L_s i_{qs} + L_m i'_{qr} \tag{6.8}$$

$$\varphi_{ds} = L_s i_{ds} + L_m i'_{dr}$$
$$\varphi'_{qr} = L'_r i'_{qr} + L_m i_{qs}$$
$$\varphi'_{dr} = L'_r i'_{dr} + L_m i_{ds}$$
$$L_s = L_{ls} + L_m$$
$$L'_r = L'_{lr} + L_m$$
$$\omega: Reference\ frame\ angular\ velocity$$

The previous equations have been derived by applying the Park's transformation in the machine's voltage equations. The whole procedure to extract these equations is documented in Appendix B. The parameters in the equations (6.7) and (6.8) are explained in table 5.

Table 5: Definition of asynchronous machine parameters

Parameter	Definition
R_s, L_{ls}	Stator resistance and leakage inductance
L_m	Magnetizing inductance
L_s	Total stator inductance
V_{qs}, i_{qs}	q axis stator voltage and current
V_{ds}, i_{ds}	d axis stator voltage and current
ϕ_{qs}, ϕ_{ds}	Stator q and d axis fluxes
R'_r, L'_{lr}	Rotor resistance and leakage inductance
L'_r	Total rotor inductance
V'_{qr}, I'_{qr}	q axis rotor voltage and current
V'_{dr}, I'_{dr}	d axis rotor voltage and current
ϕ'_{qr}, ϕ'_{dr}	Rotor q and d axis fluxes
p	Number of pole pairs
ω_r	Electrical angular velocity (ω_m x p)
T_e	Electromagnetic torque

6.3.2. Mechanical Part

The asynchronous machine block has as input a specified torque. The machine speed is determined by the machine inertia J (or inertia constant H for the pu machine) and by the difference between the applied mechanical torque T_m and the internal electromagnetic torque T_e. The sign convention for the mechanical torque is the following: when the speed is positive, a positive torque signal indicates motor mode and a negative signal indicates generator mode. The mechanical part is described by the following equations:

$$\frac{d\omega_m}{dt} = \frac{1}{2H}(T_e - F\omega_m - T_m) \quad (6.9)$$

$$\frac{d\theta_m}{dt} = \omega_m \tag{6.10}$$

where

ω_m: angular velocity of the rotor

H: combined rotor, load and wind turbine inertia constant

F: Combined rotor, load and wind turbine friction coefficient

θm: rotor angular position

In the generic model, however, a different mechanical representation is used as already explained in section 6.2.2. The asynchronous machine block has its rotational speed as input. In this case, the machine speed is imposed and the mechanical part of the model (inertia J) is ignored. That is because the interaction between the generator and the wind turbine is modeled by the two-mass mechanical model, so the machine inertia is taken into account at that subsystem.

The parameters values for the induction generator model used in this thesis are presented in table 6.

Table 6: Induction generator model parameters

Parameter	Value
P_N	1.5 MW
V_N	575 V
Number of Poles	3
f_N	60 Hz
R_s	0.004843 pu
L_{ls}	0.1248 pu
R'_r	0.004377 pu
L'_{lr}	0.1791 pu
L_m	6.77 pu
Lumped Inertia Constant (WT included)	5.3 sec
F	0.01

6.4. STATCOM

6.4.1. Overall Structure

The STATCOM modeled in this thesis represents an IGBT-based STATCOM (fixed DC voltage), but without the details of the inverter and the harmonics included. The Pulse-Width-Modulation (PWM) technique is used to synthesize a sinusoidal waveform from

the DC voltage source (capacitor). This sinusoidal voltage is varied by changing the modulation index (m) of the PWM modulator. The general structure of the model is presented below:

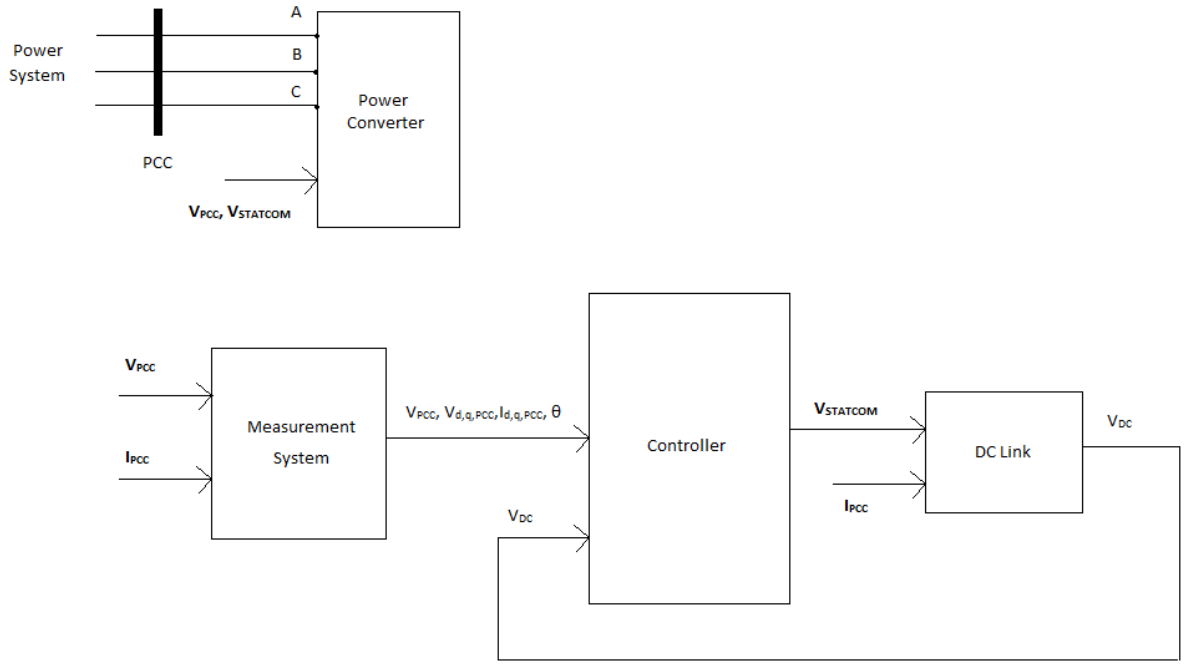

Figure 49: STATCOM model

As it can be observed, it comprises the following subsystems:

6.4.2. Measurement System

The STATCOM uses the type of control described in section 5.3.3. Specifically, it performs decoupled control of active and reactive power by using the dq0 transformation. The measurement unit calculates the dq components of the voltage and current at the point of common connection (PCC). It does so by setting the positive-sequence component of the voltage as the reference d-axis. It is reminded here that the transformation matrix used for the symmetrical components transformation is:

$$[S]^{-1} = \begin{bmatrix} 1 & 1 & 1 \\ 1 & a^2 & a \\ 1 & a & a^2 \end{bmatrix} \tag{6.11}$$

where $a = e^{j\frac{2\pi}{3}}$. The inverse transform uses the matrix

$$[S] = \frac{1}{3}\begin{bmatrix} 1 & 1 & 1 \\ 1 & a & a^2 \\ 1 & a^2 & a \end{bmatrix} \tag{6.12}$$

The measurement system also includes a phase-locked loop (PLL) which synchronizes on the positive-sequence component of the three-phase PCC voltage. The output of the PLL (angle θ=ωt) is used to provide the angle reference required by the abc-dq0 transformation.

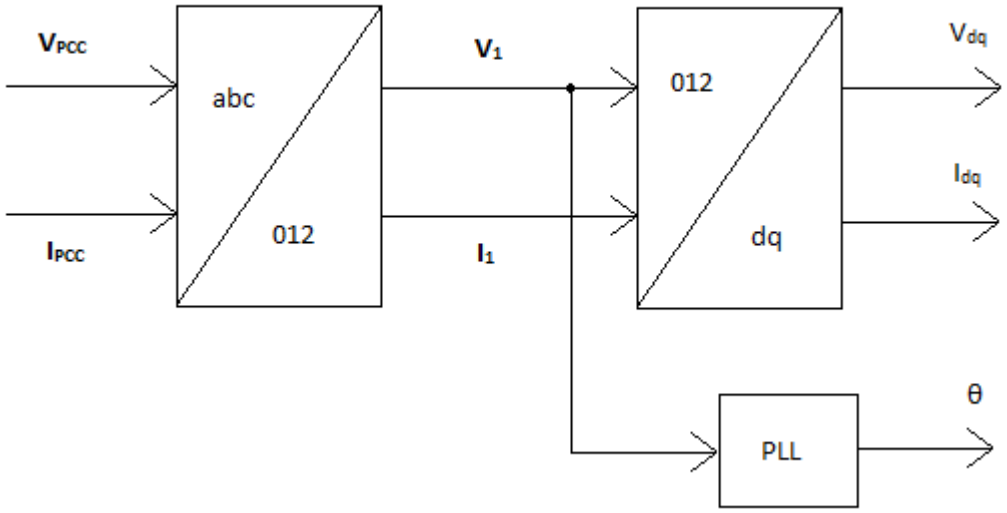

Figure 50: STATCOM measurement system

6.4.3. Power Converter Model

The power converter was modeled through an average model. This choice was deemed more appropriate than a more detailed model, as for dynamic analyses and control design purposes, knowledge about the high frequency details of variables is often not necessary, since the compensators and filters in a closed-loop control system typically exhibit low-pass characteristics and do not react to high-frequency components. Furthermore, an averaged model also enables us to describe the converter dynamics as a function of the modulating signal.

An equivalent per-phase circuit for a STATCOM is shown in figure 51. We assume that the STATCOM output voltage is coupled with the power system through an RL branch.

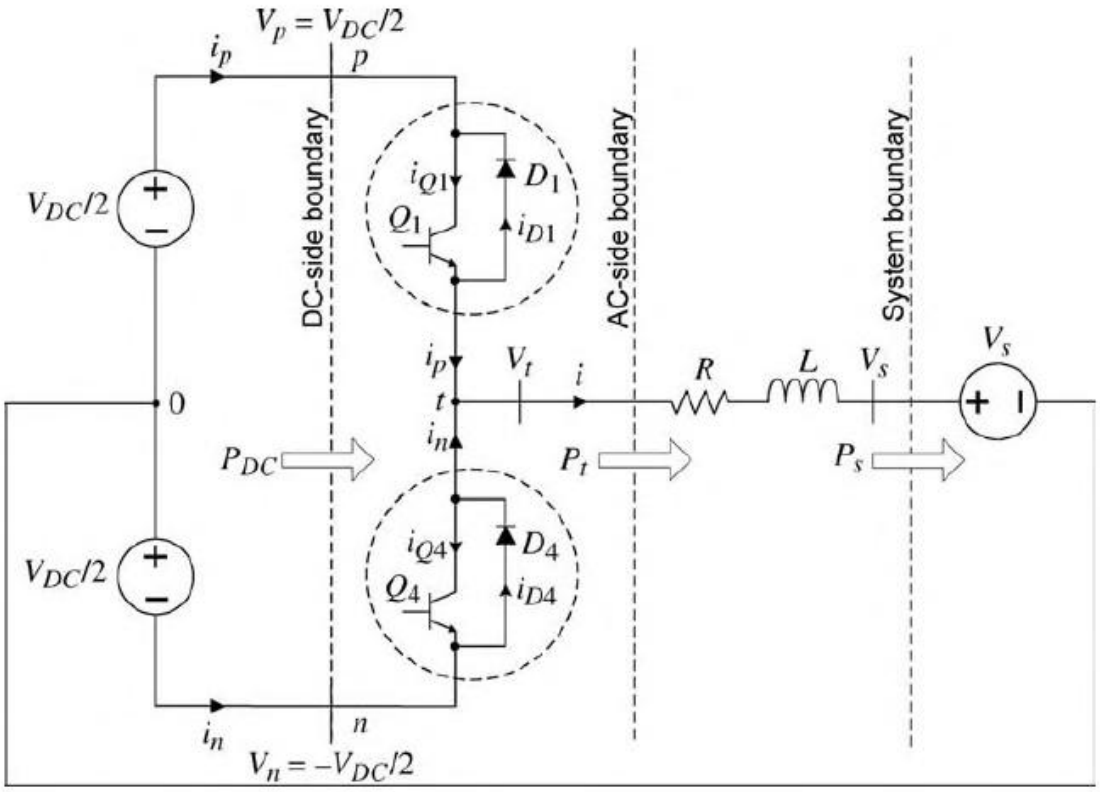

Figure 51: STATCOM per-phase equivalent

As it has already been stated, the STATCOM control is employed through the dq0 transformation. For this reason, the STATCOM RL branch equations have been expressed in the arbitrary reference frame (see Appendix A.4 for details). More specifically, for the AC STATCOM current, we have:

$$\begin{bmatrix} V_{ta} \\ V_{tb} \\ V_{tc} \end{bmatrix} = R \begin{bmatrix} i_a \\ i_b \\ i_c \end{bmatrix} + L \frac{d}{dt} \begin{bmatrix} i_a \\ i_b \\ i_c \end{bmatrix} + \begin{bmatrix} V_{sa} \\ V_{sb} \\ V_{sc} \end{bmatrix} \Rightarrow$$

$$\begin{bmatrix} v_{td} \\ v_{tq} \end{bmatrix} = R \begin{bmatrix} i_d \\ i_q \end{bmatrix} + L \frac{d}{dt} \begin{bmatrix} i_d \\ i_q \end{bmatrix} + \omega_s L \begin{bmatrix} 0 & -1 \\ 1 & 0 \end{bmatrix} \begin{bmatrix} i_d \\ i_q \end{bmatrix} + \begin{bmatrix} v_{sd} \\ v_{sq} \end{bmatrix} \quad (6.13)$$

$$where\ \omega_s = 2\pi f_{nom}$$

Using the Laplace transform and per-unit quantities, we get:

$$i_d = \frac{\omega_s}{Ls}\left(v_{sd} - v_{td} - R i_d + L i_q\right) \quad (6.14)$$

$$i_q = \frac{\omega_s}{Ls}\left(v_{sq} - v_{tq} - Ri_q - Li_d\right) \tag{6.15}$$

These currents are injected into the power system through a controlled current source. The overall power converter system structure is depicted below:

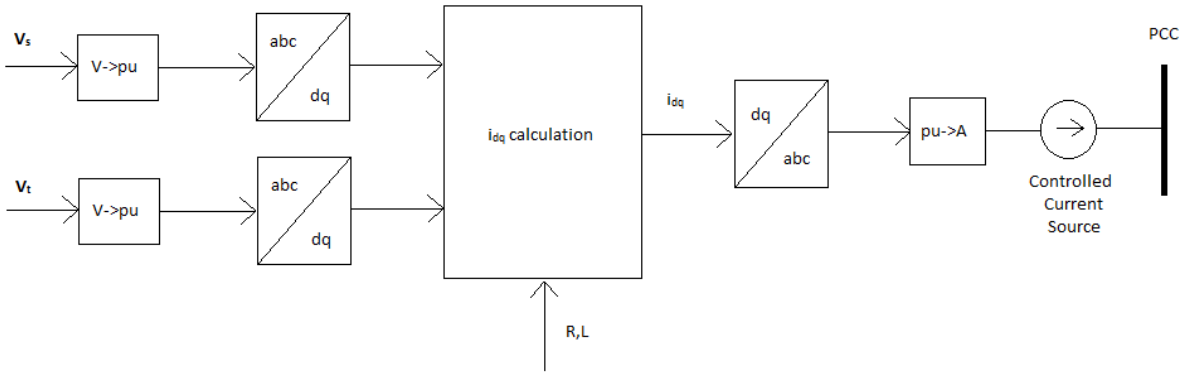

Figure 52: Power converter model

6.4.4. Control System

As mentioned before, for all of the cases examined in this thesis, we consider linear converter operation. Hence, $0 \leq m \leq 1$, and the STATCOM generated voltage in the averaged model is described by:

$$V_t = \frac{\sqrt{3}}{\sqrt{2}} m \frac{V_{DC}}{2} \tag{6.16}$$

In the dq frame, we have:

$$\begin{aligned} v_{td} &= \frac{V_{DC}}{2} m_d \\ v_{tq} &= \frac{V_{DC}}{2} m_q \end{aligned} \tag{6.17}$$

where $m = \sqrt{m_d^2 + m_q^2}$

Hence, the variables m_d and m_q are described by the following equations:

$$m_d = 2\frac{v_{td}}{V_{DC}}$$
$$m_q = 2\frac{v_{tq}}{V_{DC}} \quad (6.18)$$

Using equations (6.17), equation (6.13) can be rewritten as:

$$L\frac{di_d}{dt} = -Ri_d + \omega_s L i_q - v_{sd} + m_d\frac{V_{DC}}{2}$$
$$L\frac{di_q}{dt} = -Ri_q - \omega_s L i_d - v_{sq} + m_q\frac{V_{DC}}{2} \quad (6.19)$$

If we further define:

$$v_d = \omega_s L i_q - v_{sd} + m_d\frac{V_{DC}}{2}$$
$$v_q = -\omega_s L i_d - v_{sq} + m_q\frac{V_{DC}}{2} \quad (6.20)$$

equations (6.19) are written:

$$L\frac{di_d}{dt} = -Ri_d + v_d$$
$$L\frac{di_q}{dt} = -Ri_q + v_q \quad (6.21)$$

Equations (6.21) represent a linear first-order differential equation system. Therefore, i_d and i_q can be controlled by controlling the variables v_d and v_q.

The control is assisted by a feed-forward system that provides at the point of the compensation a measurement of $\mathbf{V_s}$. This practice helps in smoothing the control output and in avoiding the start-up transients.

The model for the control system was constructed based on the system of figure 40. It mainly consists of an outer regulation loop with an AC and a DC voltage regulator and an inner regulation loop with a current regulator. It is illustrated in figure 53.

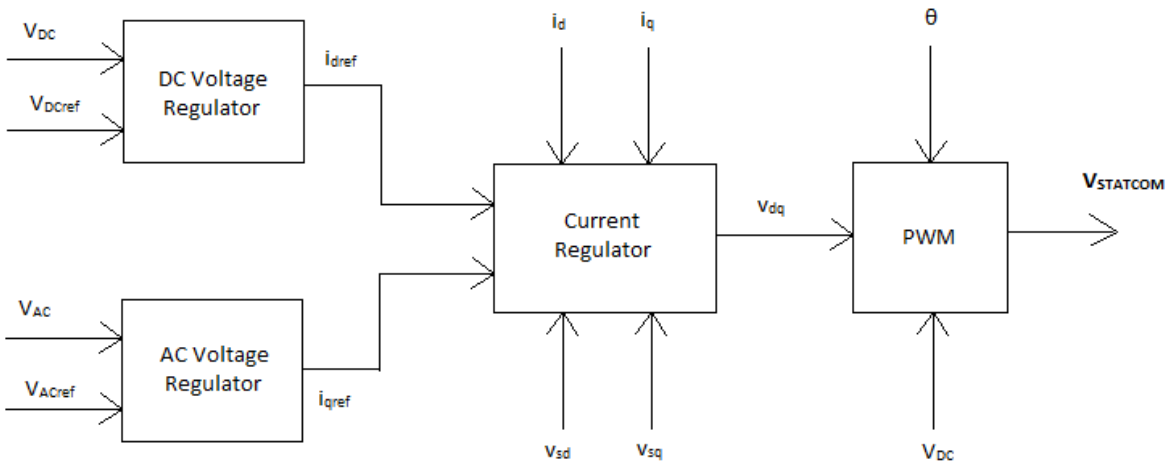

Figure 53: STATCOM controller model

The DC and AC voltage regulators each consists of a PI controller which generates the reference values for i_d and i_q respectively. Their gains were chosen accordingly, so that the responses would be relatively fast and smooth at the same time. A droop value of 0.03 was also used for the AC voltage regulator.

The current regulator in the inner loop is the core of the control system. Two PI controllers are used for the i_d and i_q regulation as indicated in the control system of figure 40. Their gains are chosen based on the analysis in [23]. Namely:

$$k_p = \frac{L}{\tau_i}$$
$$k_i = \frac{R}{\tau_i} \qquad (6.22)$$

τ_i is the desired time constant of the closed-loop control system. It should be chosen to have a small value so that a fast current-control response is accomplished, but at the same time it should be adequately large such as $1/\tau_i$, that is, the bandwidth of the closed-loop control system be considerably smaller than the switching frequency of the converter. Depending on the requirements of a specific application and the converter switching frequency, τ_i, is typically selected in the range of 0.5-5 ms. In our model, it was chosen τ_i=0.5 ms.

The current regulator, as constructed in the Simulink environment, is depicted in figure 54. The dq components of the PCC voltage provide feed-forward compensation, so that the output value can be “predicted”.

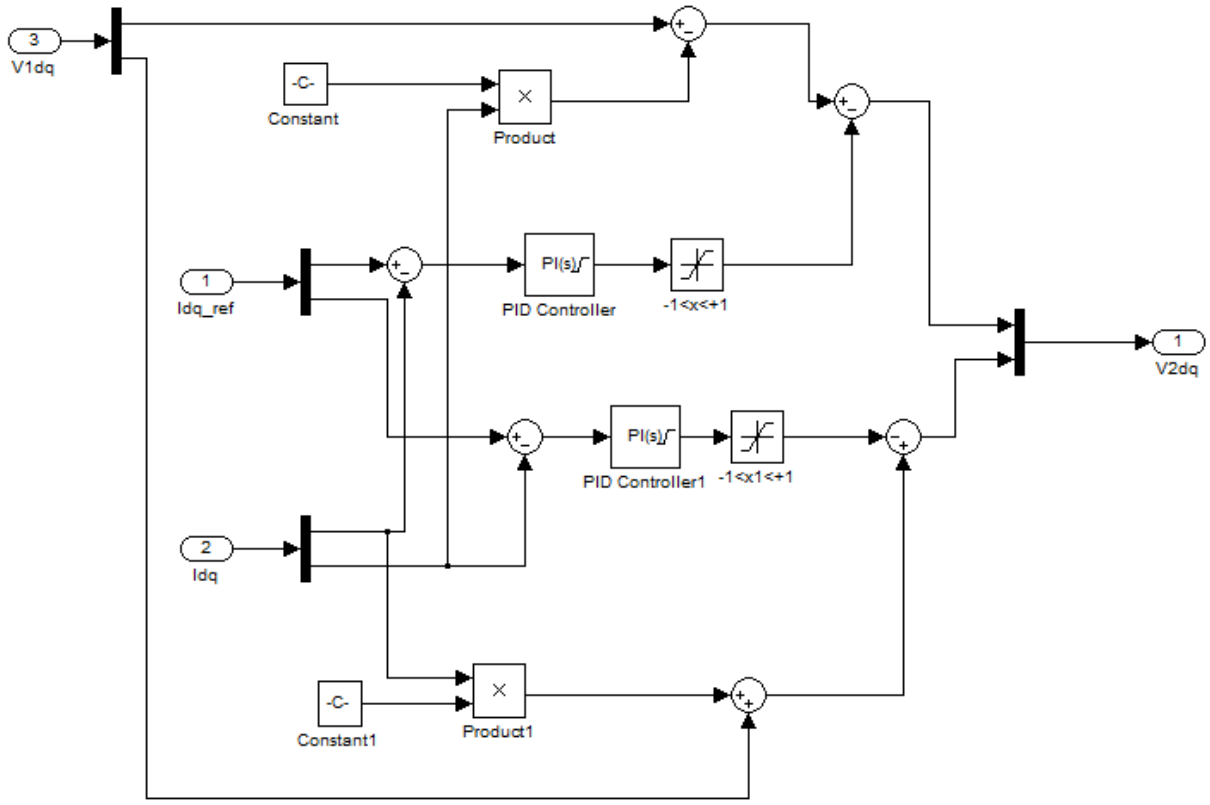

Figure 54: STATCOM current regulator

Having determined the values of the control variables v_d and v_q and, consequently the values of m_d and m_q, the STATCOM output voltage can be determined. Its rms value is calculated as:

$$V_{t,rms} = \frac{\sqrt{3}}{\sqrt{2}} m \frac{V_{DC}}{2} \tag{6.23}$$

where $m = \sqrt{m_d^2 + m_q^2}$

The voltage angle is the sum of the angle of **m** and the output of the PLL (angle θ).

6.4.5. DC Link Model

The average model of the converter is based on the energy conservation principle. This means that it relies on the assumption that the instantaneous power must be the same on the DC side and the AC side of the converter (assuming an ideal converter) [44]:

$$V_{DC} I_{DC} = v_a i_a + v_b i_b + v_c i_c \tag{6.24}$$

The DC current in the DC-link capacitor can be then computed from the measured AC instantaneous power and the DC-link voltage as:

$$I_{DC} = \frac{v_a i_a + v_b i_b + v_c i_c}{V_{DC}} \tag{6.25}$$

The DC-link subsystem is simply the implementation of the latter equation. A capacitor (represented by an integrator) is charged by a DC current source with value computed by equation (6.25). It is depicted in figure 55.

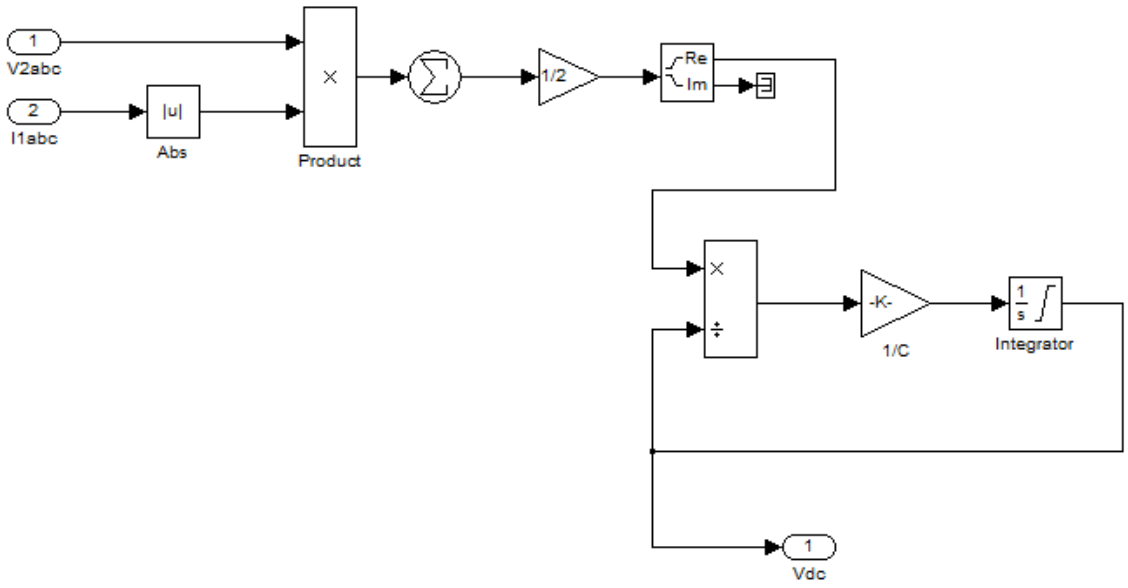

Figure 55: DC-Link model

The parameters used for the STATCOM model are presented in the following table.

Table 7: Simulated STATCOM parameters

Parameter	Value
Converter Rating	3 MVA
Converter Resistance	0.22 pu
Converter Inductance	0.022 pu
DC link Nominal Voltage	4000 V

DC link Capacitance	1125 µF
K_{pAC}	5
K_{iAC}	1000
K_{pDC}	0.0001
K_{iDC}	0.02
K_{pi}	44
K_{ii}	440

6.5. Electric Grid

The grid is modeled as a balanced three-phase voltage source with an internal R-L impedance. The R and L values are specified indirectly by specifying the short-circuit ratio (X/R ratio) and the short-circuit level of the source. In our simulations, it is:

$$V_{N(rms,ph-ph)} = 120\ kV$$

$$S_{SC} = 1000\ MVA$$

$$SCR = 3$$

6.6. Transformers and Transmission Lines

The transmission lines are represented by a lumped PI section. That means, that contrary to the distributed line model, where the resistance, inductance and capacitance are uniformly distributed along the line, here they are lumped in a single PI section. The transmission line parameters, as well as those of the transformers, are presented in tables 8 and 9.

Table 8: Transmission line parameters

Parameter	Value
Frequency	60 Hz
Positive-sequence resistance	0.1153 Ohms/km
Zero-sequence resistance	0.413 Ohms/km
Positive-sequence inductance	0.00105 H/km
Zero-sequence inductance	0.00332 H/km
Positive-sequence capacitance	$11.33 \cdot 10^{-9}$ F/km
Zero-sequence capacitance	$5.01 \cdot 10^{-9}$ F/km

The TL1's length is 1 km, while the TL2's is 25 km.

Table 9: Transformer 1 parameters

Parameter	Value
Winding 1 connection	Wye-grounded
Winding 2 connection	Wye-neutral
S_N	4 MVA
f_N	60 Hz
$V_{1N(rms)}$	25 kV
$V_{2N(rms)}$	575 kV
R_1	0.025/30 pu
L_1	0.025 pu
R_2	0.025/30 pu
L_2	0.025 pu
R_m	500 pu
L_m	infinite

Table 10: Transformer 2 parameters

Parameter	Value
Winding 1 connection	Wye-grounded
Winding 2 connection	Delta
S_N	47 MVA
f_N	60 Hz
$V_{1N(rms)}$	120 kV
$V_{2N(rms)}$	25 kV
R_1	0.08/30 pu
L_1	0.08 pu
R_2	0.08/30 pu
L_2	0.08 pu
R_m	500 pu
L_m	500 pu

Finally, the shunt capacitors connected at each WTG terminals, are delta-connected and inject to the system 400 kVAr each.

7. Simulation Results

7.1. Changes in Wind Speed

The wind farm response to changes in wind speed will be examined in this chapter. As described in section 6.2.1.3, each wind turbine in the test model is equipped with a pitch angle controller with an active power reference signal. When active power generation exceeds nominal, i.e. for wind speeds higher than the nominal one, the pitch controller acts, rotating the blades around their own axes and curtailing active power generation. Since the response cannot be immediate, a rate limiter of 2 degrees per second has been set for a more realistic representation. Also, the maximum blade pitch angle is set to 45 degrees.

In this simulation, changes throughout a wide range of wind speeds are tested. First, we assume nominal wind speed (9 m/s). Then, the wind starts to increase with unit steps until the value of 15 m/s and then it decreases, also with unit steps, until the value of 6 m/s.

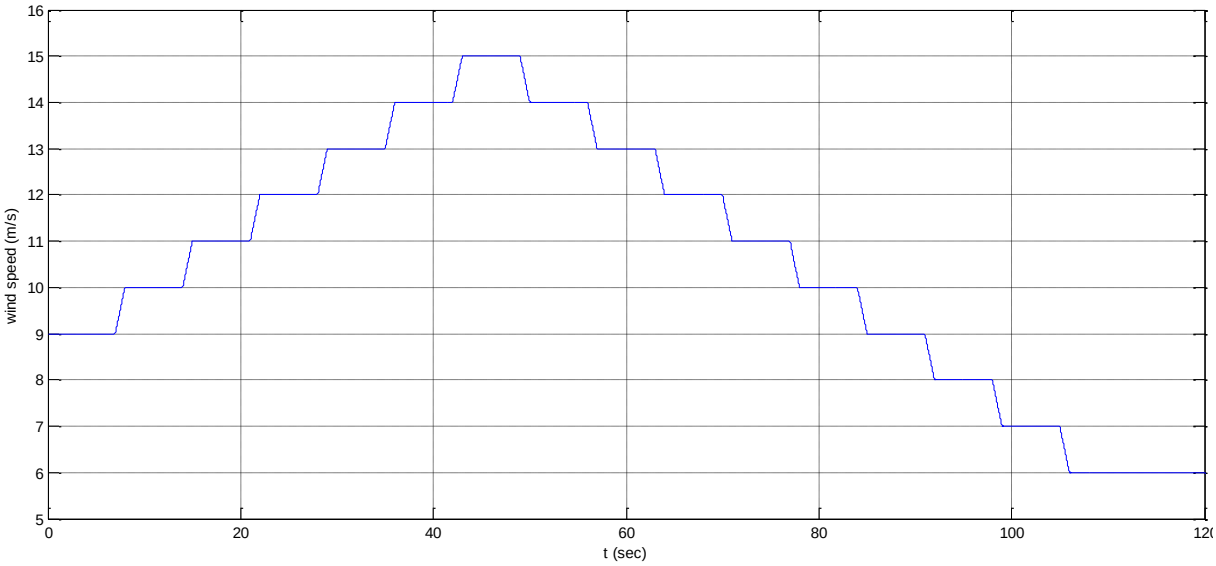

Figure 56: Wind speed input

Each step takes place every 7 seconds and the simulation time is 120 seconds. Similar to the pitch angle response, the wind naturally cannot change speed instantly. For a more faithful representation, a wind speed change limit of 1 m/s per second has been imposed.

The generated active power is shown in figure 57.

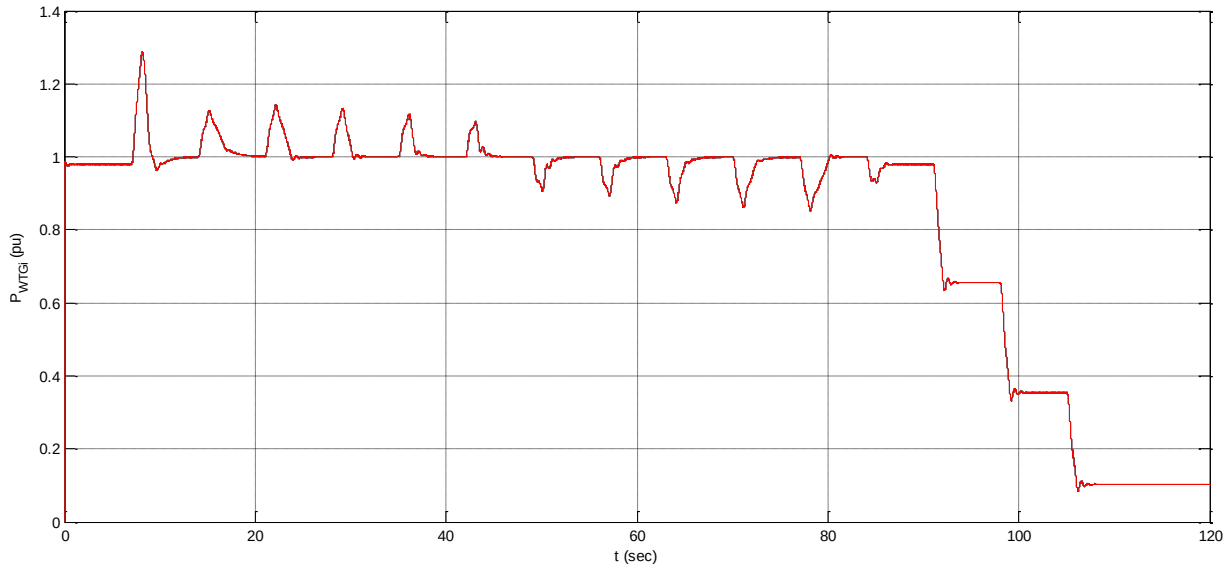

Figure 57: Active power output to wind change

The first wind gust increases the mechanical input and consequently, the generated real power. At that same moment, when the active power starts increasing above nominal (at 7 sec), the pitch control acts. Due to the limit imposed to its rate, it cannot instantly set the pitch angle to the corresponding value and thus, the active power output sees an increase up to approximately 1.3 per unit. The moment when the blade pitch angle has acquired the proper value, active power has reached a peak and starts restoring its value to the reference (1 per unit). The same pattern is followed for each wind gust, but less angle opening is required each time. The latter is in accordance with the wind turbine characteristics, i.e. at higher pitch angles the coefficient of performance decreases and so does the available portion of the aerodynamic power that can be extracted. Since the power is less, a smaller pitch angle is required to restore it to the nominal value.

When the wind starts decreasing, the sequence of events is inversed; the rotor speed and, therefore, the active power output, decreases. The blades, then, ordered by the pitch control, start reducing their angle to compensate for that decrease. Again, the real power faces a decrease before the pitch can be able to gain its corresponding value. For wind speeds below nominal (9 m/s), the pitch angle is zero and retains this value. The active power at those wind speeds varies proportionally with the wind.

The pitch angle variation is presented below.

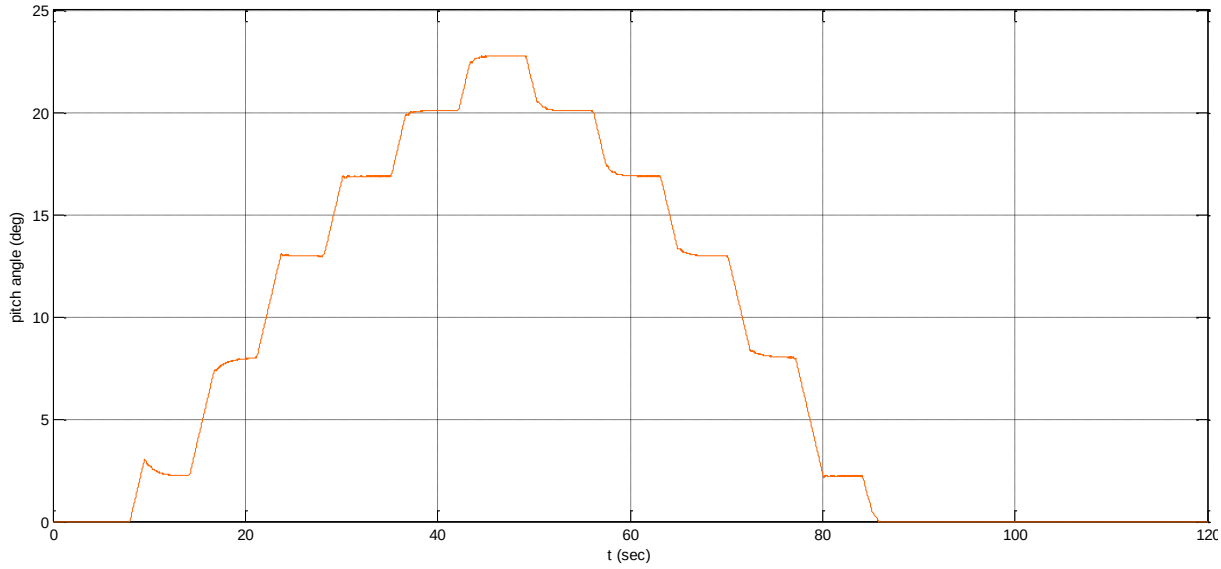

Figure 58: Pitch angle output to wind change

We can confirm from figure 58 that the higher the pitch angle, the smaller the next required pitch angle is.

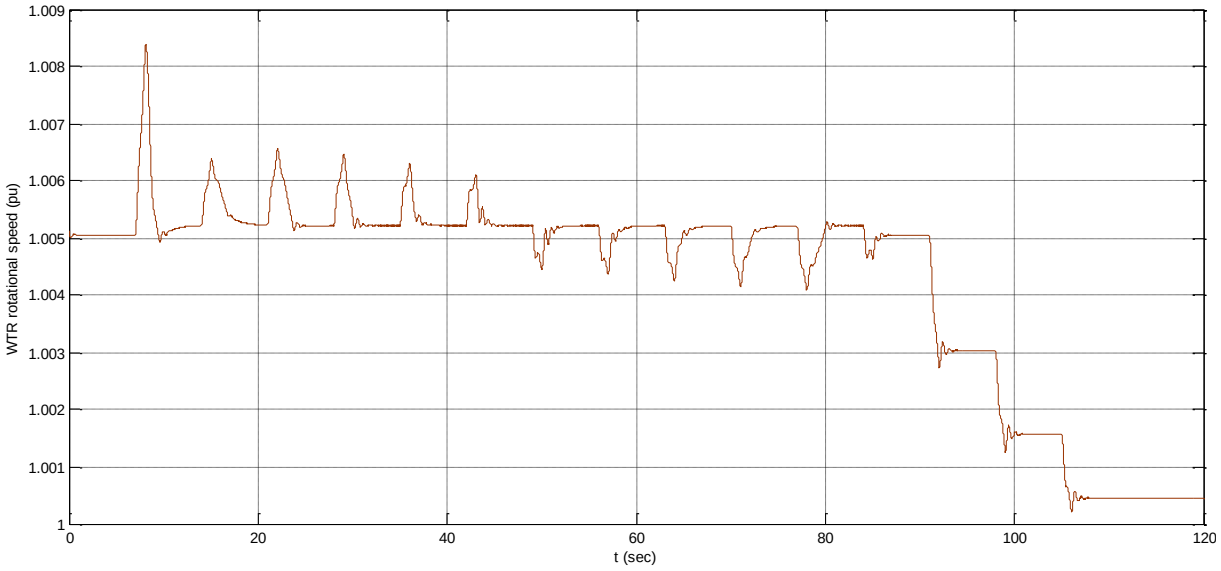

Figure 59: WTR speed output to wind change

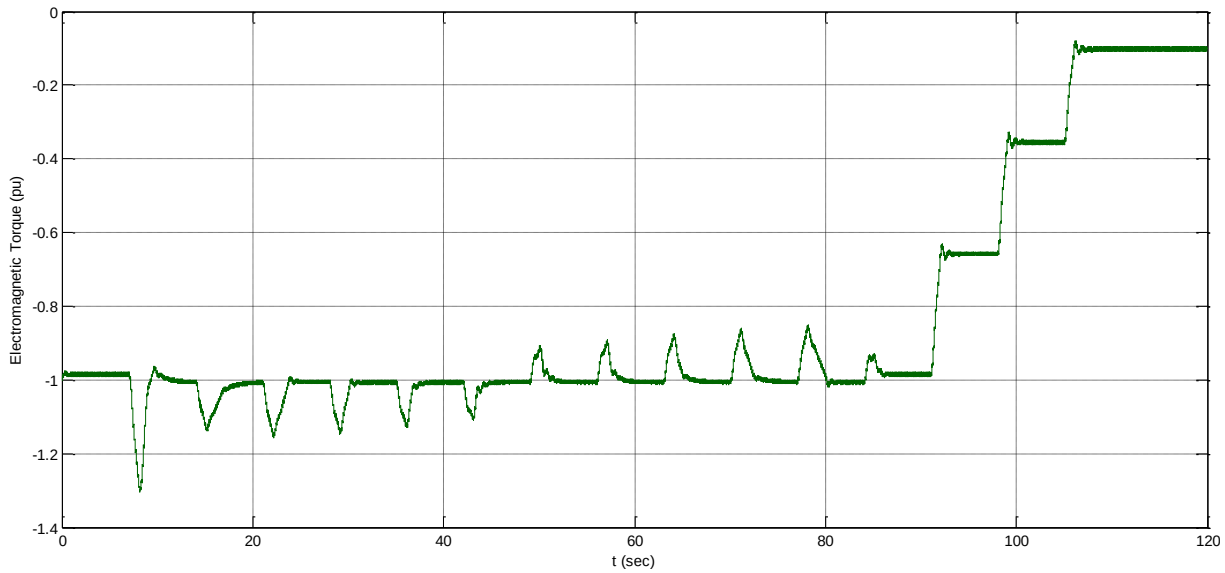

Figure 60: Electromagnetic torque output to wind change

As it can be verified by figures 59 and 60, the wind turbine rotor speed and the electromagnetic torque variations are directly proportional to the wind speed variations. The electromagnetic torque is assumed negative because the induction machine operates as generator. The first wind gust results in the highest variation as with the real power, and the WTG reaches a slip value of -8.3% and a torque value of -1.3 per unit.

It also has to be highlighted that the pitch controller capability to sustain the active power generation to the desired level highly depends on the rate with which the wind speed changes. Wind gusts of up to 2 m/s per second are handled successfully from the pitch controller and if we assume an increase rate of wind speed no more than 2 m/s per second, the wind turbine can remain in operation for a maximum 35 m/s wind speed.

7.2. System Response to PCC Fault

7.2.1. Case Description

In this section, a three-phase to ground fault is assumed to occur at the PCC. The wind farm operates at nominal conditions before the fault (wind speed 9 m/s). For different fault durations, the responses of PCC voltage and wind turbine generator real and reactive power are examined. The responses of the test model and the generic model are compared, with and without the STATCOM.

For the real and reactive power, the following sign convention has been adopted: real power is positive when it is being transferred to the grid. Reactive power, on the other hand, is positive when it is being absorbed by the wind turbines.

7.2.2. PCC Fault Cleared after 100 ms

A three-phase to ground fault is simulated to occur at the PCC at t=3 sec and it is cleared after 0.1 sec (at t=3.1 sec).

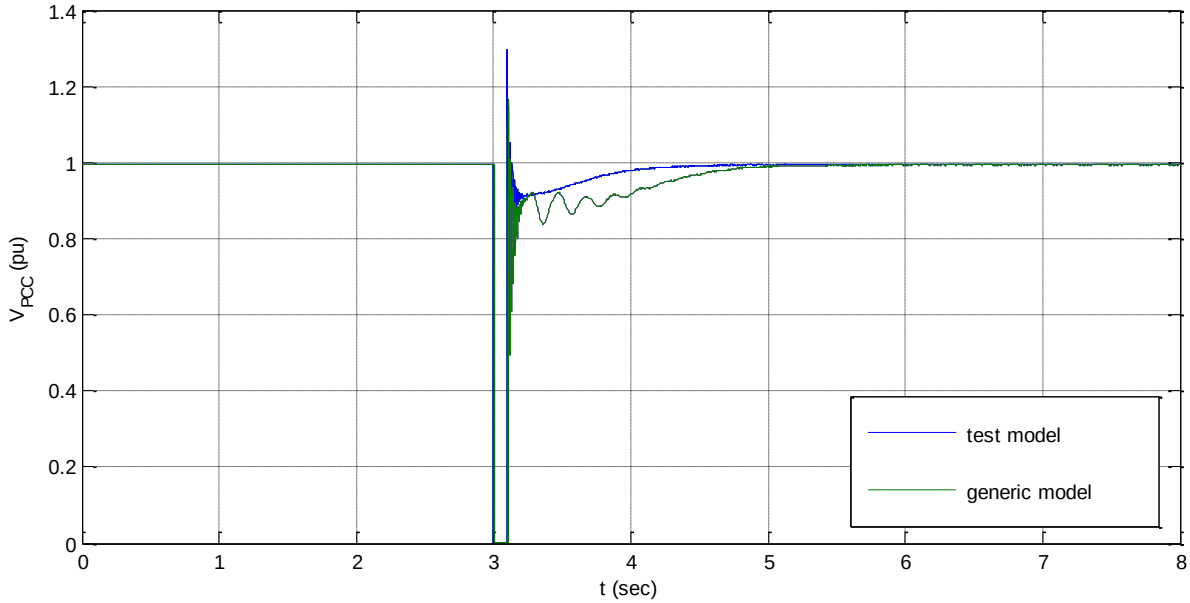

Figure 61: V_{PCC} without STATCOM (100 ms fault duration)

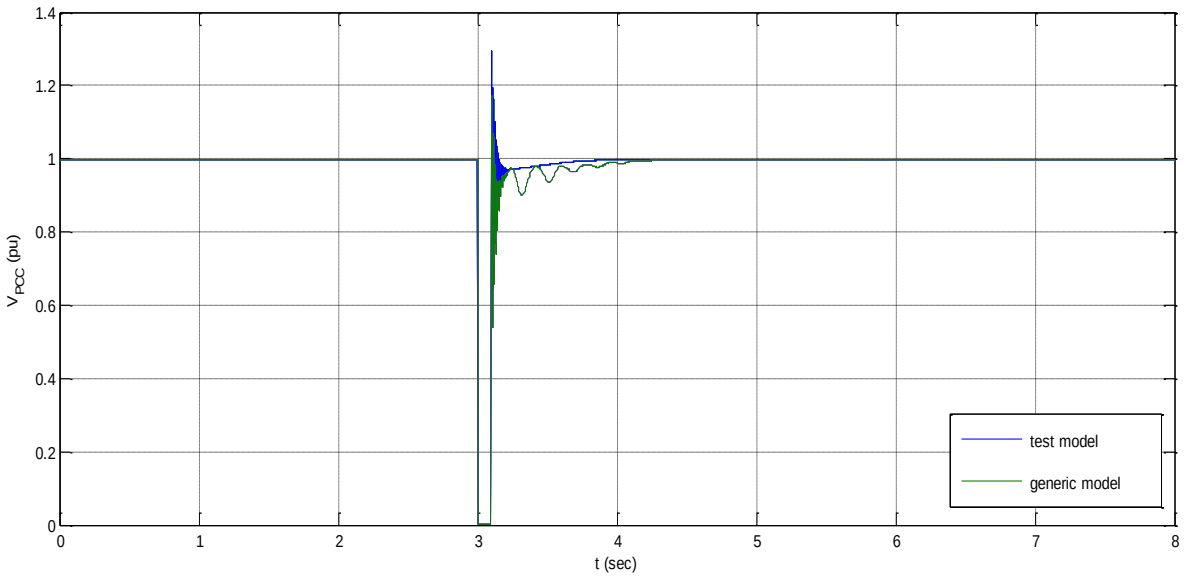

Figure 62: V_{PCC} with STATCOM (100 ms fault duration)

It can easily be observed that the voltage response of the test model and the generic are quite similar. The transient oscillations last for the same time interval, although in the generic model response, some additional oscillations occur until the beginning of the fourth second approximately. These torsional oscillations, however, are expected, as they

are the result of the two-mass mechanical model representation and depict the interaction between the two masses.

It is also testified that, in the case of the test model, the voltage restores its nominal value smoother and quicker than in the generic model case. That indicates that the torsional interaction between the two-masses has a significant impact on the system dynamic behavior.

When the STATCOM is connected, the voltages in both cases return to their nominal values quicker, i.e. the voltage is almost completely restored at the beginning of the fourth second. This illustrates the impact of the reactive support of the STATCOM; the additional reactive power supplied helps the voltage regain quicker its original value. Furthermore, the torsional oscillations have been decayed.

The details of the voltage transient behavior can be observed more thoroughly in the zoomed figures below:

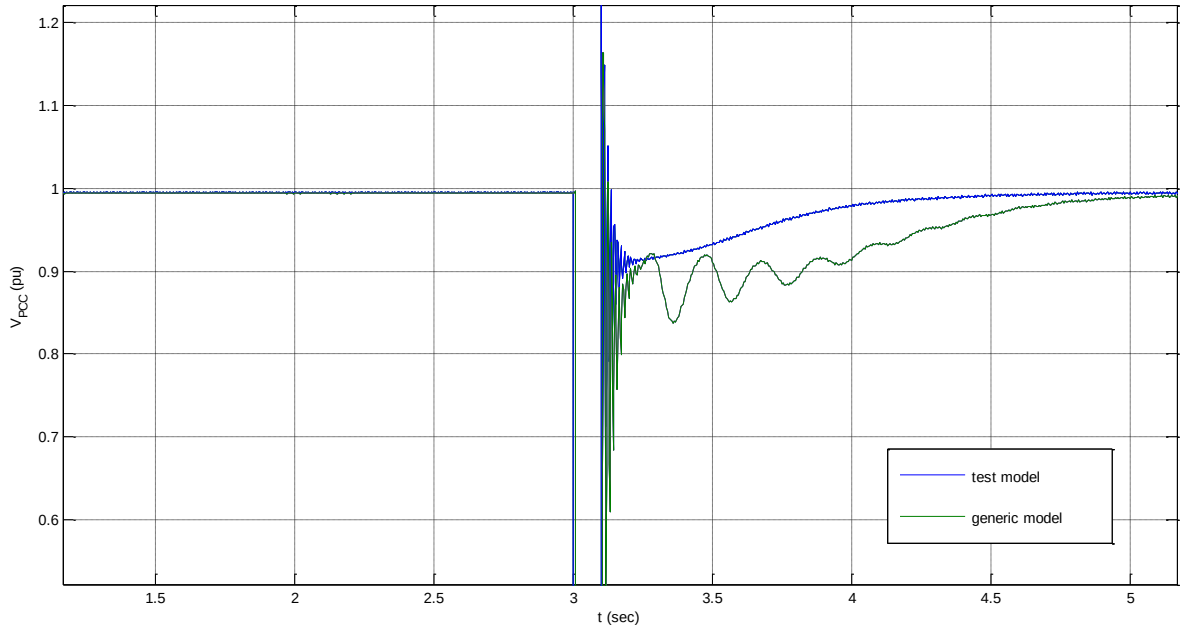

Figure 63: V_{PCC} without STATCOM (100 ms fault duration, zoomed)

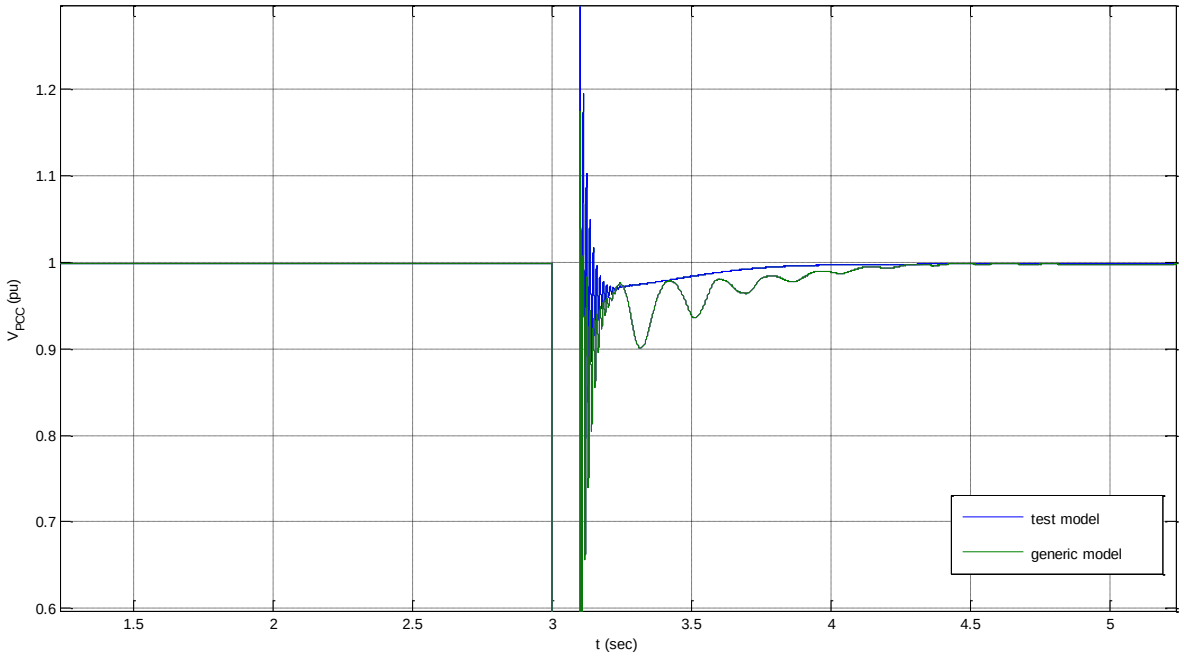

Figure 64: V_{PCC} with STATCOM (100 ms fault duration, zoomed)

We can see that the transient oscillations have the same frequency, as expected. However, in the generic model, the voltage oscillates around a value that is lower that the corresponding of the test model. That is another indicator of the fact that the generic model is more 'sensible' to faults, something that is mainly attributed to the use of the two-mass mechanical model.

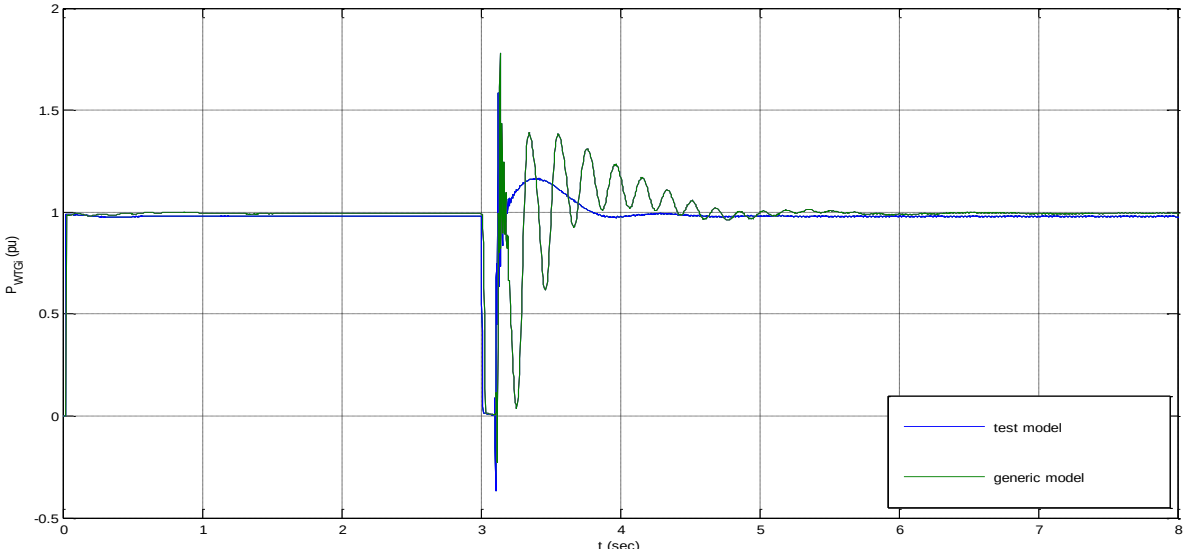

Figure 65: WTG active power without STATCOM (100 ms fault duration)

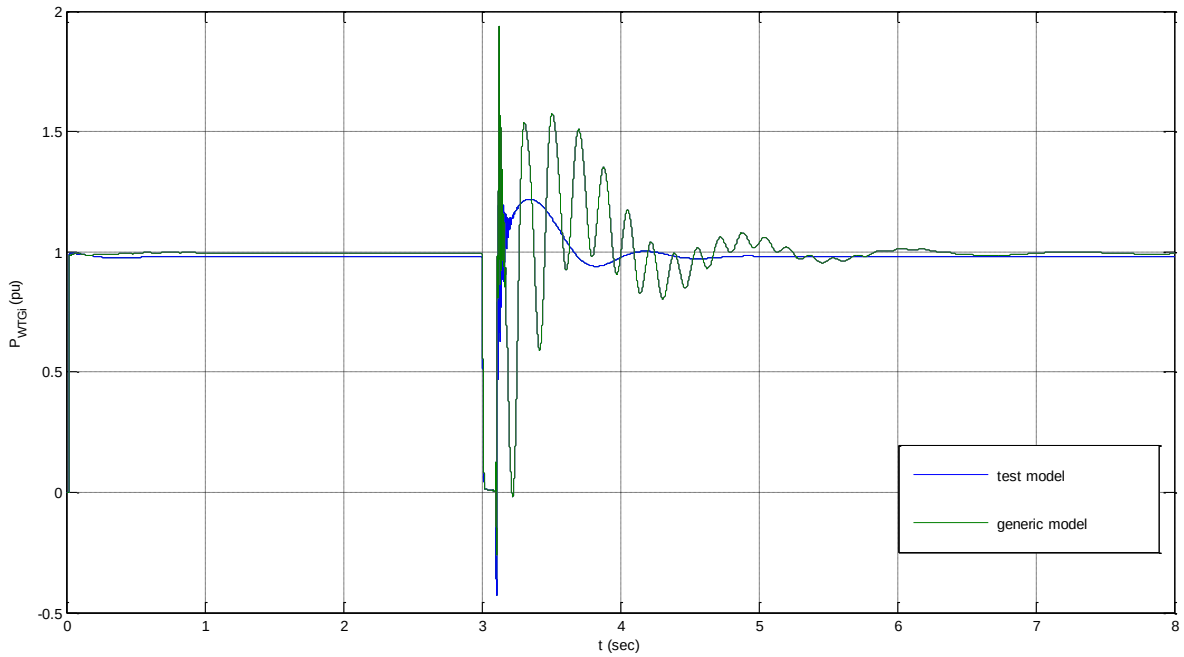

Figure 66: WTG active power with STATCOM (100 ms fault duration)

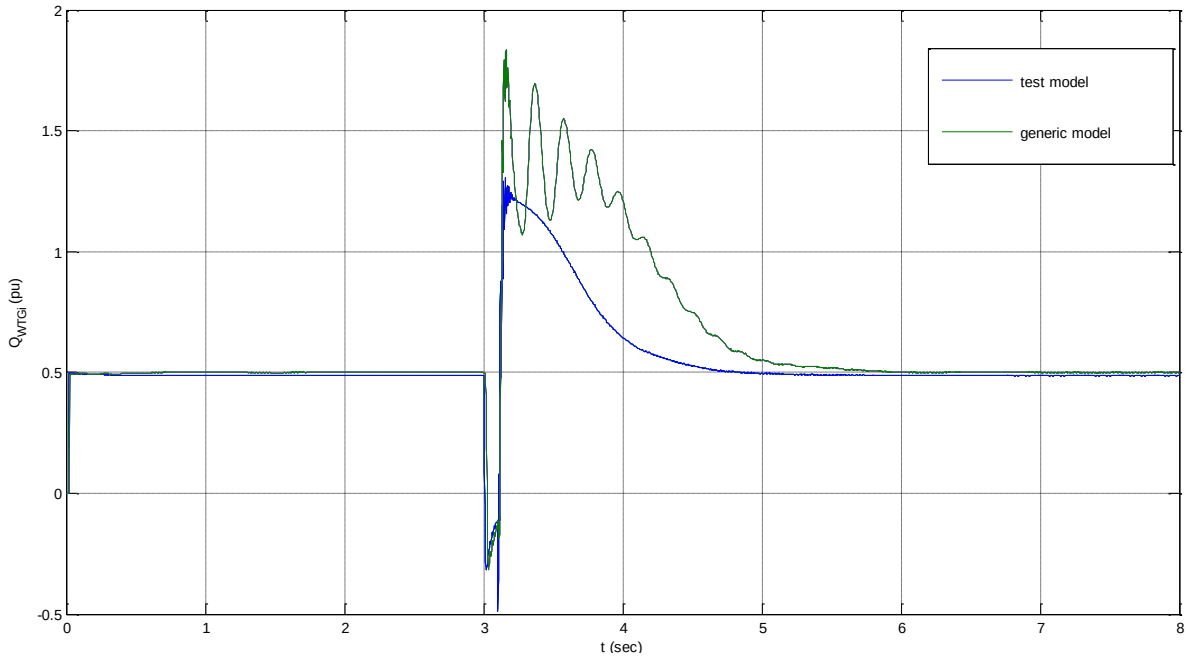

Figure 67: WTG reactive power without STATCOM (100 ms fault duration)

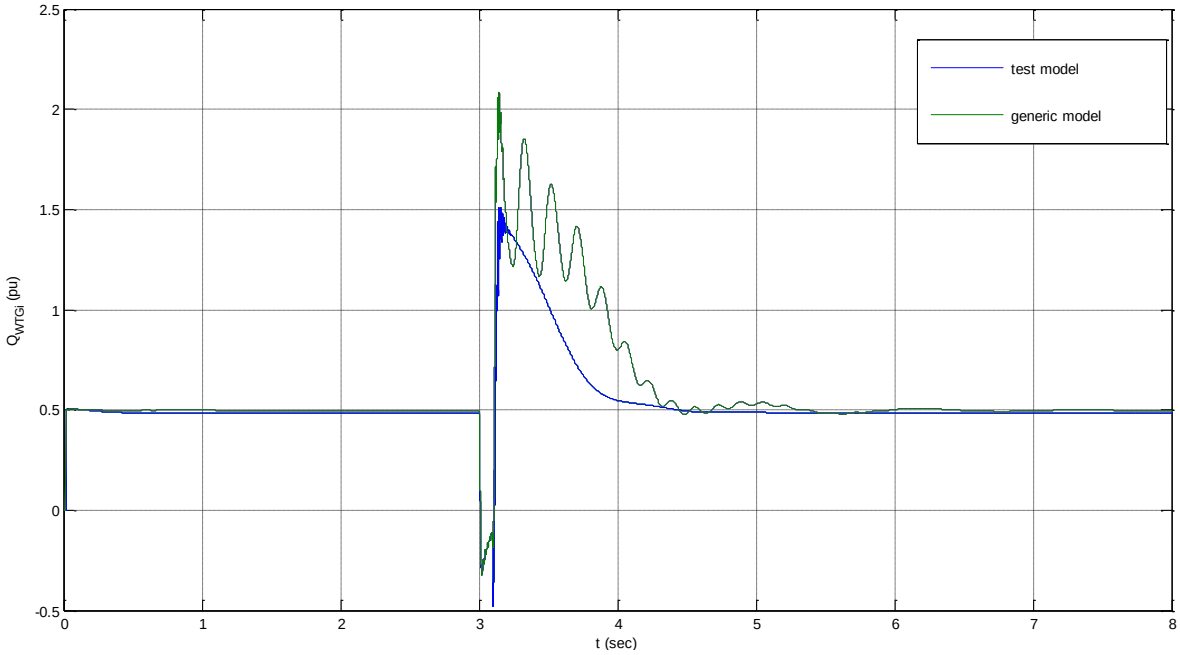

Figure 68: WTG reactive power with STATCOM (100 ms fault duration)

During a fault, the following sequence of events takes place: First, the generator terminal voltage drops. This drop results to a drop in the generated electrical power, since these quantities are proportional. In our case, the voltage and consequently, the active power drop to zero during the fault. The wind, naturally, is unaffected, so mechanical power continues to be supplied. Due to the resulting imbalance between supplied mechanical power and generated electrical power, the generator speeds up corresponding to a more negative slip operation. When the fault is cleared, the squirrel cage induction generator draws a large amount of reactive power from the grid because of its high rotational speed. If the rotor accelerates more quickly than the voltage restores, the reactive power consumption increases even more, leading to a decrease in the terminal voltage and thus to a further disturbance of the balance between mechanical and electrical power and to a further rotor acceleration. In that case, the system becomes unstable and the turbine should be disconnected from the grid to allow restoration of the voltage [45].

In our simulation, we see that the reactive power demand is sufficiently fulfilled, so the system remains stable. The generic model has higher reactive needs, a fact that agrees with the statement that it is more sensible to faults.

In the reactive power output, the impact of the STATCOM is most directly illustrated. The reactive power demand is significantly decreased when the STATCOM is connected for both models. The STATCOM however, triggers some additional oscillations in the active

power output, a fact that is accounted to a transient in the STATCOM active current at the time the fault is cleared.

7.2.3. PCC fault Cleared after 150 ms

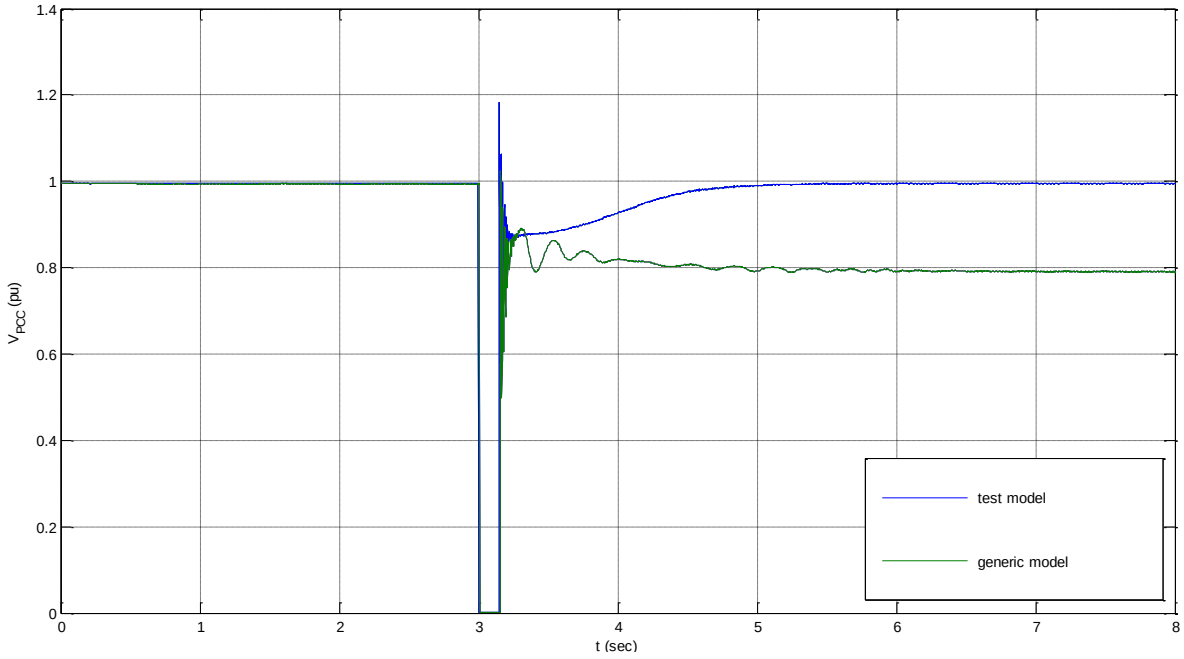

Figure 69: V_{PCC} without STATCOM (150 ms fault duration)

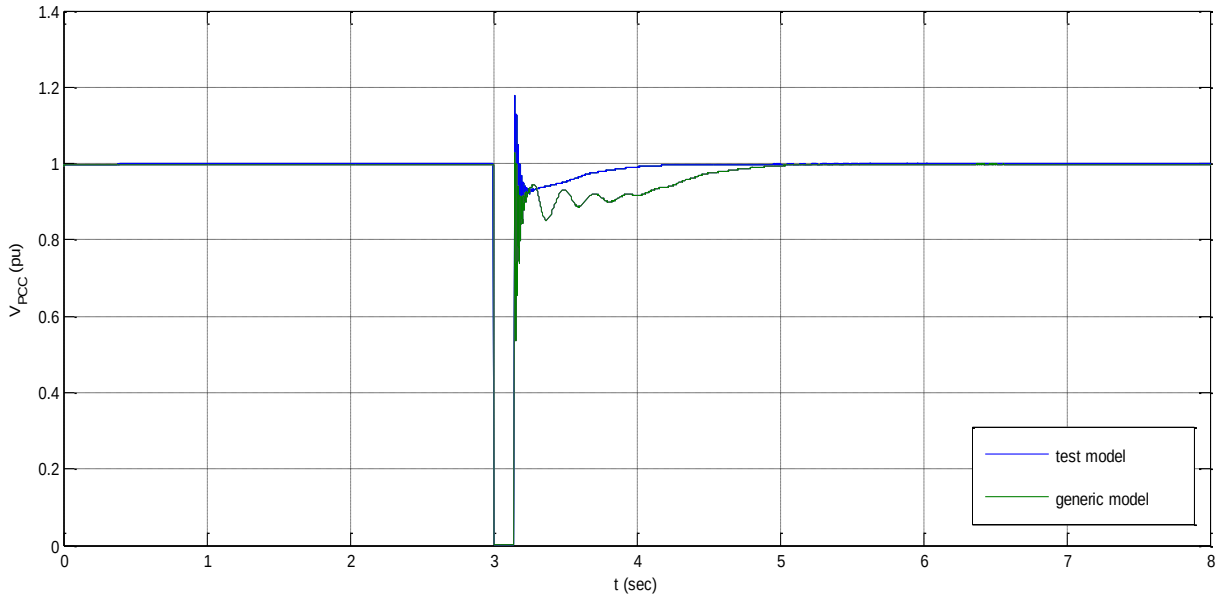

Figure 70: V_{PCC} with STATCOM (150 ms fault duration)

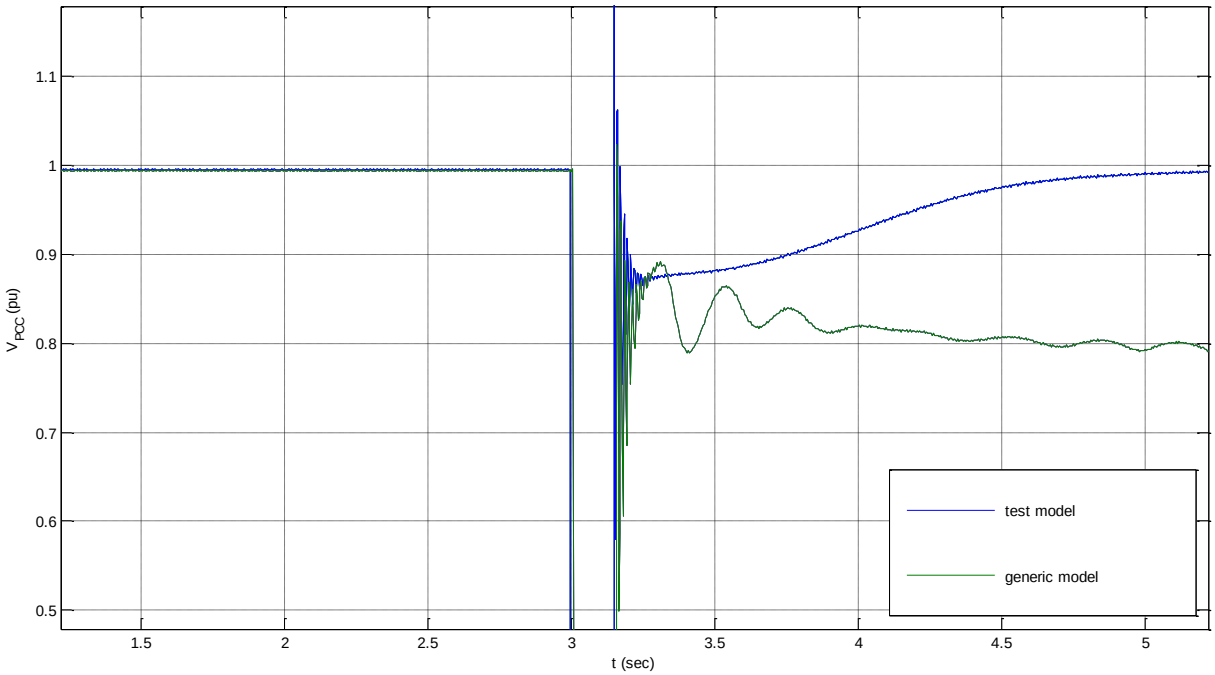

Figure 71: V_{PCC} without STATCOM (150 ms fault duration, zoomed)

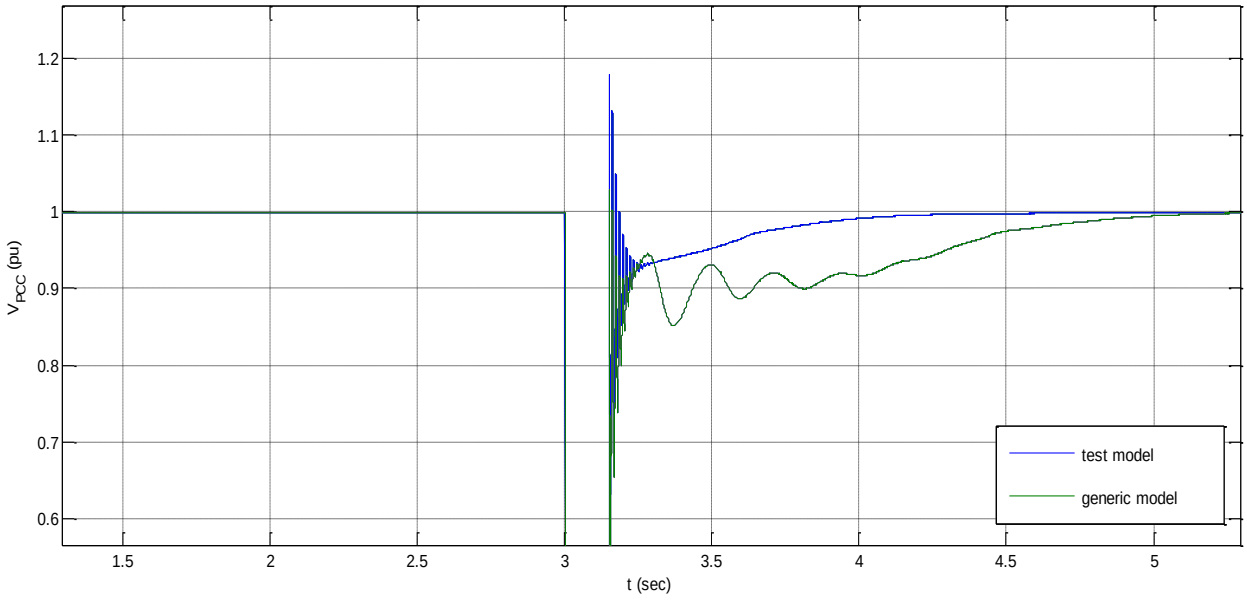

Figure 72: V_{PCC} with STATCOM (150 ms fault duration, zoomed)

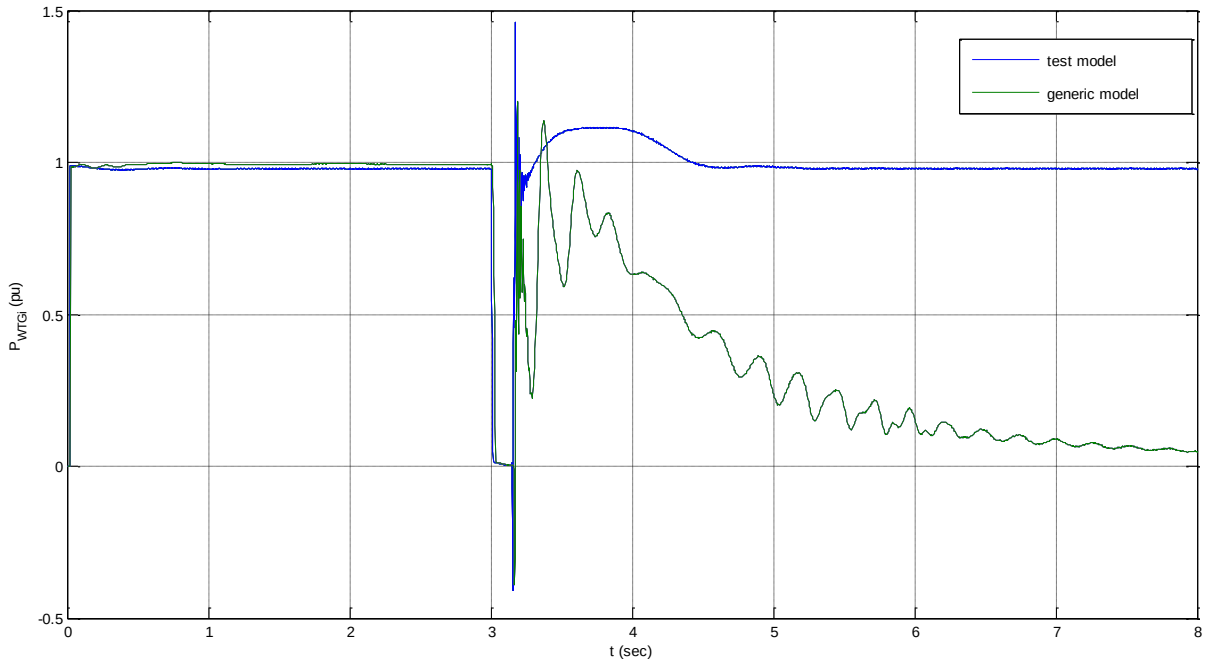

Figure 73: WTG active power without STATCOM (150 ms fault duration)

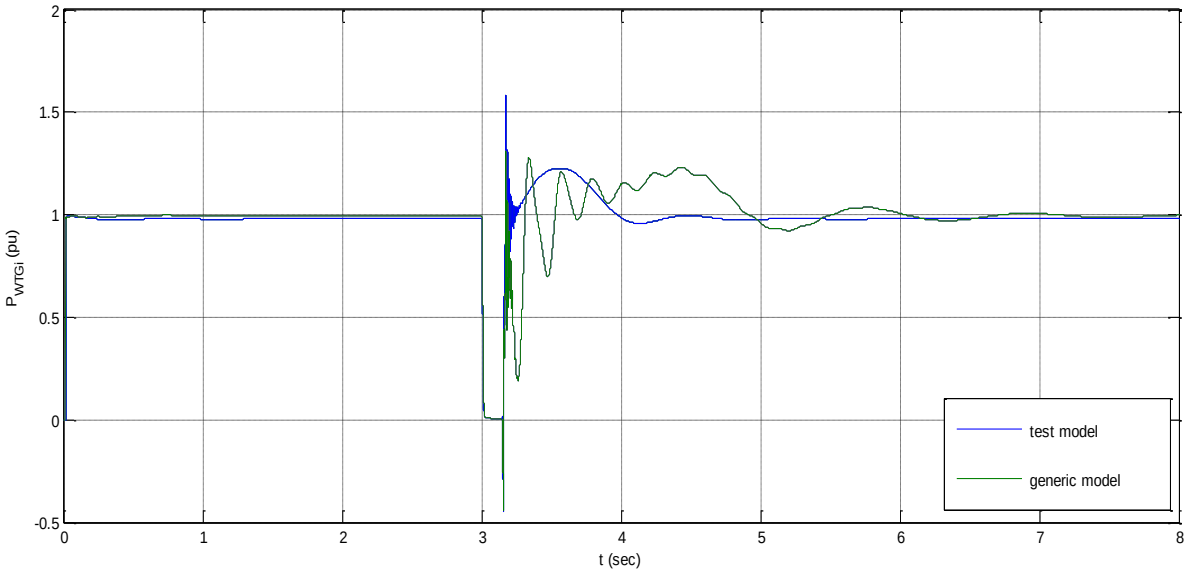

Figure 74: WTG active power with STATCOM (150 ms fault duration)

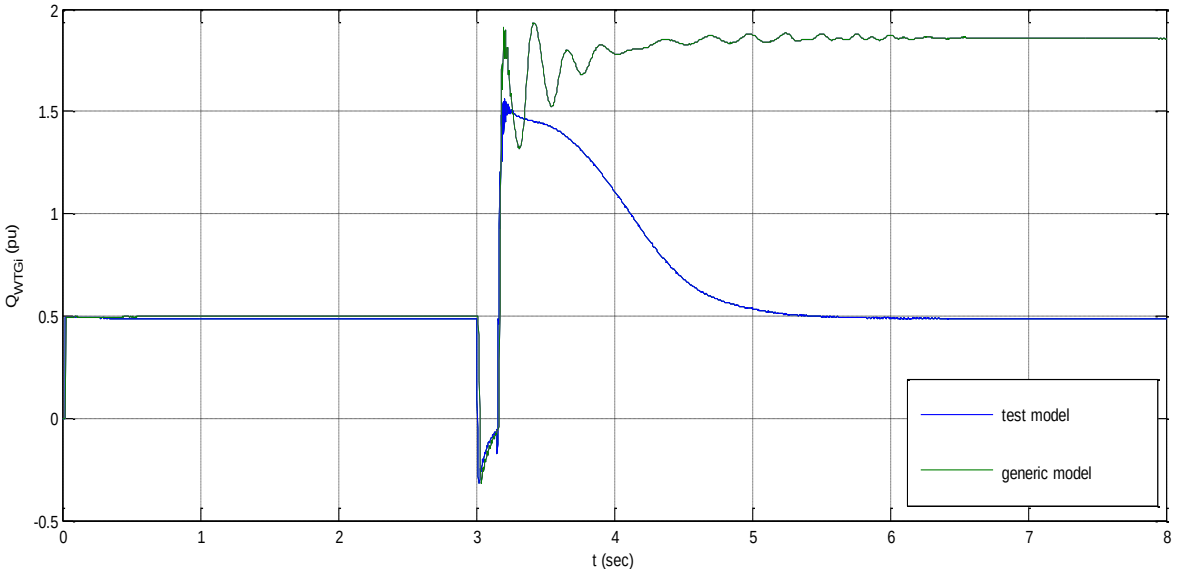

Figure 75: WTG reactive power without STATCOM (150 ms fault duration)

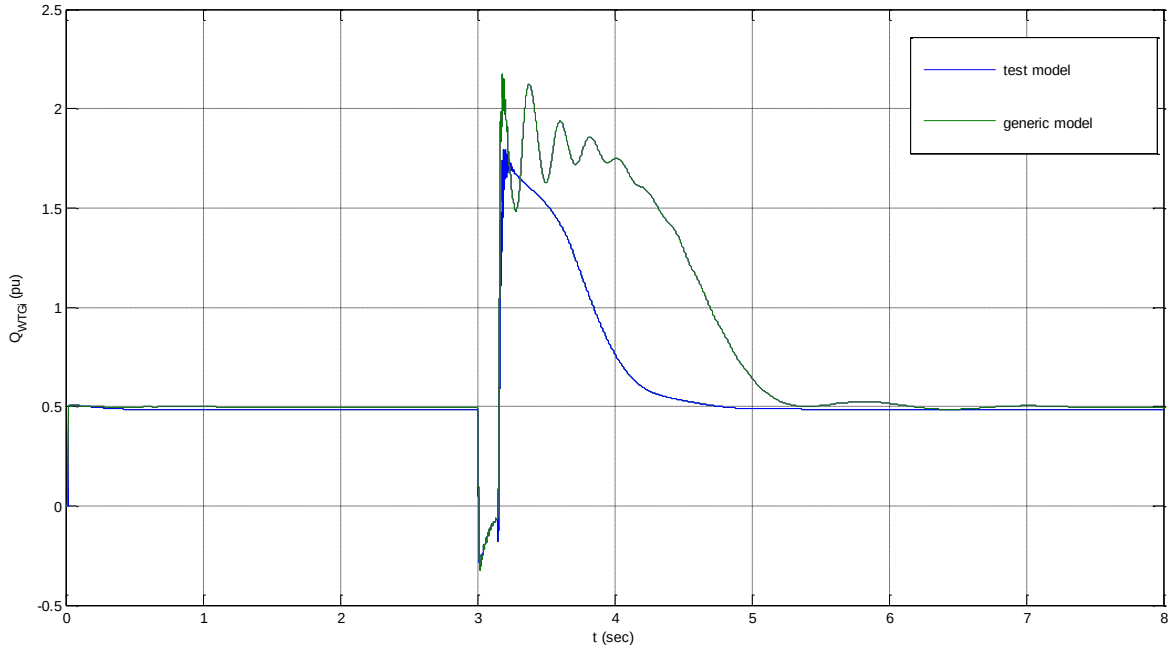

Figure 76: WTG reactive power with STATCOM (150 ms fault duration)

The voltage, active and reactive power responses for the two models and for a fault duration of 150 ms show that the generic model cannot withstand such a fault without a mean of external reactive support apart from the shunt capacitors. The voltage collapses to a value of 0.8 per unit, real power declines with some oscillations to zero and the

reactive power consumption reaches a plateau of approximately 1.8 per unit, a quantity that can no longer be supplied. The test model, on the other hand, remains stable.

The STATCOM, however, provides the necessary reactive power supplement needed for the generic model turbine, in order to restore its normal operation. It also makes the test model restoration smoother.

7.2.4. PCC Fault Cleared after 200 ms

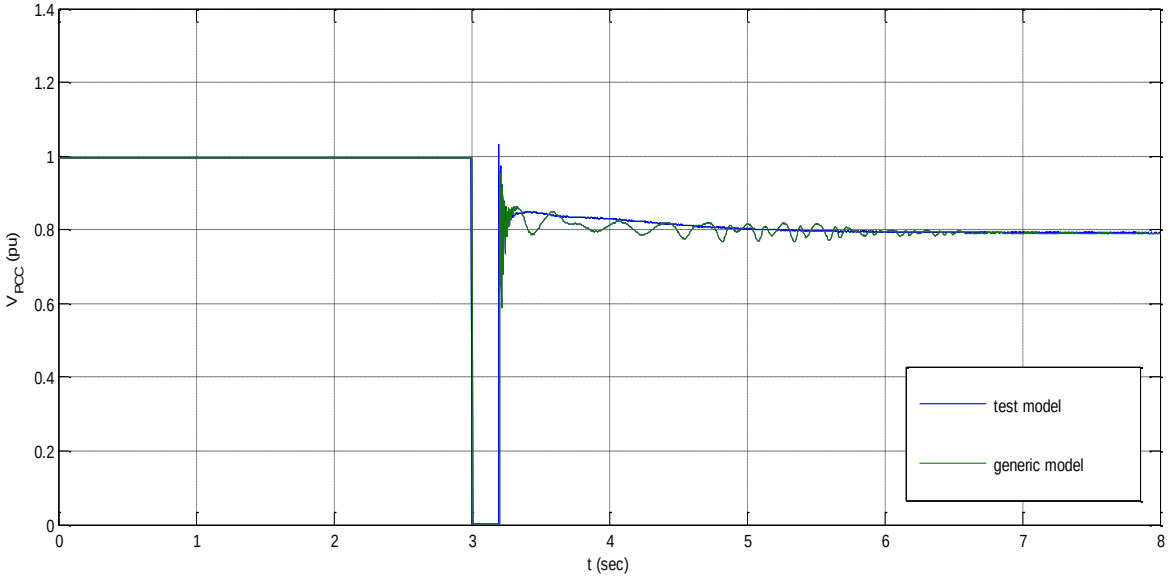

Figure 77: V_{PCC} without STATCOM (200 ms fault duration)

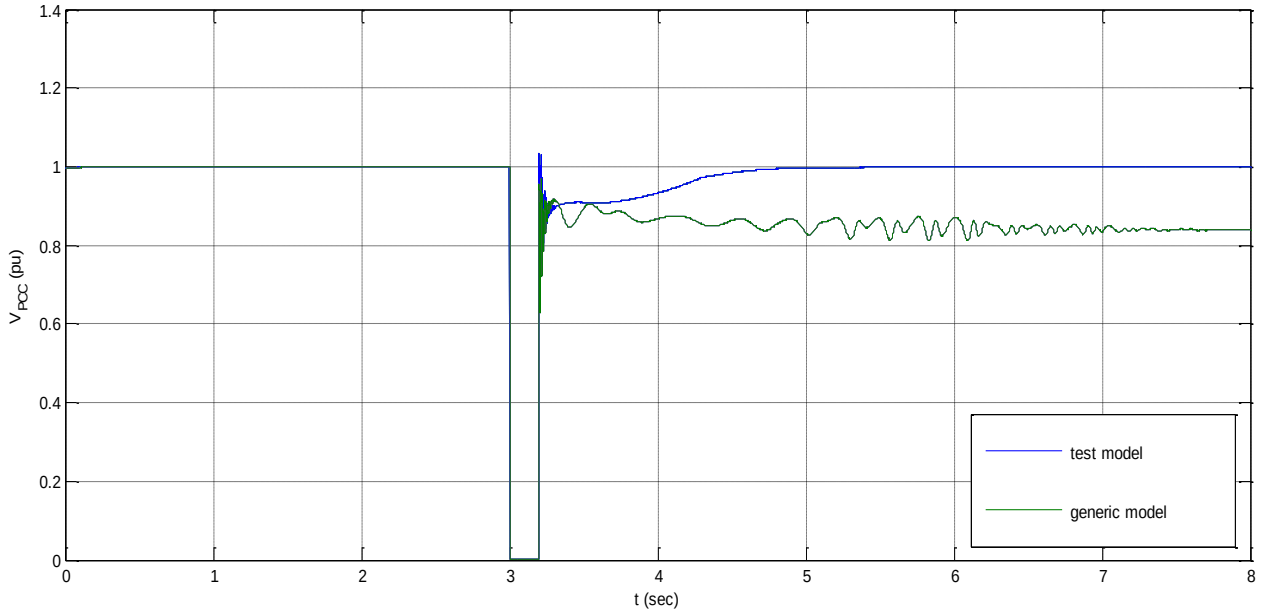

Figure 78: V_{PCC} with STATCOM (200 ms fault duration)

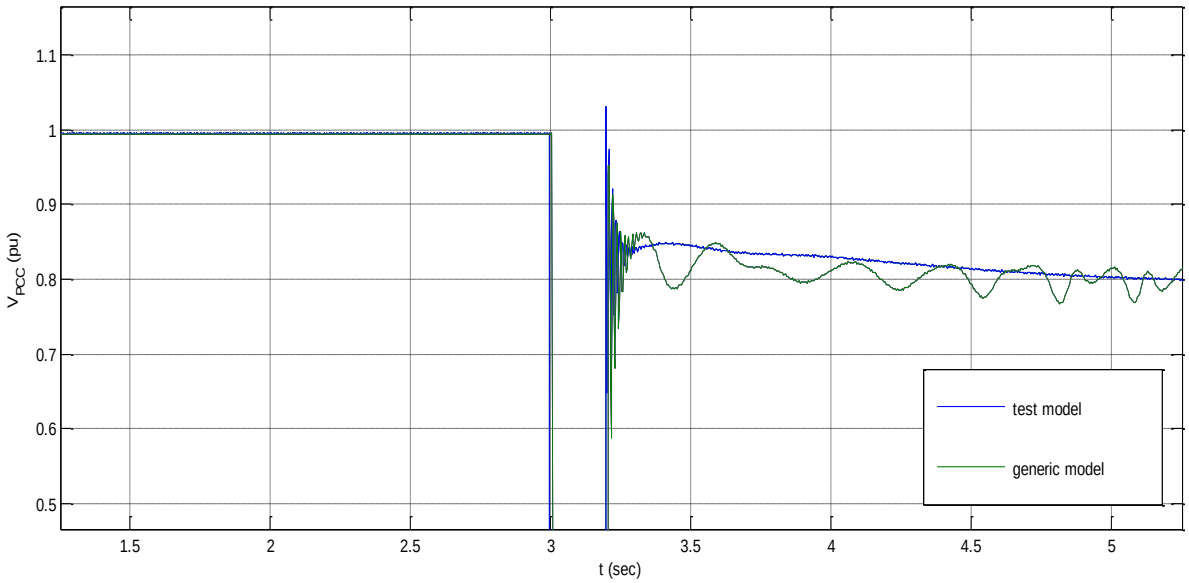

Figure 79: V_{PCC} without STATCOM (200 ms fault duration, zoomed)

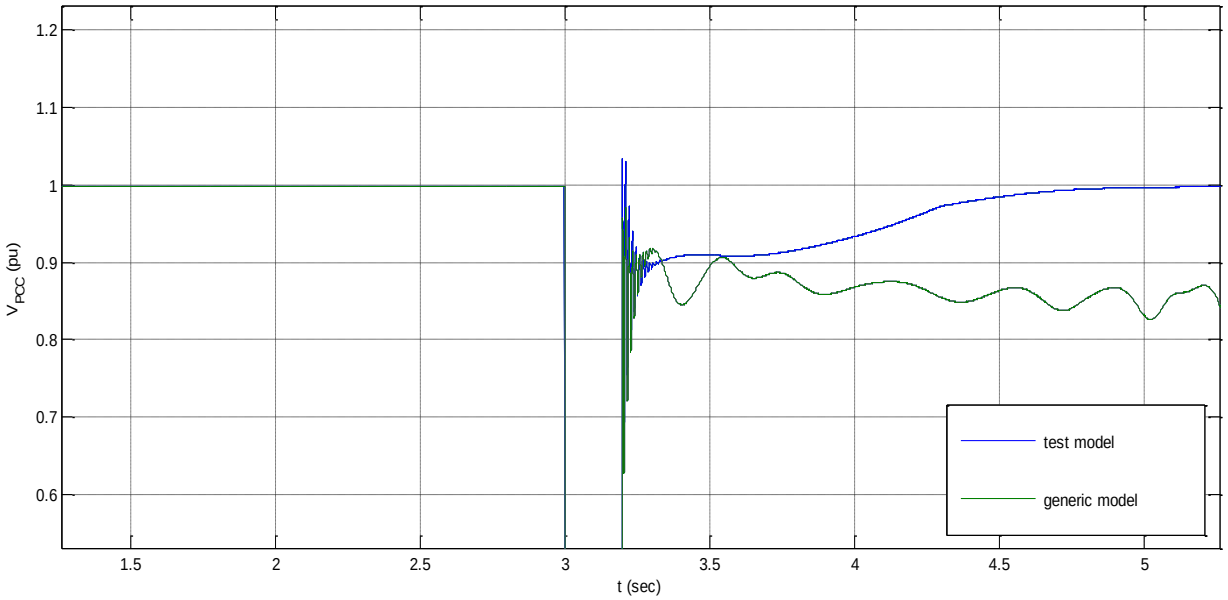

Figure 80: ms V_{PCC} with STATCOM (200 ms fault duration, zoomed)

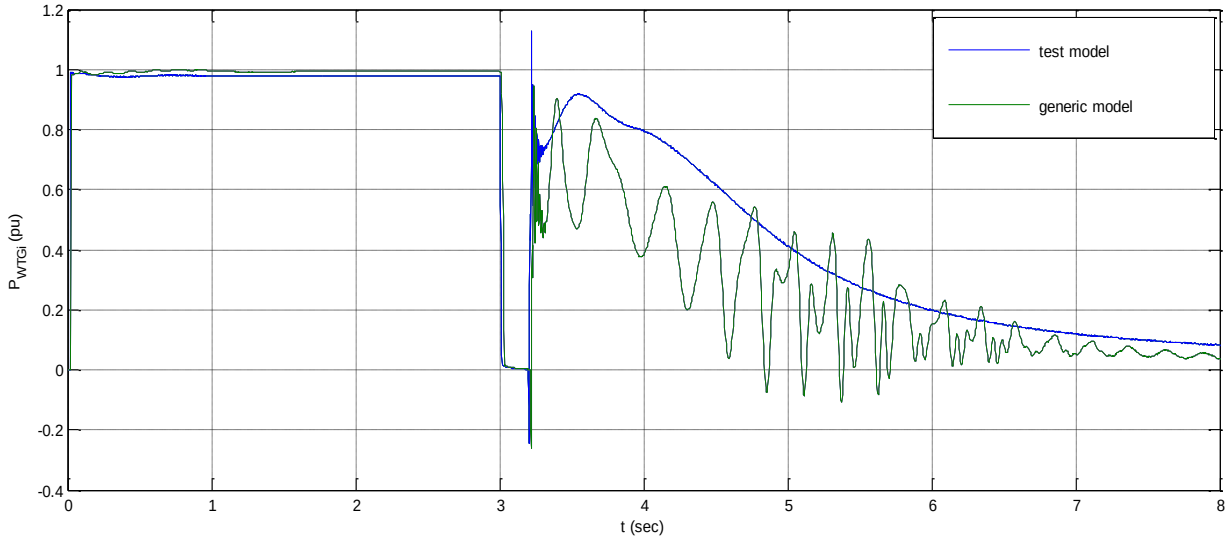

Figure 81: WTG active power without STATCOM (200 ms fault duration)

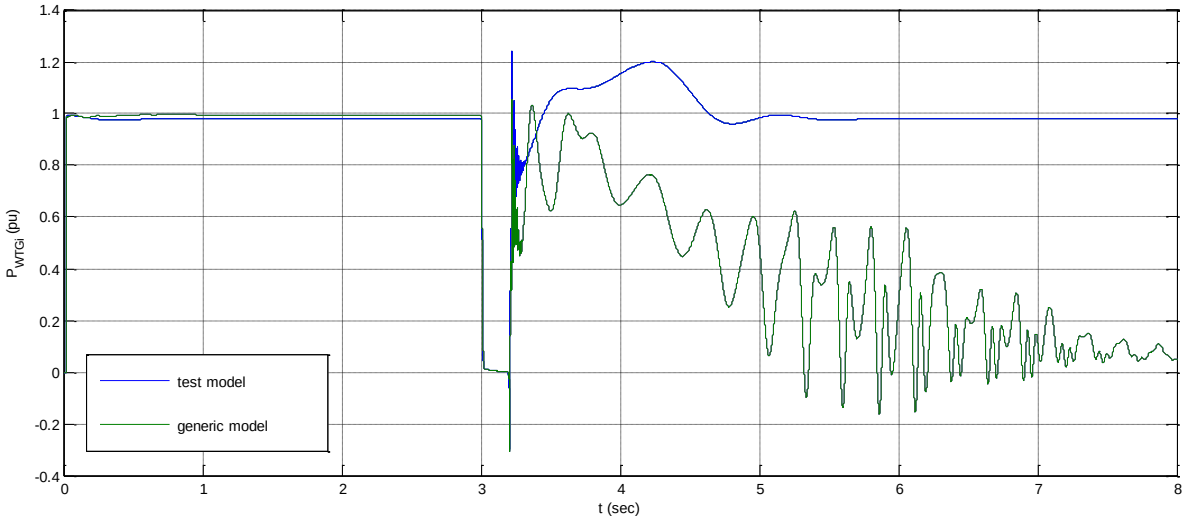

Figure 82: WTG active power with STATCOM (200 ms fault duration)

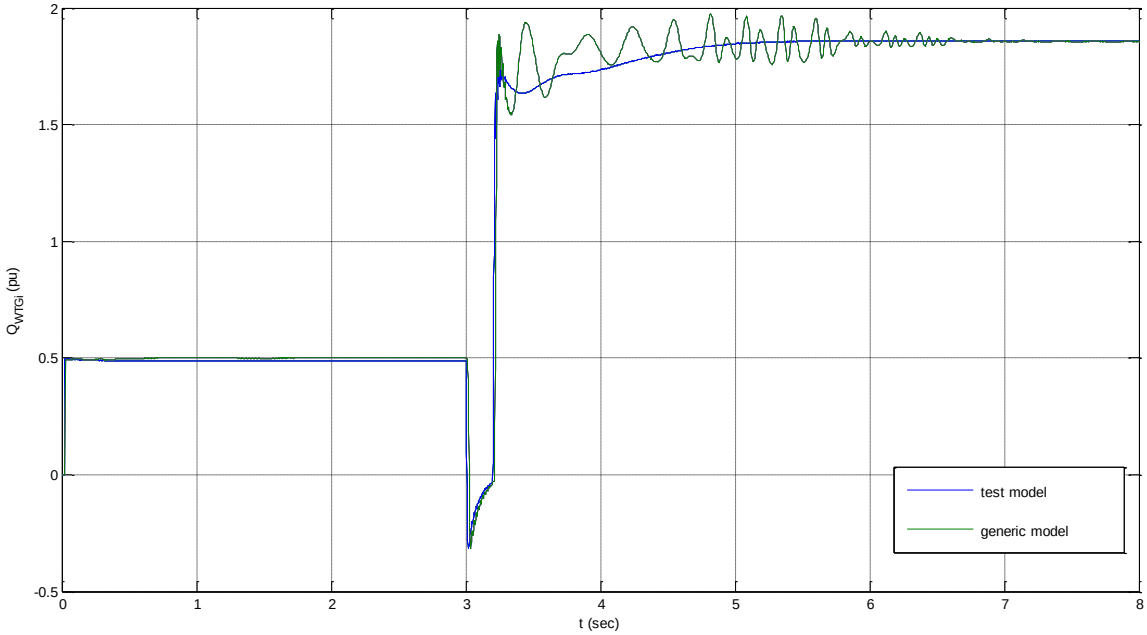

Figure 83: WTG reactive power without STATCOM (200 ms fault duration)

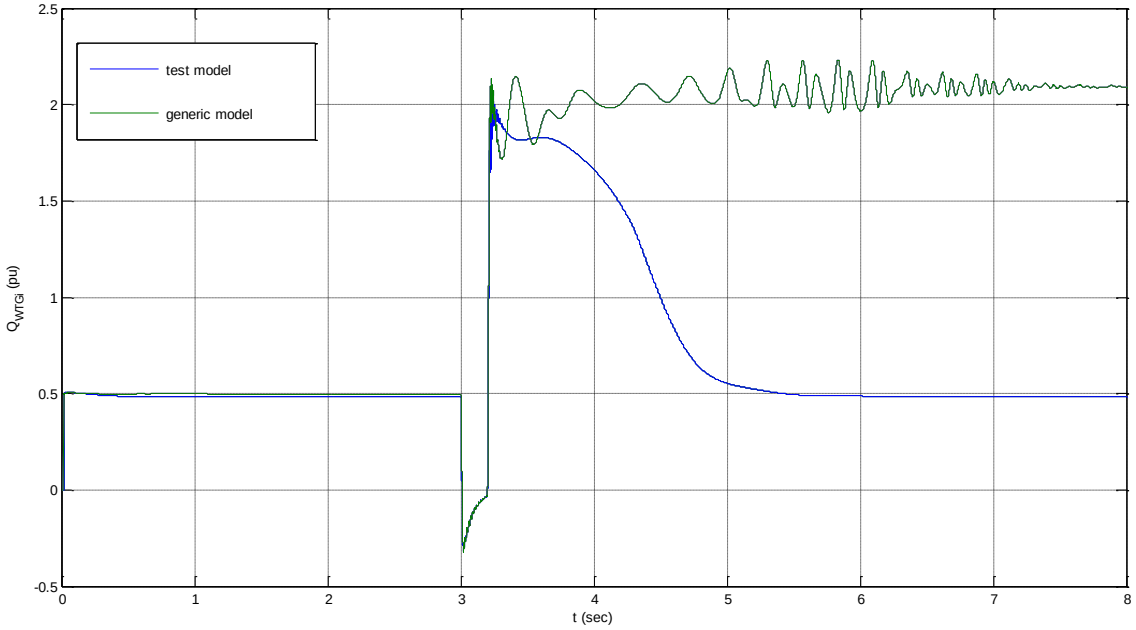

Figure 84: WTG reactive power with STATCOM (200 ms fault duration)

In case of a fault with a duration of 200 ms, both models are not able to recover and become unstable without the STATCOM support. The generic model outputs, in addition, exhibit intense oscillations. The STATCOM support is enough only for the test model; the generic, even with the STATCOM connected on its PCC, becomes unstable.

7.2.5. System Critical Clearing Time and Fault Damping

The time needed in each case, for the system to damp the fault (restoration of reactive power) is presented in the following table for comparison.

Table 11: Time needed for the fault to be damped for each case

Fault duration	Test Model	Test Model with STATCOM	Generic Model	Generic Model with STATCOM
100 ms	1.7 s	1.4 s	2.8 s	2.15 s
150 ms	1.95 s	1.7 s	-	3.15 s
200 ms	-	2 s	-	-

In table 12, another value is presented for each model, in order to illustrate even more the transient behavior of each model. That value is the fault critical clearing time (CCT) and is defined as the maximal fault duration for which the system remains transiently stable. The CCT for each model was approximated in the ms digit.

Table 12: CCT for the test and the generic model (with and without STATCOM)

Model	CCT (ms)
Test Model	186
Generic Model	124
Test Model with STATCOM	223
Generic Model with STATCOM	169

The CCTs for each of the models simulated indicate that the test model remains stable for faults of durations of up to 62 ms more that the generic without the STATCOM and of up to 54 ms with the STATCOM. The fault tolerance that each value gains with the STATCOM is 37 ms for the test model and 45 ms for the generic, values that are relatively close. From that we can deduce that the impact of STATCOM for each model is, overall, similar.

Taking into account the responses, the time needed for the fault to be damped for the different fault durations and the CCTs of the test model and the generic, it is evident that the test system gives more optimistic results, regarding the system stability and the power quality. This is mainly attributed, as mentioned, to its one-mass mechanical model representation, which ignores the interaction between the turbine and the generator rotor. In the generic model, where the two-mass mechanical model is used, the mechanical oscillations after the fault are reflected in the active and reactive power outputs and thus in the terminal voltage. This fact verifies the statement that we cannot rely on a one-mass mechanical model representation for a dynamic stability study.

7.3. Test Model PCC Fault Response with Two-Mass Mechanical Model

7.3.1. Case Description

In this simulation, the one-mass mechanical representation of the test model is superseded by the two-mass mechanical model, in order to make a more legitimate comparison with the generic model. However, since the induction generator model used in the test model integrates the machine inertia, the proper modification shall be made in the mechanical model described in section 6.2.2.2. Specifically, the mechanical system output is no longer the generator rotational speed, but the mechanical power and the generator speed is fed as an input in the two-mass model. Also, the branch that included the integrator with the generator inertia is eliminated. The modified system is shown in figure 85.

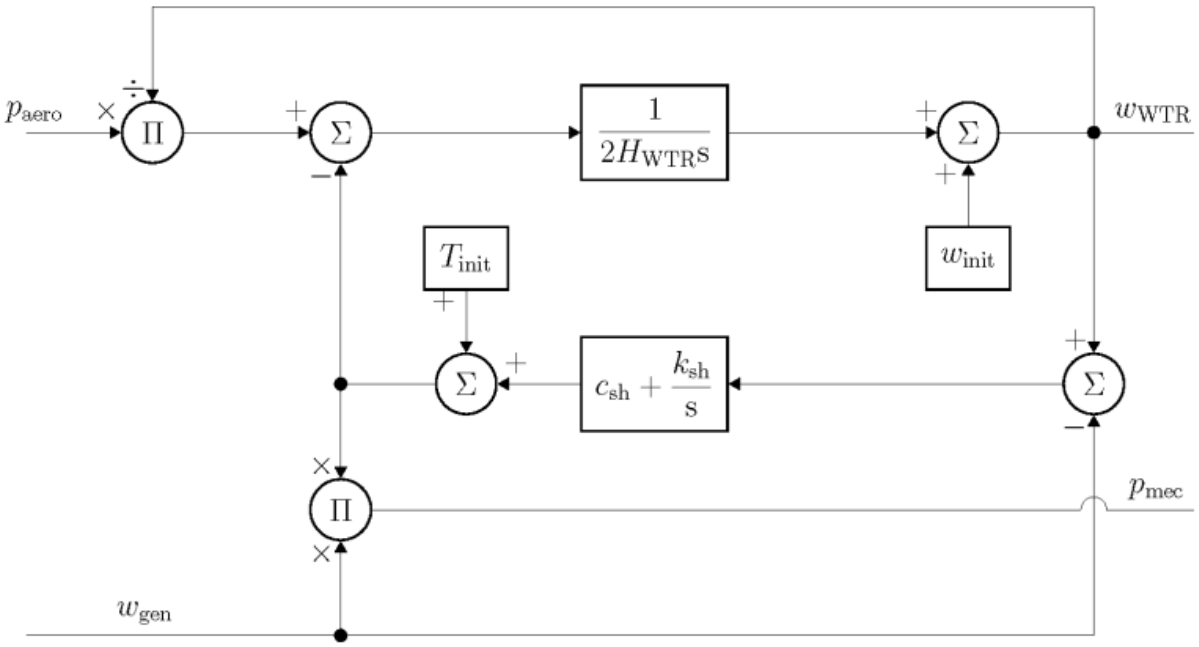

Figure 85: Modified block diagram for two-mass model [42]

7.3.2. System Response to a PCC Fault Cleared after 100 ms

The case of the fault at PCC which is cleared after 100 ms is simulated with this modified model. The responses are depicted below:

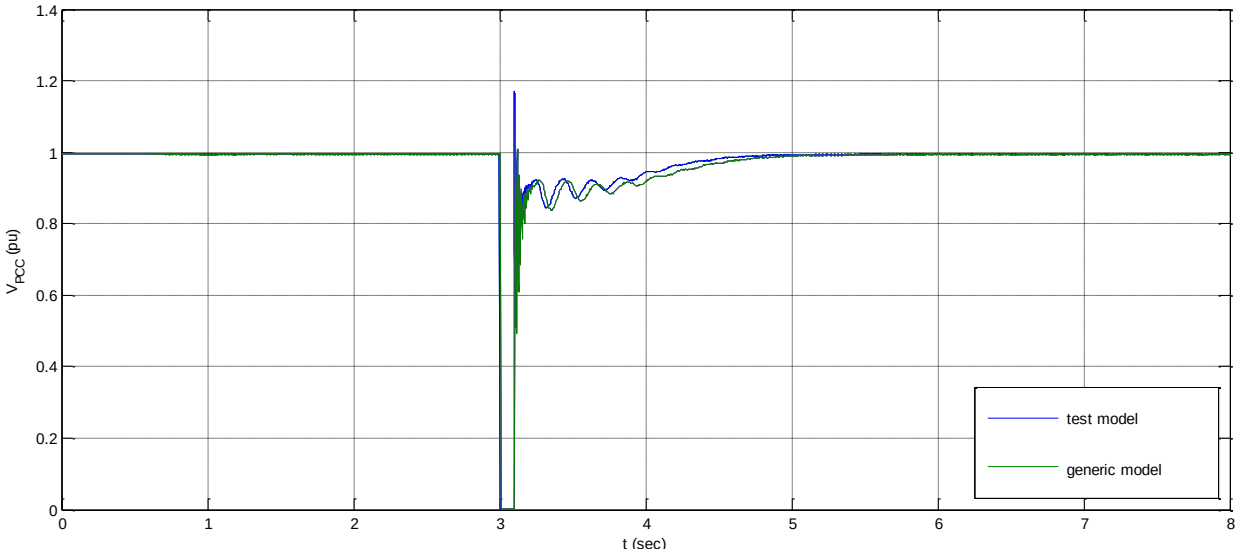

Figure 86: V_{PCC} for two-mass test model and generic (100 ms fault)

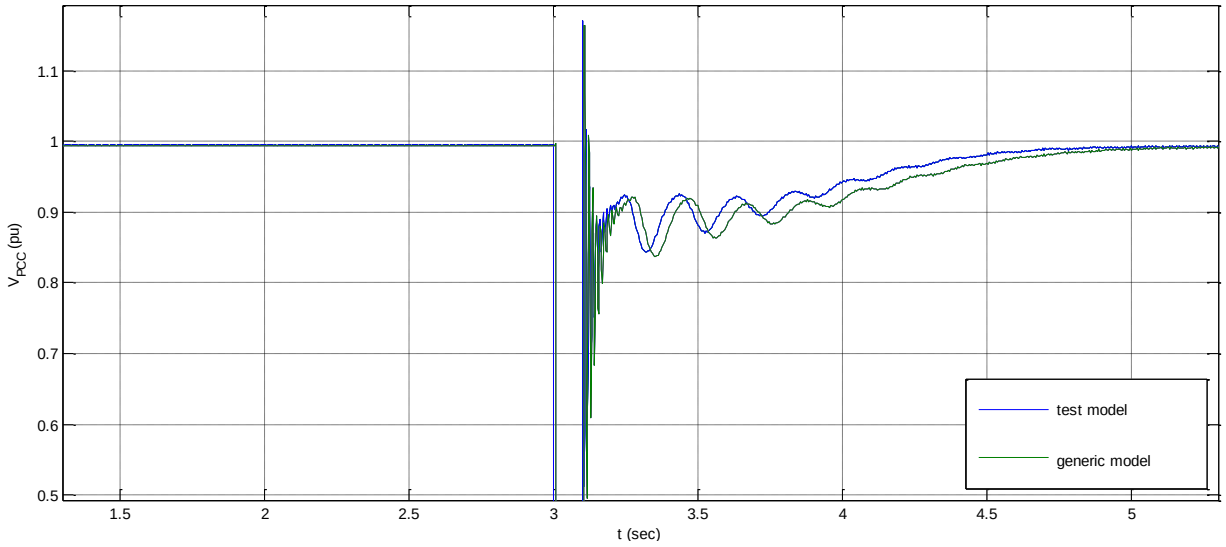

Figure 87: V_{PCC} for two-mass test model and generic (100 ms fault, zoomed)

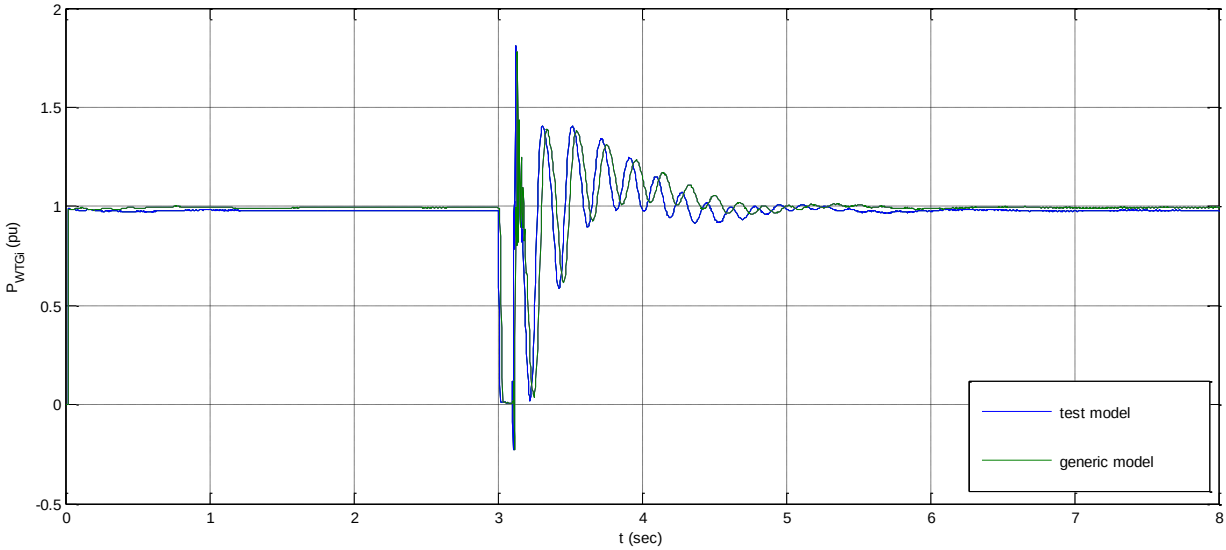

Figure 88: WTG active power for two-mass test model and generic (100 ms fault)

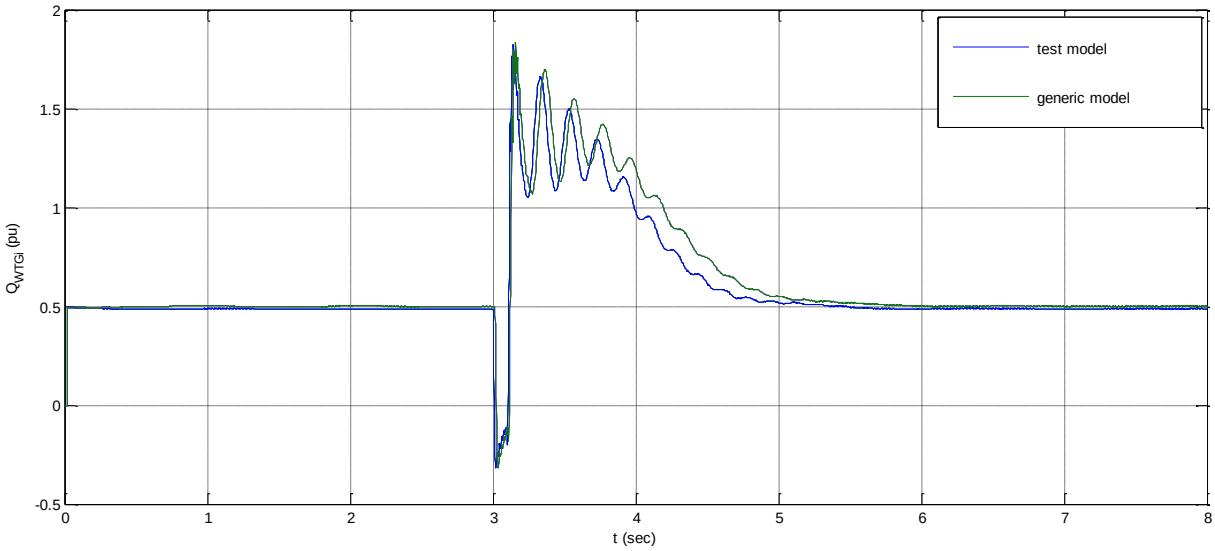

Figure 89: WTG reactive power for two-mass test model and generic (100 ms fault)

We can see that the outputs are almost identical. The generic model needs a little more time to damp the fault, i.e. approximately 0.5 sec more to completely restore its reactive power. In addition, the CCT for the two-mass test model is 140 ms, 16 ms more that the generic, a value that can be characterized small, but still the results are more optimistic. Nevertheless, we can deduct that the test model has, overall, a faithful and reliable representation of the generic model.

7.4. System PCC Fault Response with a Modified Pitch-Controller Introduced

7.4.1. Case Description

In order to increase the wind farm's transient stability margin even more, a modified pitch controller is introduced in this section that contributes to the fault damping. This is achieved, simply by changing the controller reference to the nominal WTG rotational speed. The modified controller as modeled in Simulink is shown below:

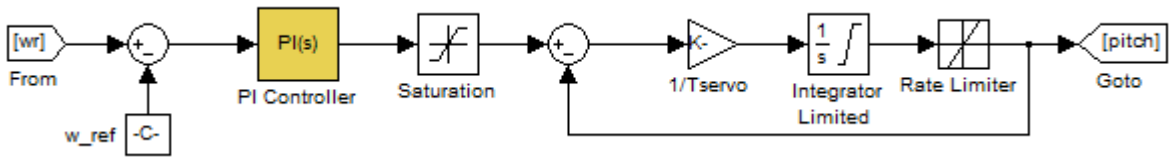

Figure 90: Modified pitch controller

A measurement of the wind turbine rotor speed is compared to the reference speed (for nominal operation 1.005 per unit) and the error signal is controlled by a PI controller. The control delay due to the servomechanism is taken into account (via the T_{servo} time constant) and limits have been imposed to the maximum blade pitch angle, as well as their rate of change for a more realistic representation. The minimum angle has been set to zero, in order for the controller to act only in cases that the rotor overspeeds. The parameters for this modified pitch controller are shown in table 13.

Table 13: Modified pitch controller parameters

Parameter	Value
ω_{ref}	1.005 pu
K_P	2
K_I	50
T_{servo}	1 ms
Minimum pitch blade angle	0 degrees
Maximum pitch blade angle	40 degrees
Maximum rate of change	±8 degrees/sec

A PCC fault that is cleared after 150 ms simulated in order to examine the system dynamic behavior with the modified pitch controller and to compare the response with the corresponding case (section 7.2.3). For this simulation the STATCOM is not connected to the PCC terminals.

The modified pitch controller is also implemented in the generic model. However, as it has already been mentioned, the generic models were developed for dynamic studies, where the wind speed is assumed constant. In this section, we “violate” this assumption, as, to depict the pitch controller effect, the pseudo-governor described in section 4.3.1 or the constant torque that was implemented in the previous demonstrations of the generic models, is substituted by the wind turbine model described in section 6.2.1.1.

7.4.2. System Response to a PCC Fault Cleared after 150 ms

The PCC voltage, wind turbine active and reactive power output and the pitch angle are shown in figures 91-95.

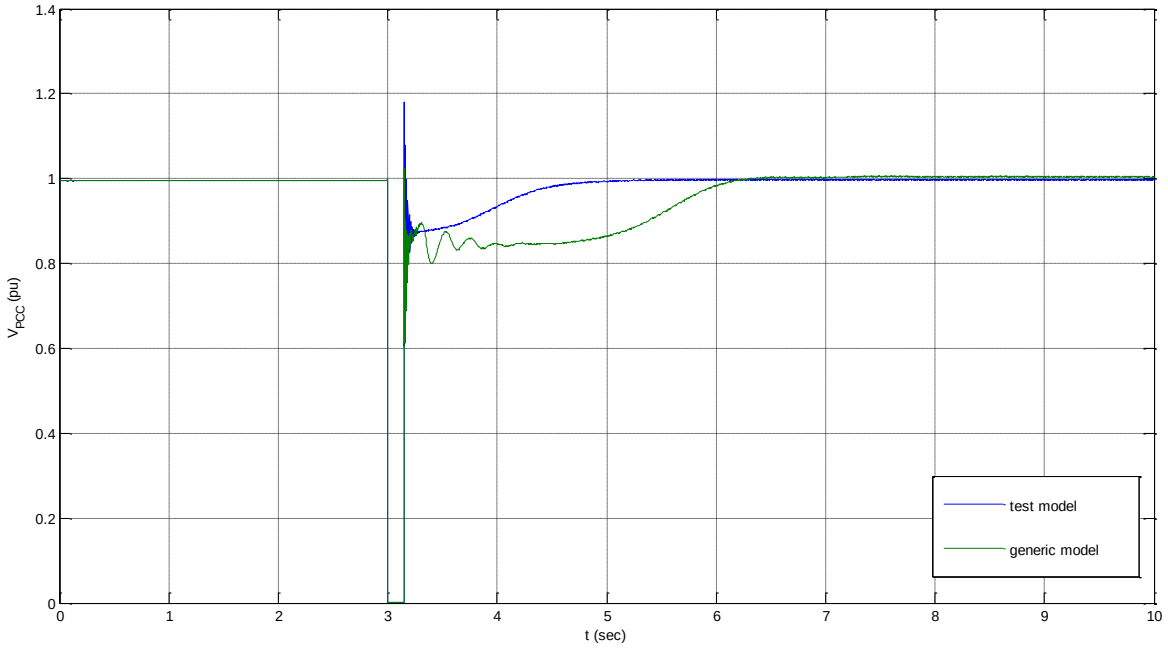

Figure 91: V_{PCC} with modified pitch controller and 150 ms fault duration

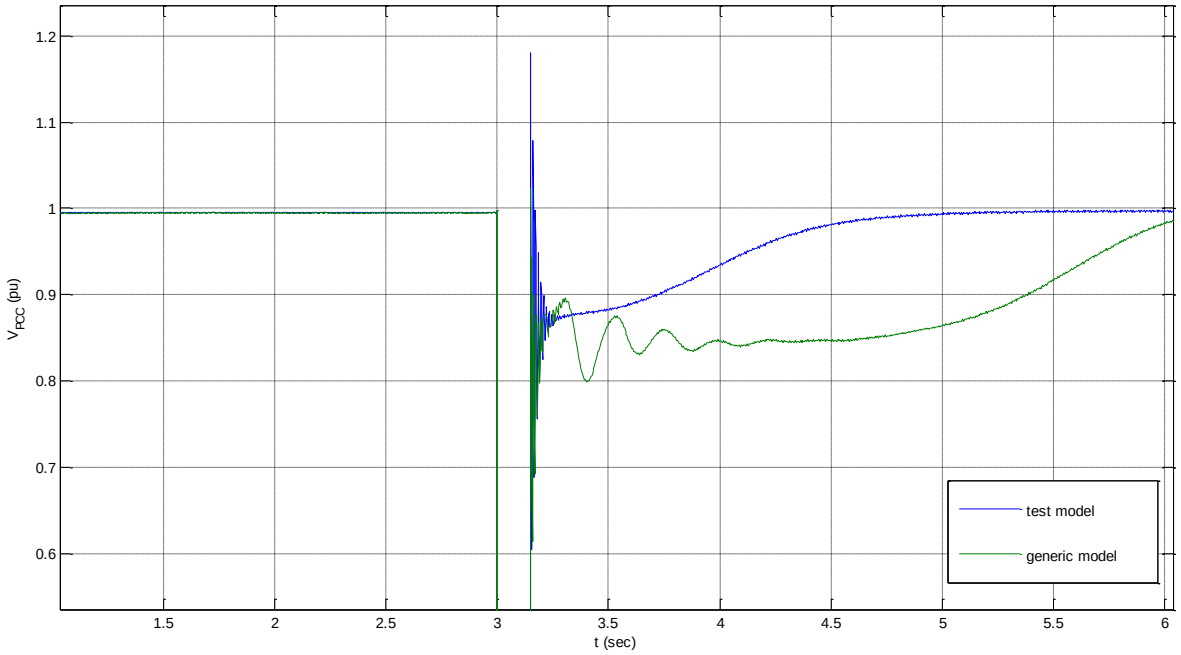

Figure 92: V_{PCC} with modified pitch controller and 150 ms fault duration (zoomed)

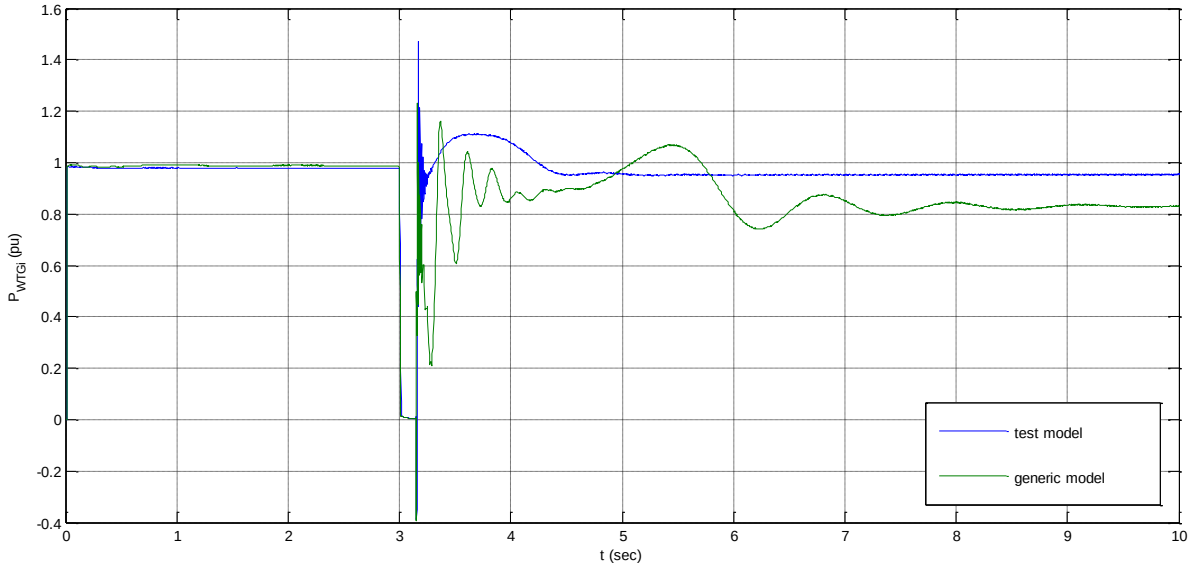

Figure 93: WTG active power with modified pitch controller and 150 ms fault duration

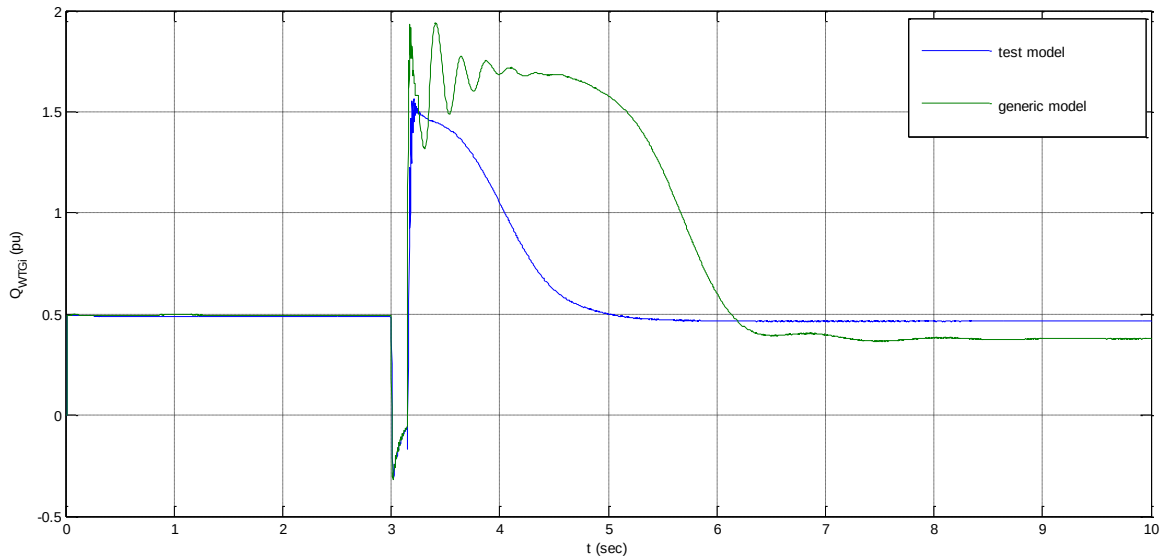

Figure 94: WTG reactive power with modified pitch controller and 150 ms fault duration

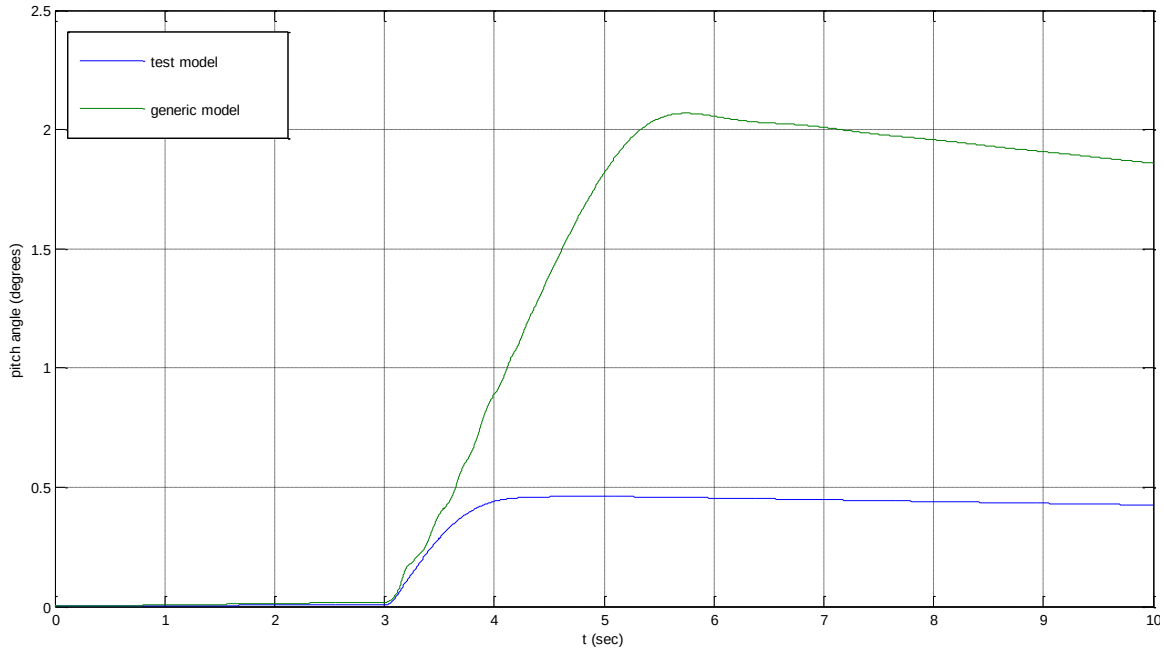

Figure 95: WT blade pitch angle with modified pitch controller and 150 ms fault duration

Comparing the responses with those without the pitch controller (neither the STATCOM) and the same fault duration (figures 69, 73 and 75), the first thing that is noticed is that the modified pitch controller achieves the stability of the generic model, in contrast with the initial controller. A blade angle of up to 2 degrees curtailed the active power generation, which was stabilized at the value of 0.8 per unit, to keep the wind turbines of the generic model within operation.

On the other hand, the blade angle required in the test model is minimal, i.e. only 0.5 degrees. That is because the fault did not have such a significant impact in the specific model, compared to the generic. Consequently, the active power curtailment and the contribution in the fault damping of the modified pitch controller are less profound in this case.

The biggest difference is spotted in the reactive power output, as the generic model requires excessive amounts of reactive power and for more than the double time interval than the test model. This could be possibly characterized as a result that raises a question to whether the generic model should be used in conjunction with the wind turbine model described in section 6.2.1.1.

The CCTs for the models with the modified pitch controller are 203 ms and 156 ms for the test and the generic model respectively. The corresponding CCTs with the regular controller (which had no effect during the fault) were 186 ms and 124 ms.

7.5. System PCC Fault Response with Coordinated STATCOM and Modified Pitch Control

7.5.1. Case Description

Since it was demonstrated that both the STATCOM and the modified pitch controller can enhance the system stability and therefore the wind farm's LVRT capability, in this section, a coordinated control of both of these methods is examined. A similar work has been presented in [46]. All of the components' parameters are the same while the system's response to a fault in the PCC is simulated; first, it is cleared after 150 ms and then after 200 ms.

7.5.2. System Response to a PCC Fault Cleared after 150 ms

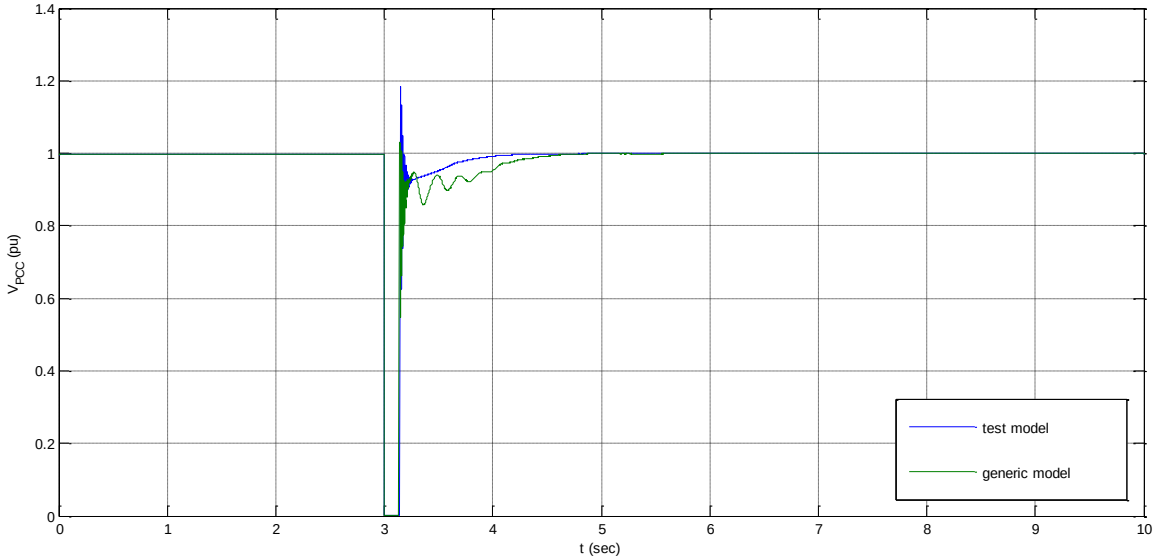

Figure 96: V_{PCC} with modified pitch controller and STATCOM and 150 ms fault duration

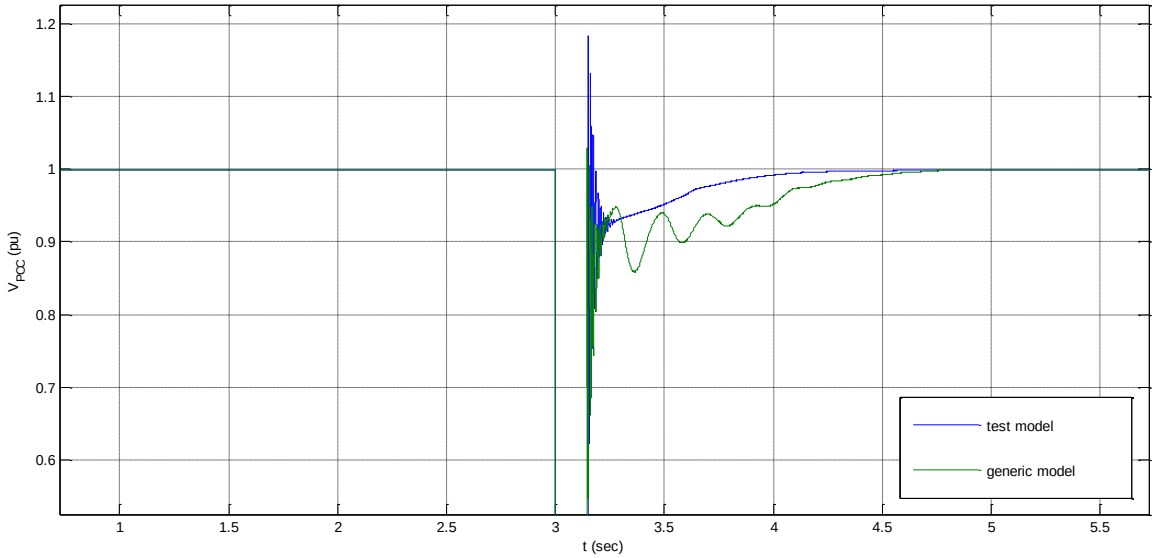

Figure 97: V_{PCC} with modified pitch controller and STATCOM and 150 ms fault duration (zoomed)

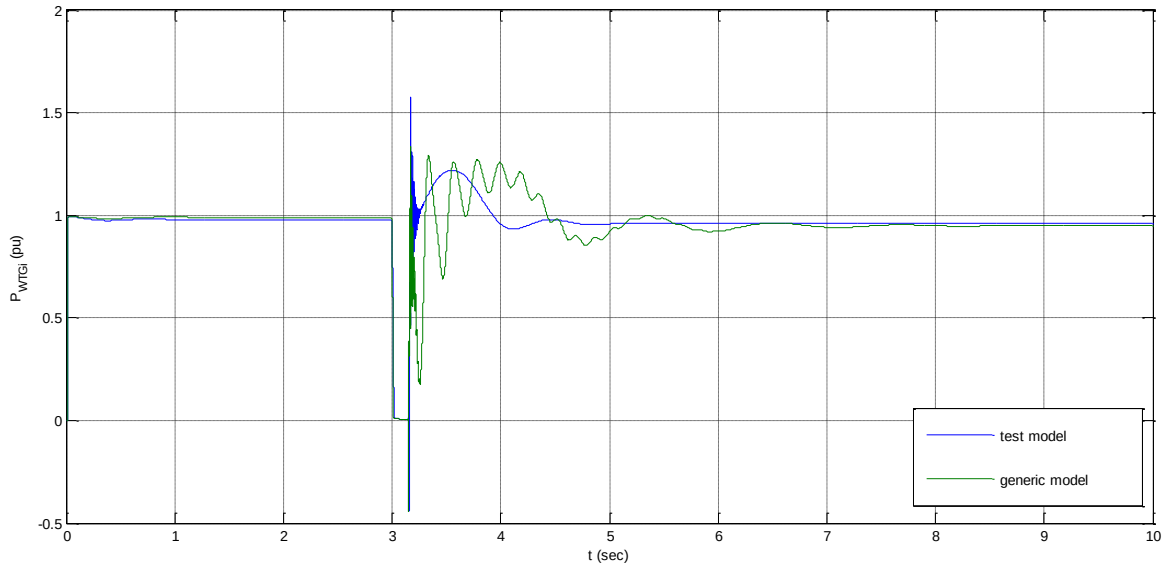

Figure 98: WTG active power with modified pitch controller and STATCOM and 150 ms fault duration

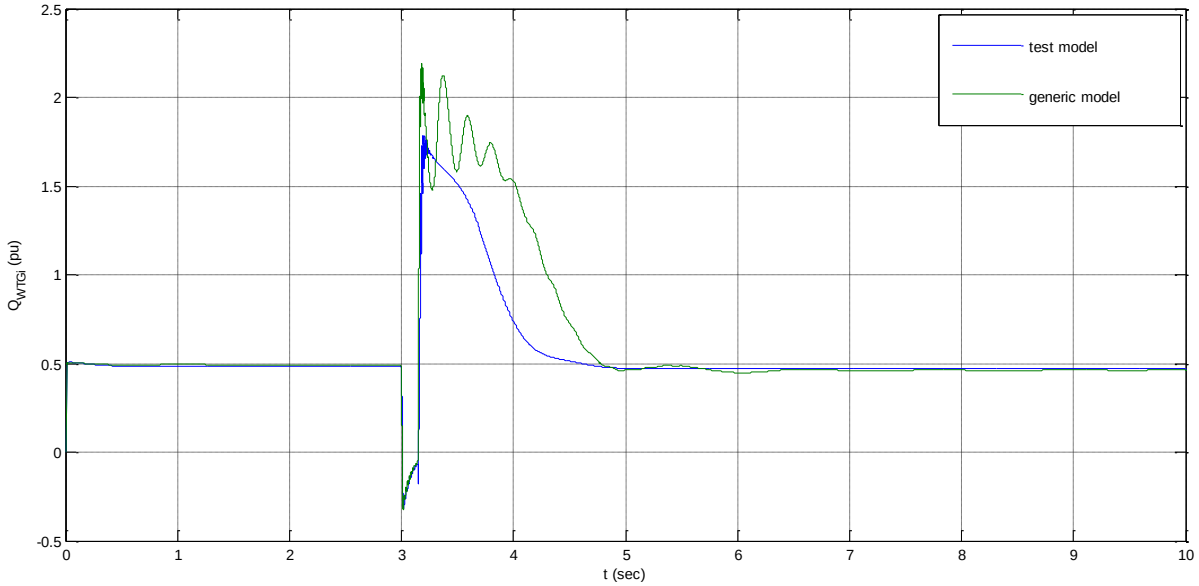

Figure 99: WTG reactive power with modified pitch controller and STATCOM and 150 ms fault duration

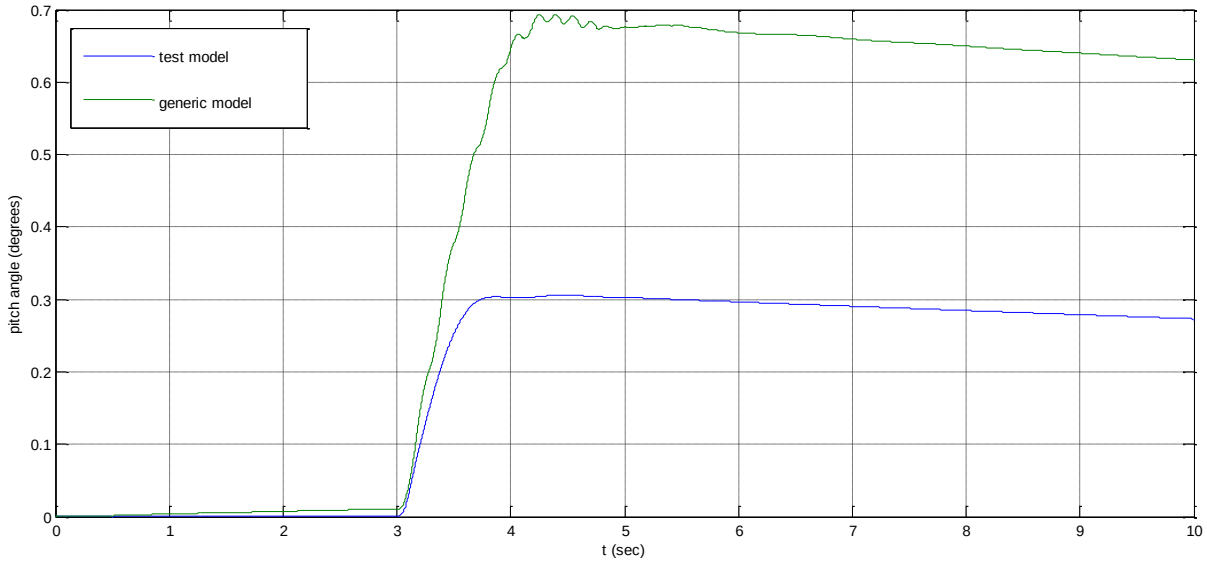

Figure 100: WT blade pitch angle with modified pitch controller and STATCOM and 150 ms fault duration

It is evident that compared to the previously examined case (modified pitch controller only), the fault's effects are significantly allayed. The reactive power injected by the STATCOM assists the voltage to restore its pre-fault value 1.5 sec earlier. From the real power and pitch angle outputs, it is shown that the STATCOM abates the need of active power curtailment to approximately 0.9 per unit, with the corresponding pitch angle to be up to 0.7 degrees. The STATCOM's active current's transient at the time of the fault clearance is also noticeable in the pitch angle response, apart from the active power, with

small oscillations. Finally, a notable difference is also spotted in the reactive power responses, where the excessive reactive amounts the generic model required have been significantly smoothed by the STATCOM.

The effects on the test model are less visible, as it had an already efficient fault response. In the specific model, the voltage restores at 4.25 sec, compared to the 5 sec without the STATCOM. The pitch angle and the corresponding active power were slightly modified, with the pitch angle value to peak to 0.3 degrees instead of 0.4 in the previous case, having a negligible difference in the active power curtailment, a fact that is in strong contrast with the generic model. With the STATCOM connected, however, in spite of the alternative generic model implementation with variable wind available, the comparison between the two models is more acceptable.

7.5.3. System Response to a PCC Fault Cleared after 200 ms

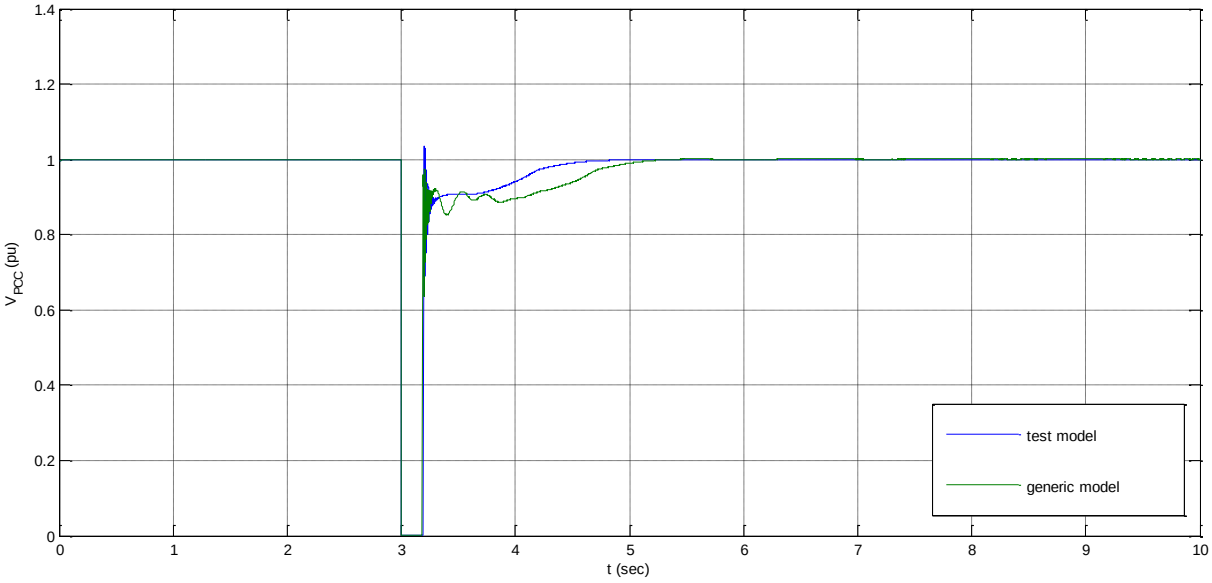

Figure 101: V_{PCC} with modified pitch controller and STATCOM and 200 ms fault duration

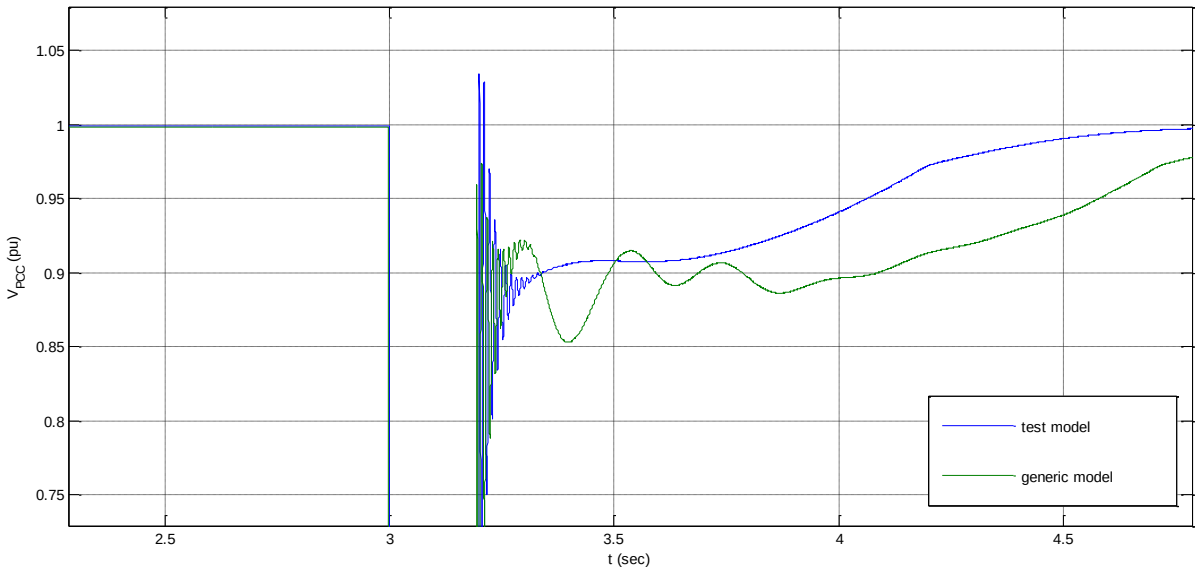

Figure 102: V_{PCC} with modified pitch controller and STATCOM and 200 ms fault duration (zoomed)

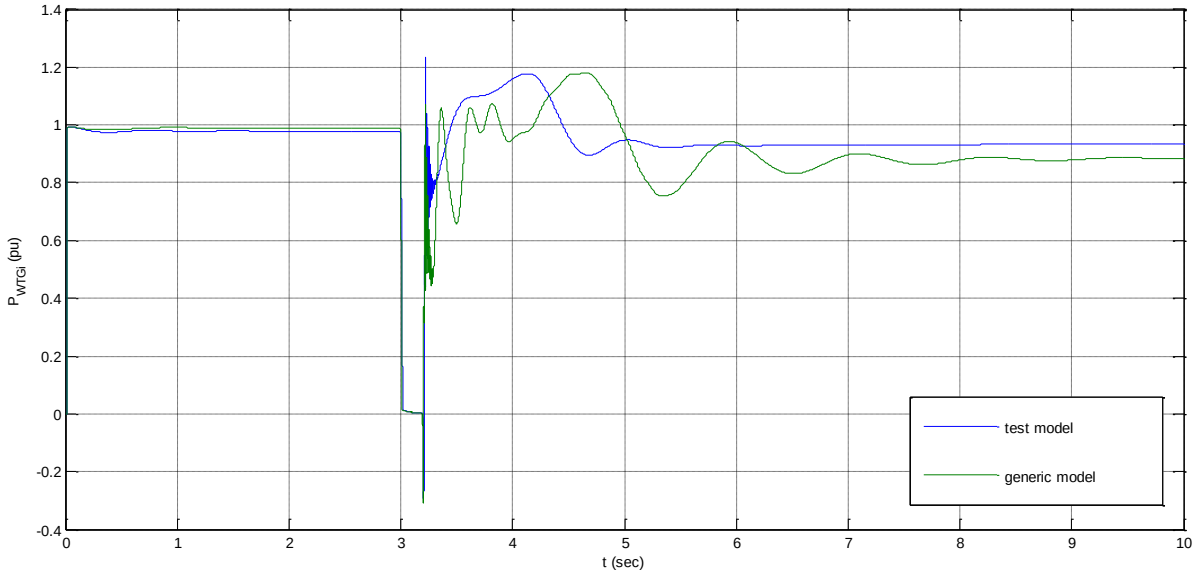

Figure 103: WTG active power with modified pitch controller and STATCOM and 200 ms fault duration

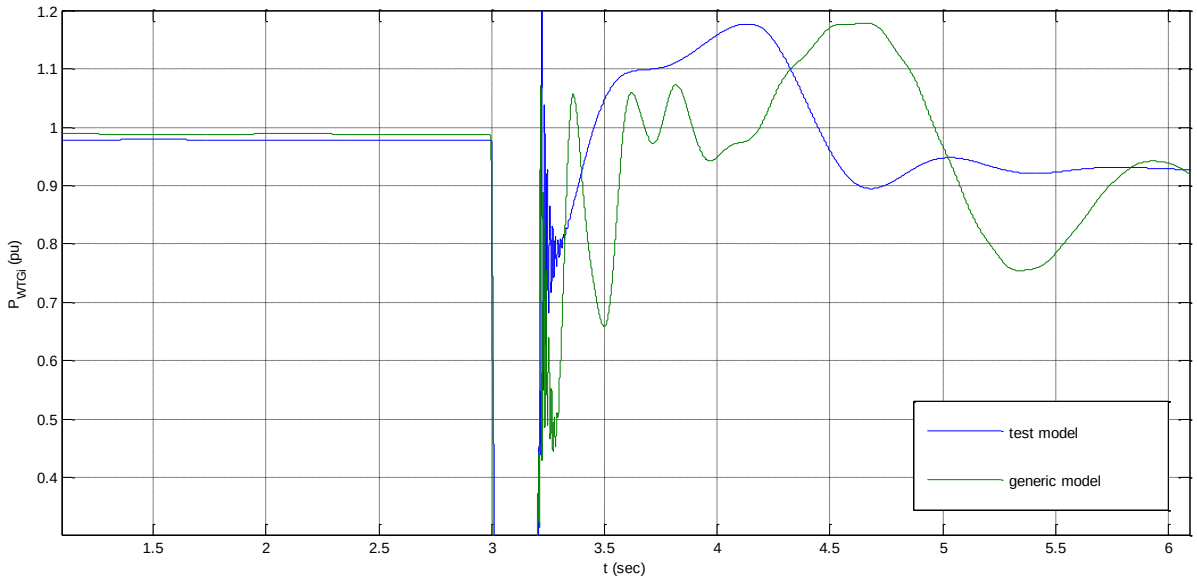

Figure 104: WTG active power with modified pitch controller and STATCOM and 200 ms fault duration (zoomed)

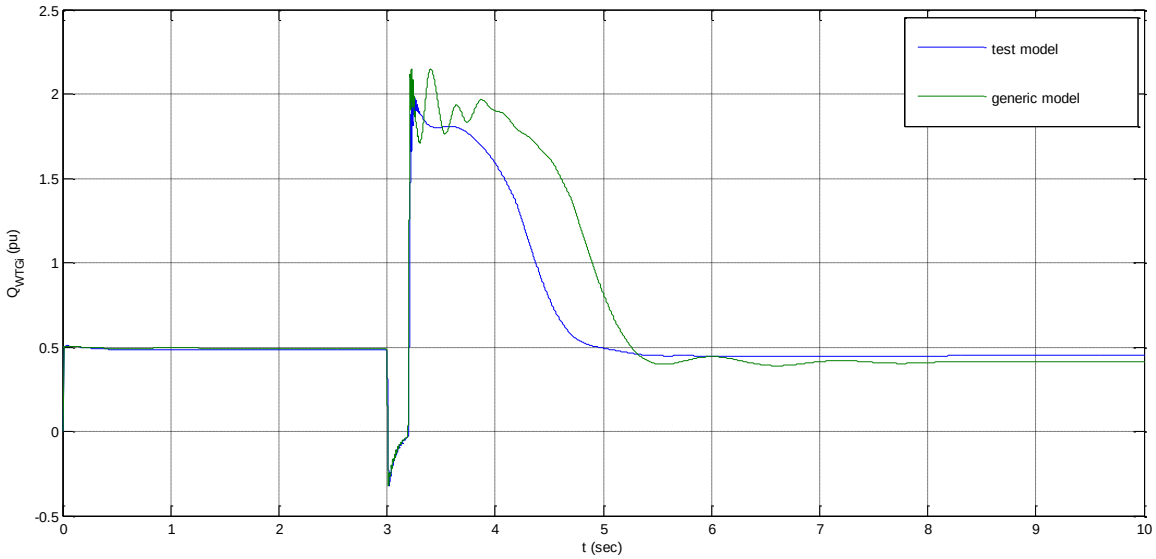

Figure 105: WTG reactive power with modified pitch controller and STATCOM and 200 ms fault duration

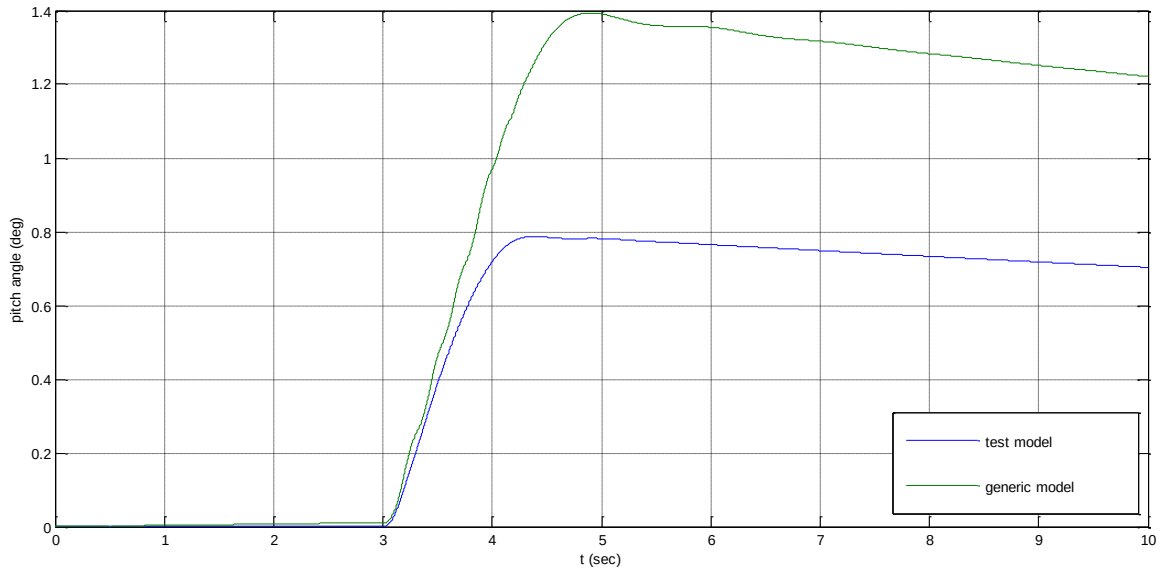

Figure 106: WT blade pitch angle with modified pitch controller and STATCOM and 200 ms fault duration

The model responses for the PCC fault with clearing time of 200 ms demonstrate that with the coordinated control of the STATCOM and the modified pitch controller, both systems are able to withstand the specific fault, something that had not been achieved in any of the previous cases. The voltage is restored at time 4.6 sec for the test model and at 5.2 sec for the generic.

In the active power responses, we see that the generic model displays relatively intense oscillations in its real power generation before it is stabilized to the value 0.88 per unit approximately. These oscillations are caused by the combination of the interaction of the two masses, the STATCOM's active current transient and the pitch regulation. The test model's active power restoration has also been smoothed, assisted by a pitch angle of up to 0.8 degrees which curtail 0.07 per unit of the generated active power (final value 0.93 per unit). The corresponding pitch angle for the generic model is 1.4 degree, double than the case where the fault was cleared 50 ms earlier.

The reactive power for the generic model is restored at approximately time 5.5 sec and for the test model at time 5 sec, 0.5 sec faster than the case where only the STATCOM was connected. It has also to be noted that when the modified pitch controller is used, the reactive power value after the fault is slightly less than the nominal (the induction generator absorbs less reactive power). This is because of the machine deceleration caused by the pitch blade angle. In higher simulation times, we would see that all these values (real/reactive power, blade pitch angle) would gradually be restored to nominal. In the pitch angle response, this is already clear; it reaches a peak and then slowly declines.

The CCTs for the models with the coordinated control of STATCOM and modified pitch controller are 245 ms for the test model and 229 ms for the generic, the highest of the cases examined and also the values with the smallest difference between the specific models. The latter is possibly partially attributed to the substitution of the constant torque used for the generic implementation with the wind turbine block of figure 42.

7.6. Connection Line Length Variation

7.6.1. Case Description

The distance, between the PCC of a wind farm and the grid, is a factor that significantly affects the system stability. Usually, the areas with high wind capability are spotted in remote locations, away for the grid, in a manner that a long connection is required. In this section, the wind farm dynamic behavior is studied, considering that the connection distance changes parametrically.

The fault simulated occurs at the PCC at t=3 sec and is cleared after 0.1 sec. The outputs for PCC voltage, WTG real and reactive power are examined, for different values of transmission line's TL2 length. Only the test model responses are examined in this section.

7.6.2. System PCC Fault Response

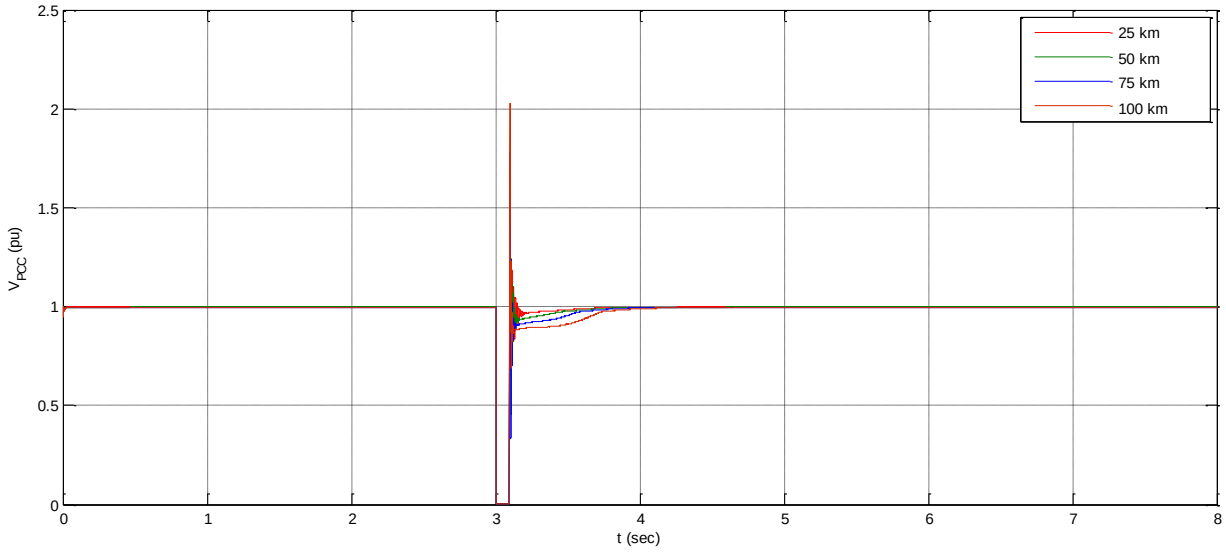

Figure 107: V_{PCC} for a fault duration of 0.1 sec and different line lengths

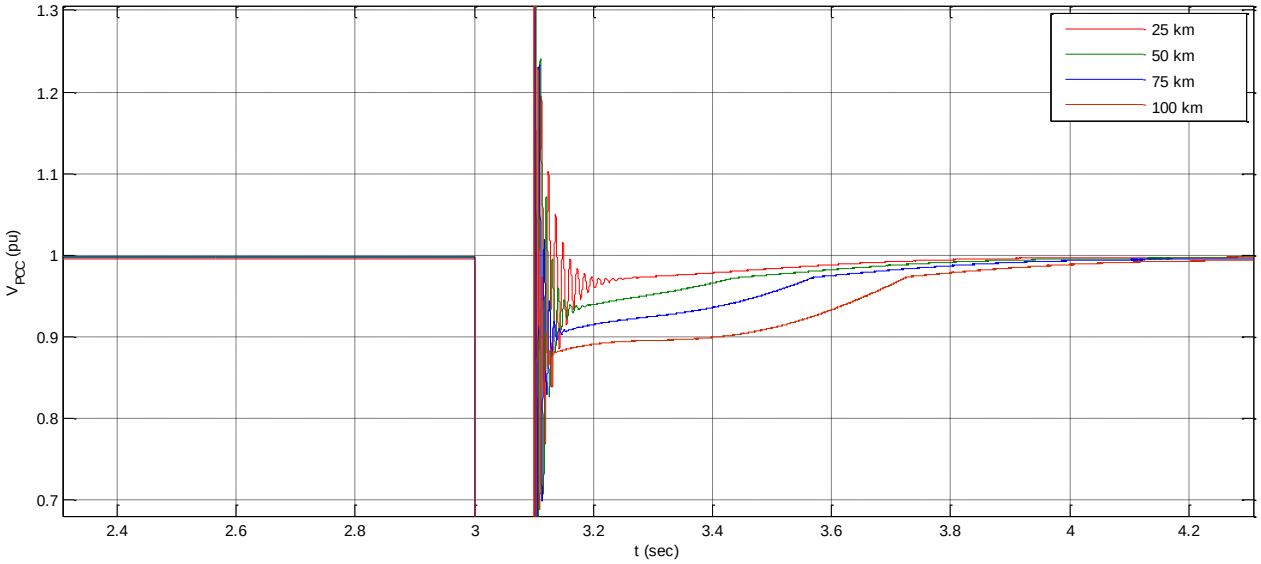

Figure 108: V_{PCC} for a fault duration of 0.1 sec and different line lengths (zoomed)

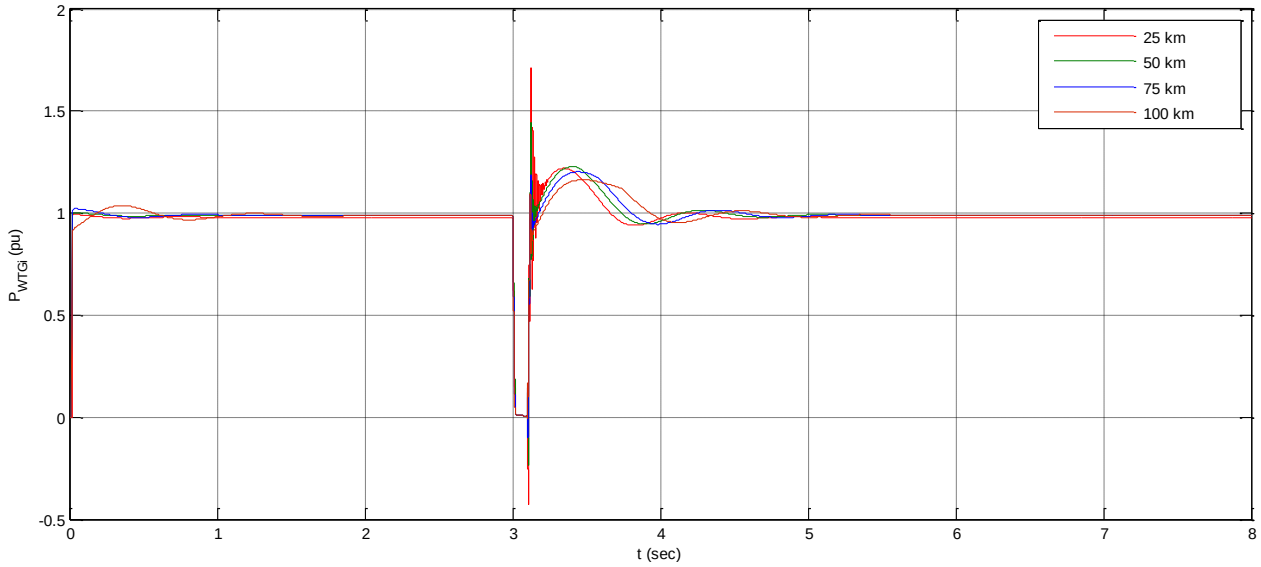

Figure 109: WTG active power for a fault duration of 0.1 sec and different line lengths

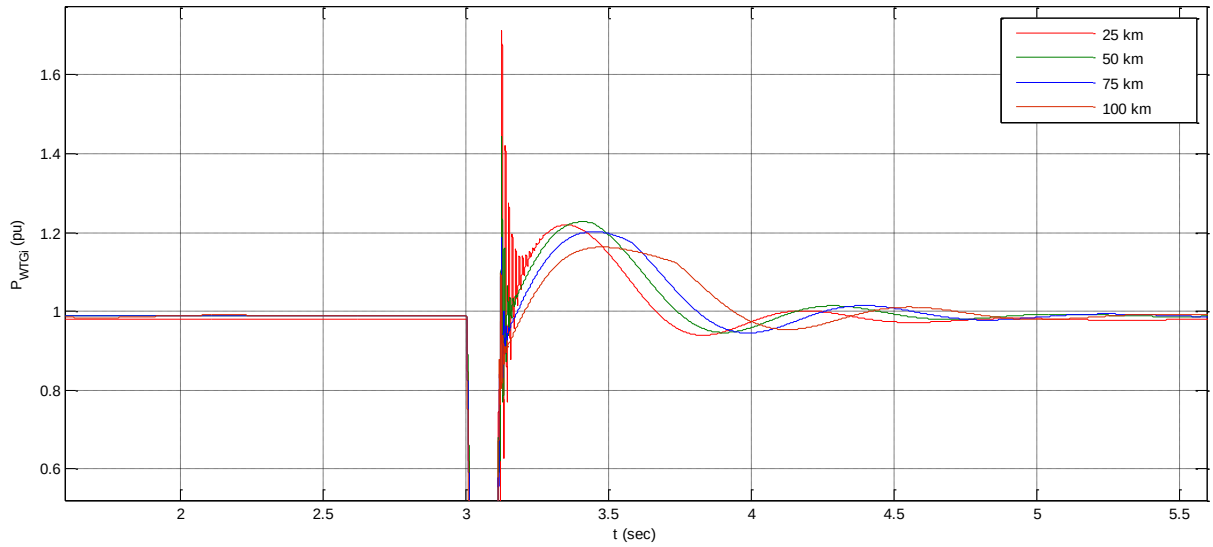

Figure 110: WTG active power for a fault duration of 0.1 sec and different line lengths (zoomed)

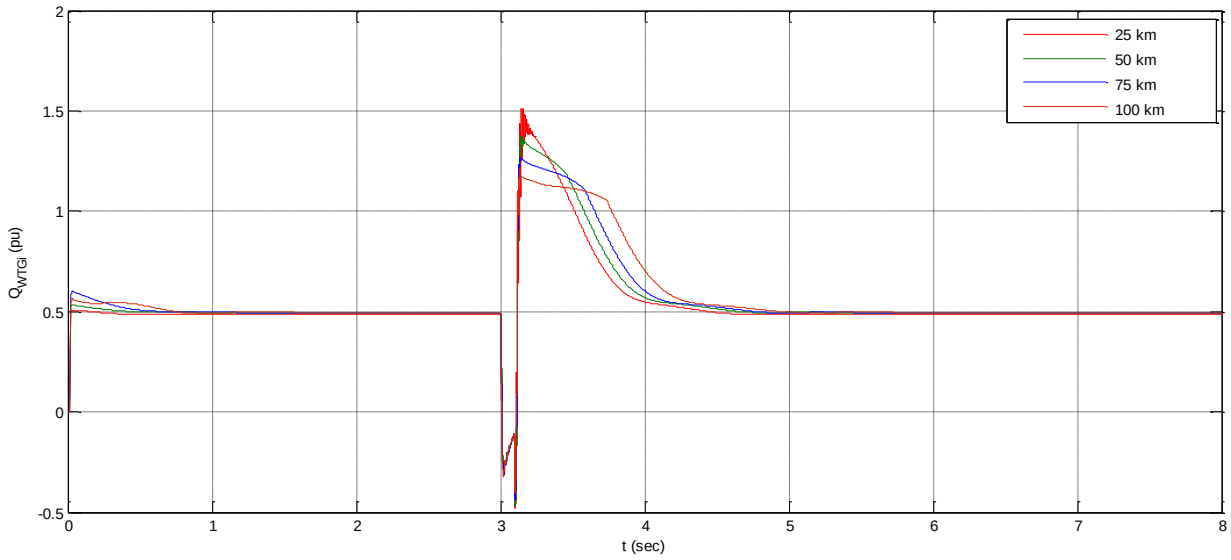

Figure 111: WTG reactive power for a fault duration of 0.1 sec and different line lengths

The system responses, at first glance, show that the line length increase is proportional to a corresponding decrease in the system stability, i.e. the CCT. Apart from that, the responses exhibit similar behavior, i.e., analogous dips, oscillations, etc.

7.6.3. Critical Clearing Time Dependence on Connection Line Length

The CCT for each of the line lengths simulated is presented in the following table:

Table 14: CCT for different line lengths

Line Length (km)	CCT (ms)
25	223
50	182
75	154
100	133

The relationship between the line length and the CCT is further examined in the plot below, where CCTs for the test model (with the STATCOM connected) were recorded, varying the line length from 20 km to 100 km and with a step size of 5 km.

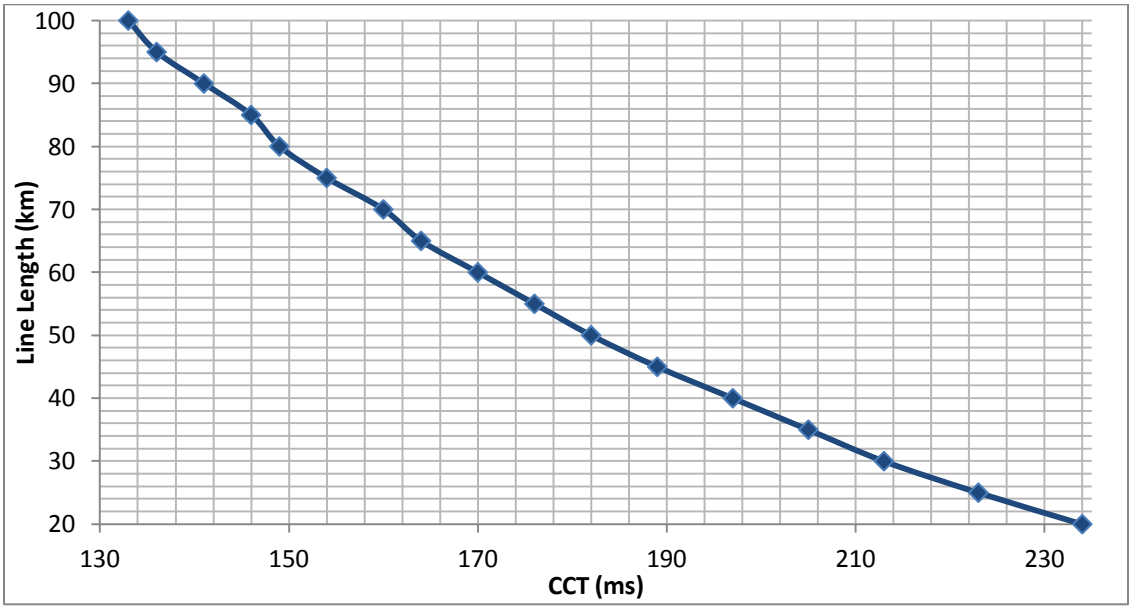

Figure 112: Line length vs CCT characteristic

The plot verifies that the line length and the CCT exhibit an inversely proportional relationship. For larger values of line lengths the slope of this characteristic increases a bit, which means that in this range, the same line length increase reduces the CCT by a smaller value than it would for line lengths of 20-60 km.

The distribution network voltage level is also a factor that influences the slope of the characteristic of figure 112. As shown in [47], this difference in the slope is more apparent

for lower distribution levels, for example, 10 kV, where, in general, the deterioration of the wind farm CCT is much worse.

7.7. Additional Fault Studies

In this section, at attempt to further investigate the system fault behavior is made, by the simulation of faults at different points of the system, or by connecting the STATCOM at a different point. For the simulations of this section, only the test model is evaluated.

7.7.1. STATCOM behind the transmission line

The PCC fault with a clearing time of 150 ms is examined again in this part, assuming that the STATCOM is removed from the PCC and is reconnected behind the transmission line (i.e. between the transmission line TL2 and the transformer T2). The test model responses are compared with the case of the same fault when the STATCOM is connected at the PCC.

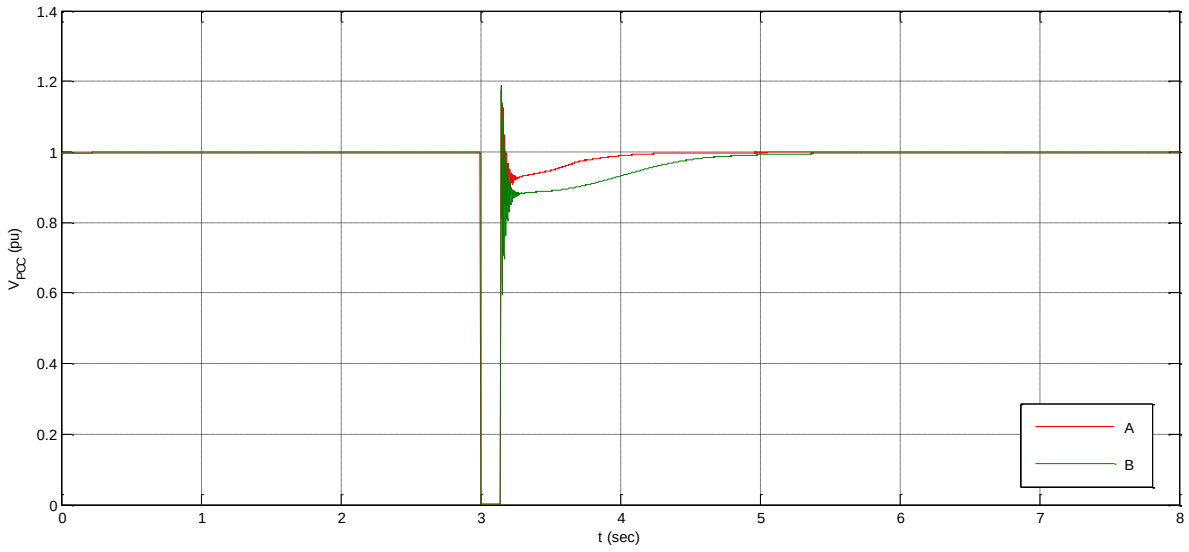

Figure 113: V_{PCC} for fault duration of 150 ms, A) STATCOM at PCC, B) STATCOM behind the transmission line

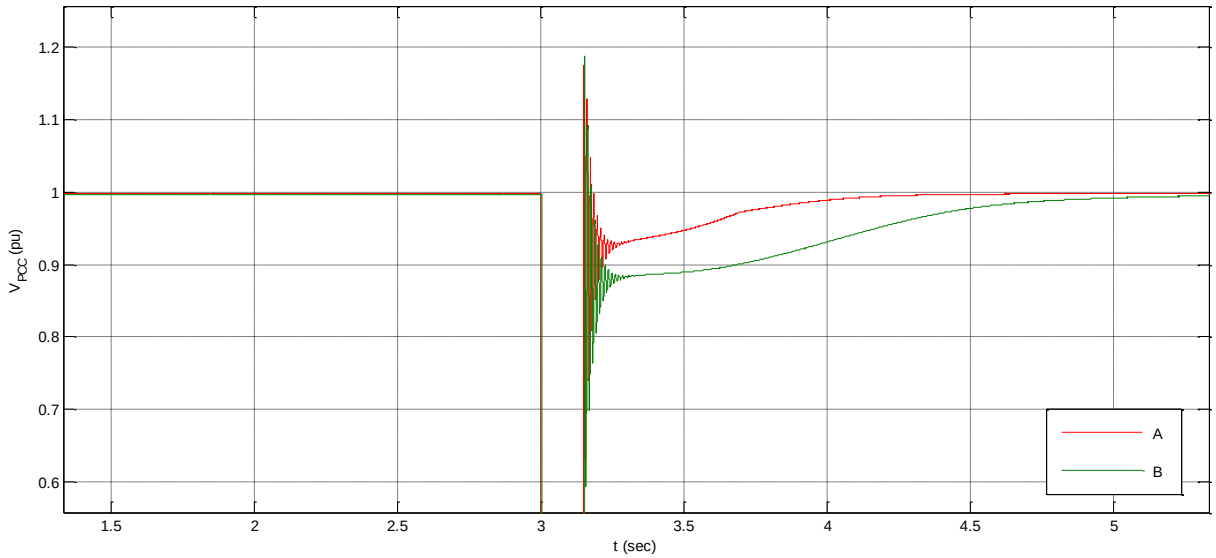

Figure 114: V_{PCC} for fault duration of 150 ms (zoomed), A) STATCOM at PCC, B) STATCOM behind the transmission line

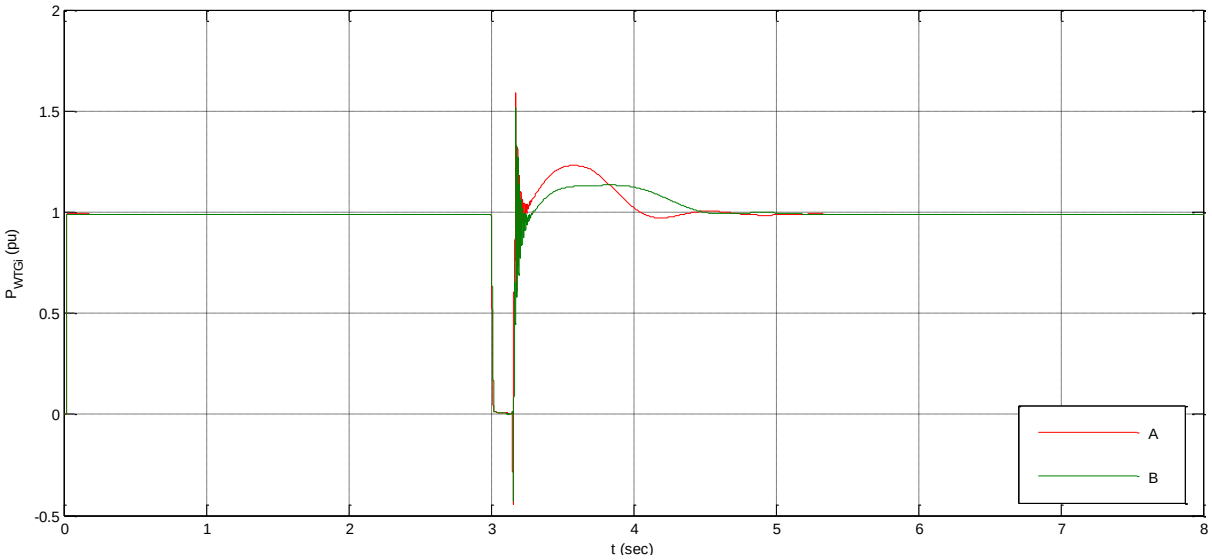

Figure 115: WTG active power for fault duration of 150 ms, A) STATCOM at PCC, B) STATCOM behind the transmission line

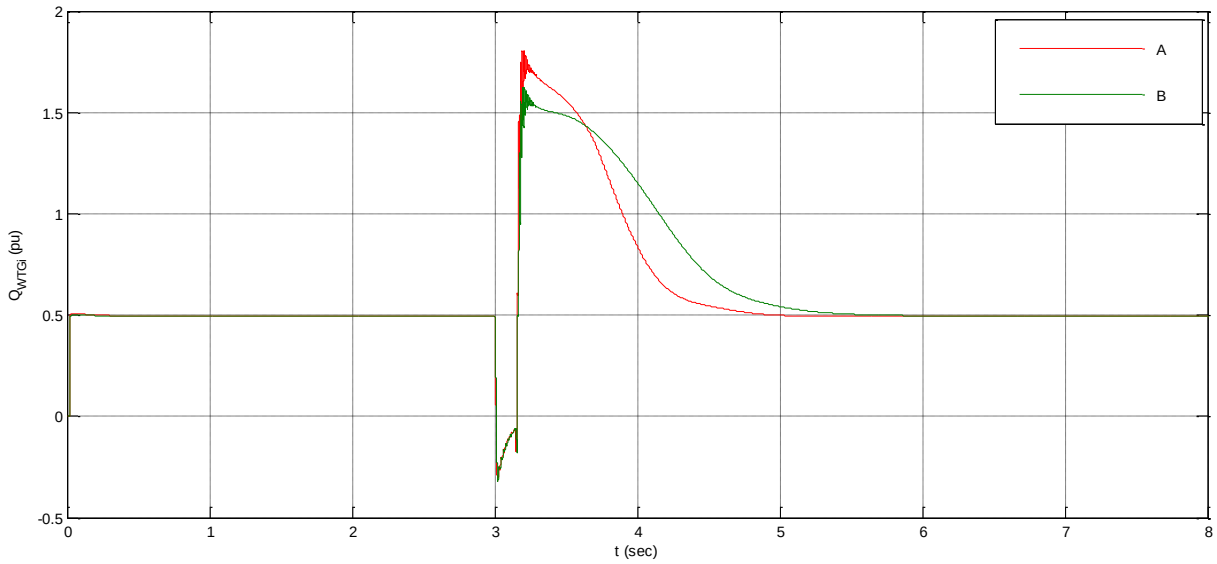

Figure 116: WTG reactive power for fault duration of 150 ms (zoomed), A) STATCOM at PCC, B) STATCOM behind the transmission line

The analogy between the responses of each case is clear. In figure 114, specifically, the zoomed in response indicates that the voltage oscillates at the same frequency and for an almost equal time interval. The STATCOM point of connection, thus, does not alter the system fault behavior, although the fault is damped faster when the STATCOM is connected at the PCC. This is reasonable, as the reactive compensation is not as instant as in the case where the fault occurred at the STATCOM terminals.

The CCT in this case is 195 ms versus the 223 ms when the STATCOM was connected at the PCC.

7.7.2. Fault Terminal

The already examined case of a three-phase-to-ground fault at the PCC is compared here with corresponding faults at different points of the system; first, at the point behind the transmission line (between transmission line TL2 and transformer T2), and, second, at the middle WTG terminals (WTG2). The STATCOM is connected at the PCC and the faults simulated are cleared after 100 ms.

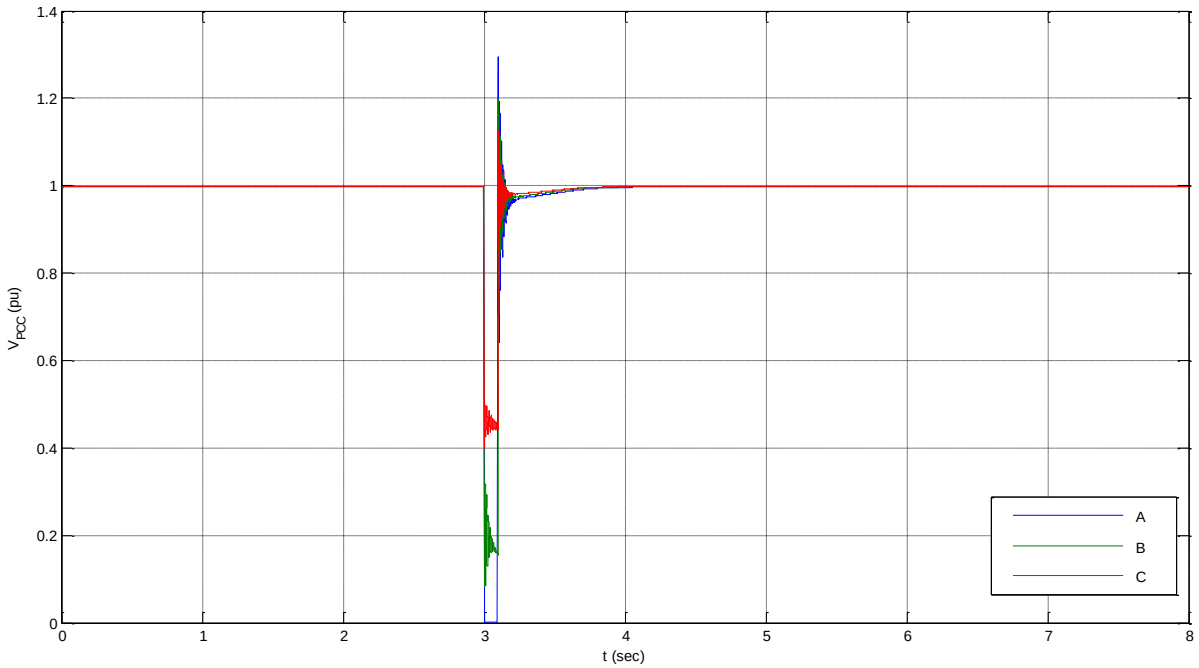

Figure 117: V_{PCC} of test model with STATCOM at PCC, A) Fault at PCC, B) Fault behind the transmission line, C) Fault at WTG2 terminals

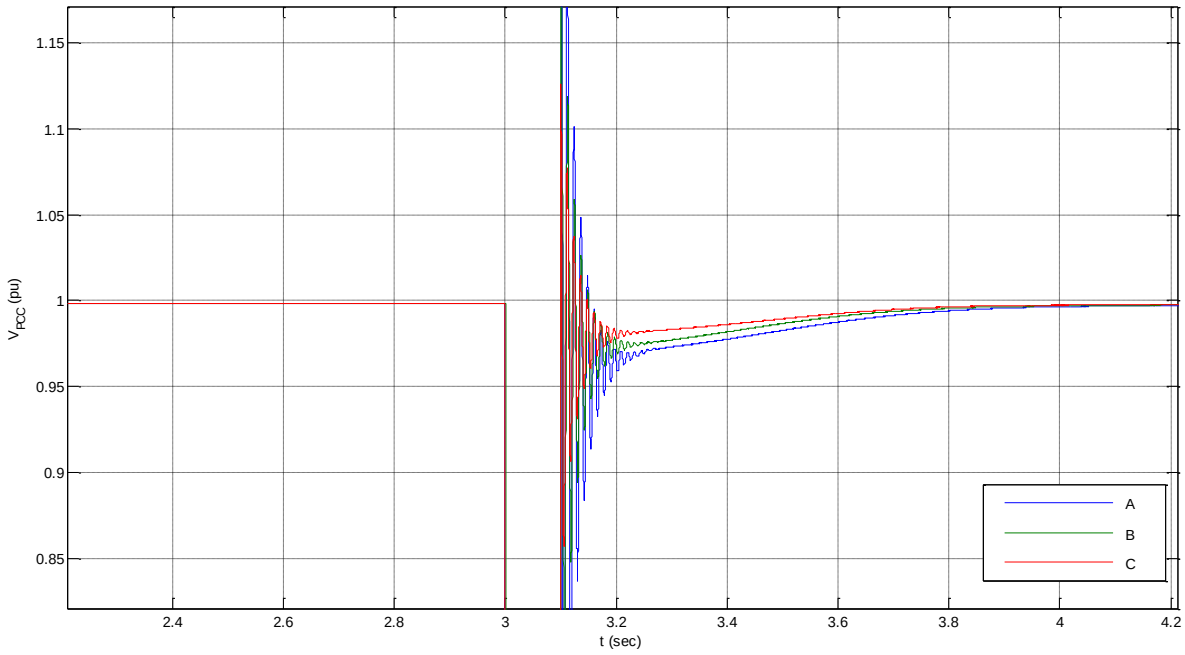

Figure 118: V_{PCC} of test model with STATCOM at PCC (zoomed), A) Fault at PCC, B) Fault behind the transmission line, C) Fault at WTG2 terminals

From the wind farm PCC voltage outputs, we see that the most threatening case for the voltage stability is the fault at the PCC, as expected, as the PCC constitutes the most vulnerable point of a wind farm installation. Following that, the fault behind the transmission line causes a voltage dip to approximately 0.18 per unit, less severe that the fault at PCC as the specific network point is more robust, but still noticeable. Finally, the fault at Wind Turbine 2 terminals results in a voltage dip to 0.42 per unit, the smallest one, as only one wind turbine is affected and can be isolated.

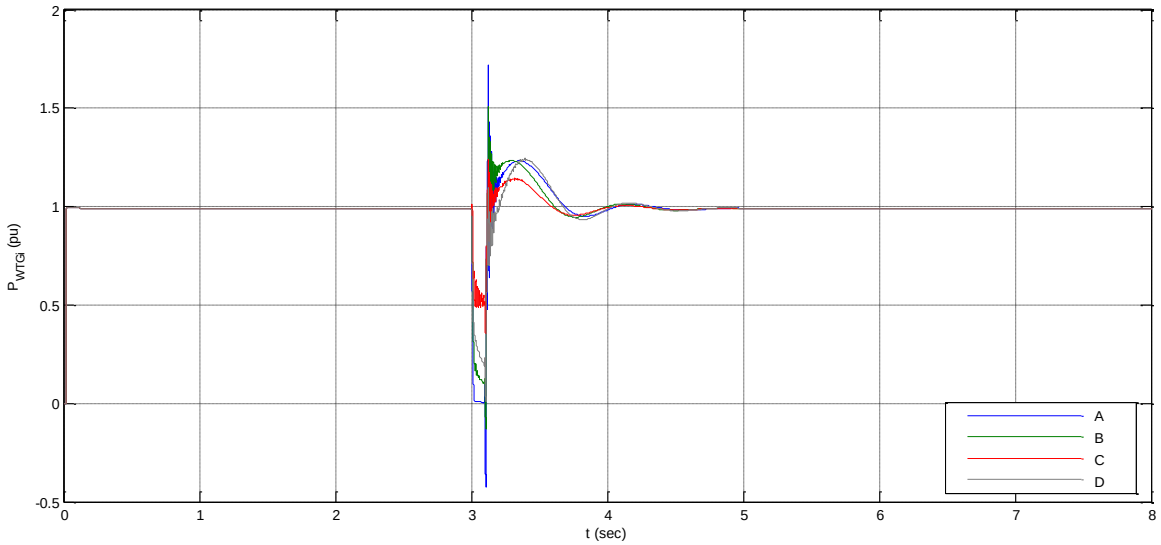

Figure 119: WTG active power of test model with STATCOM at PCC, A) Fault at PCC, B) Fault behind the transmission line, C) Fault at WTG2 terminals, WTG 1 and 3 active power output, D) Fault at WTG2 terminals, WTG 2 active power output

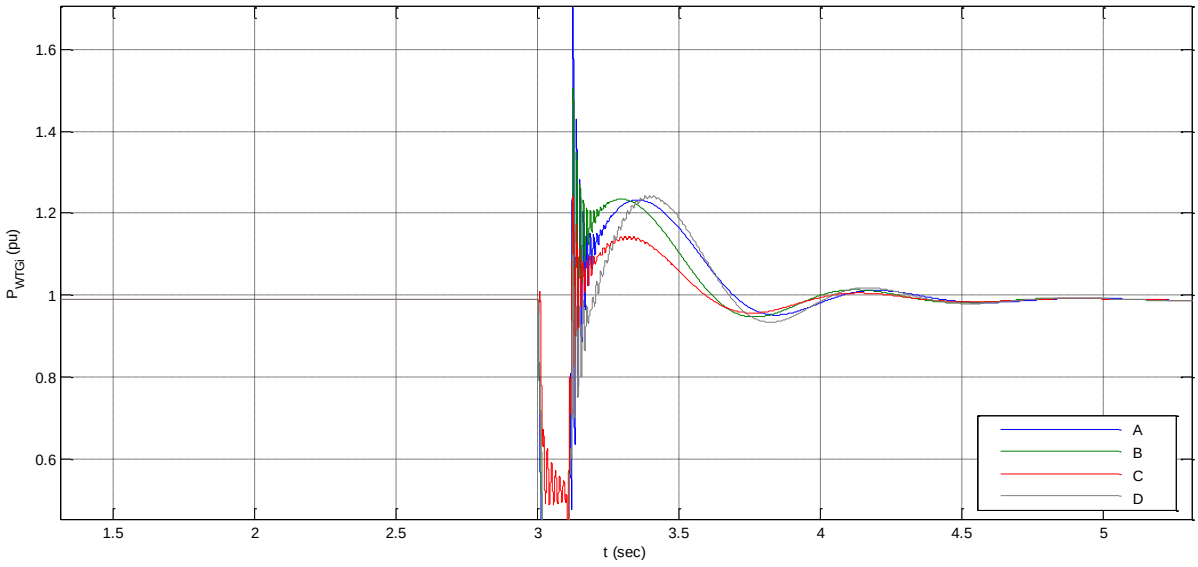

Figure 120: WTG active power of test model with STATCOM at PCC (zoomed), A) Fault at PCC, B) Fault behind the transmission line, C) Fault at WTG2 terminals, WTG 1 and 3 active power output, D) Fault at WTG2 terminals, WTG 2 active power output

The active power generation is also reduced to zero only for the fault at the PCC. The fault behind the transmission line results in a drop in each of the wind turbines active power generation to approximately 0.1 per unit. When the fault occurs to the Wind Turbine 2 terminals, the active power response of that turbine is, naturally, afflicted more that the other two; however, the impact is still less severe than in cases A and B. The active power generation of Wind Turbine 2 is reduced to approximately 0.2 per unit, while for the other two is halved. The oscillations that follow the fault exhibit a conspicuously similar pattern, with the Wind Turbine 2 to oscillate with the higher amplitude and with a larger damp time interval.

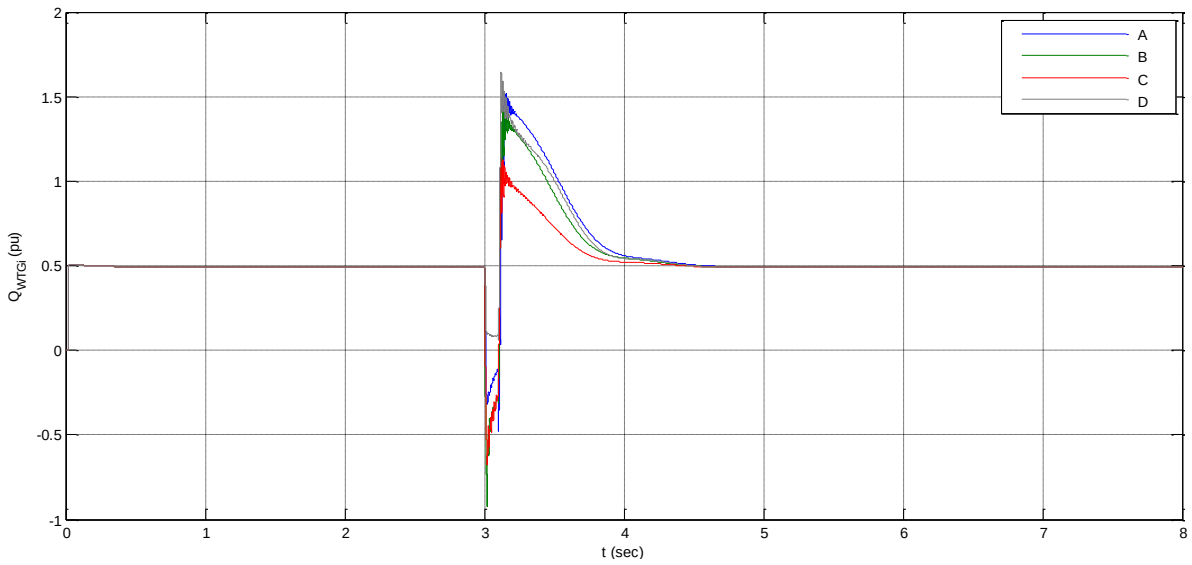

Figure 121: WTG reactive power of test model with STATCOM at PCC, A) Fault at PCC, B) Fault behind the transmission line, C) Fault at WTG2 terminals, WTG 1 and 3 reactive power output, D) Fault at WTG2 terminals, WTG 2 reactive power output

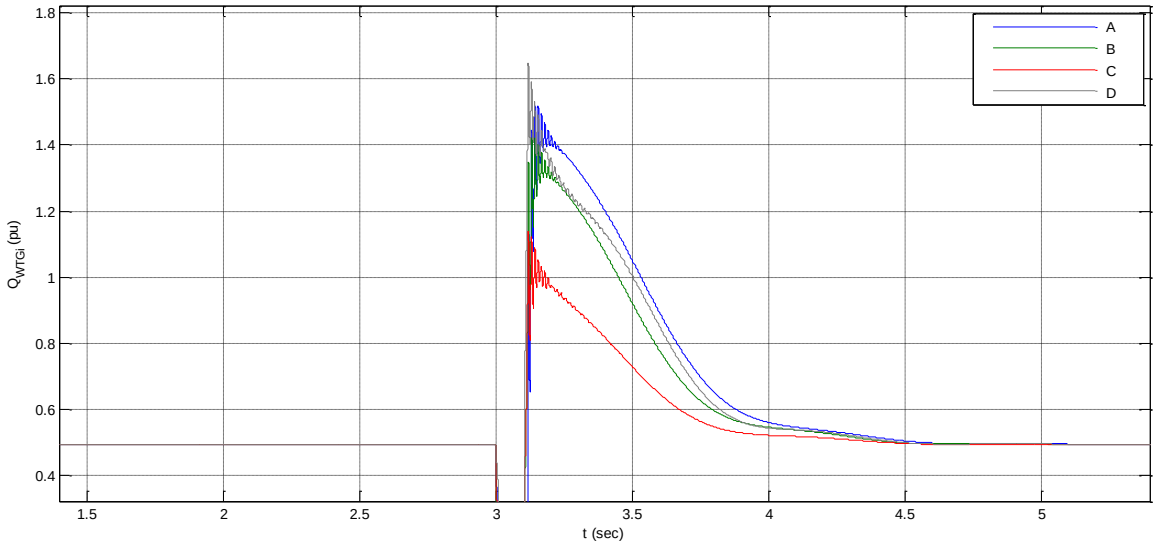

Figure 122: WTG reactive power of test model with STATCOM at PCC (zoomed), A) Fault at PCC, B) Fault behind the transmission line, C) Fault at WTG2 terminals, WTG 1 and 3 reactive power output, D) Fault at WTG2 terminals, WTG 2 reactive power output

The reactive power responses are in accordance with the aforementioned. The highest reactive demands correspond to the PCC fault, as well as to the WTG2 terminal fault for the generator 2, reaching a peak of 1.62 per unit. The peak demand for the WTG1 and WTG3 is 1.5 per unit, while for the fault behind the transmission line each WTG peaks its reactive demand at 1.2 per unit.

Overall, despite the differences spotted, all the faults are tackled quite effectively. That accounts for the small fault clearing time, but also for the STATCOM reactive compensation. The faults are damped within approximately the same time interval.

The CCTs for each case is shown in table 14.

Table 15: CCT for different fault terminals

Fault Terminals	CCT (ms)
PCC	223
Behind the transmission line	245
WTG2 terminals	308 (for WTG2 instability)

It has to be noted that the CCT for the fault at the WTG2 terminals is determined as the maximum clearing time that WTG2 remains stable. That is because it assumed that WTG2 will be disconnected by its undervoltage protection before the fault effects are spread to the rest of the system.

7.8. Result Summarization

In this section, the CCTs of each case examined are summarized to facilitate comparisons between them.

Table 16: CCTs for all cases examined

Model Used	Case Examined	CCT (ms)
Test Model	PCC fault	186
Test Model	PCC fault, STATCOM connected at the PCC	223
Test Model with Two-Mass Mechanical Representation	PCC fault	140
Test Model	PCC fault, WT modified pitch controller	203
Test Model	PCC fault, WT modified pitch controller and STATCOM connected at the PCC	245
Test Model	PCC fault, STATCOM connected behind the transmission line	195
Test Model	Fault behind the transmission line, STATCOM connected at the PCC	245
Test Model	Fault at WTG2 terminals, STATCOM connected at the PCC	308 (for WTG2)
Generic Model	PCC fault	124
Generic Model	PCC fault, STATCOM connected at the PCC	169
Generic Model	PCC fault, WT modified pitch controller	156
Generic Model	PCC fault, WT modified pitch controller and STATCOM connected at the PCC	229

The test model's CCT for a PCC fault is boosted by 19.98 % with the STATCOM, by 9.14% with the modified pitch controller and 31.72 % with the coordinated control of both. It is notable that the CCT expansion in the case of the coordinated control exceeds the sum of the other two. The use of the two-mass mechanical model in the test model results in a CCT attenuation of 24.73 %, a particularly large value that highlights the importance of selecting the system's mechanical representation based on the simulation needs.

As far as the generic model is concerned, the CCT is bolstered by 36.29 % with the STATCOM connected, 25.81% with the modified pitch controller and 84.68 % with the coordinated control of both. The STATCOM boost is larger than in the test model, as apart from the reactive support, the two-mass mechanical oscillations are also damped. The coordinating control's boost is especially high (84.68 %), a fact that shows the significance of the application of this control in fixed-speed technologies, although more tests should be performed regarding this alternative aerodynamic model that was used for the generic model implementation, to validate the results.

8. Conclusions and Future Work

In this thesis, the dynamic behavior of a wind farm comprising fixed-speed induction generators was studied. In addition to the test model, the corresponding for the case generic model was also developed, as well as a STATCOM, in order to provide addition reactive support. The STATCOM used an average converter model, while emphasis was given on its control system, which was constructed based on the decoupled active and reactive power control through the dq0 transformation. Wind turbine aerodynamic control was also performed on the test model by means of a pitch controller and the simulated wind speed changes showed that control was efficient for a wide range of wind speeds.

The system fault behavior was evaluated with the simulation of various fault cases. The comparison with the generic model showed that the one-mass mechanical model provides quite optimistic results and therefore, is not recommended for fault studies. Letting this alone, the test model mirrored the generic model well enough, as validated with the simulation during which, the two-mass mechanical model was used for the test model.

The impact of the STATCOM was notable, as the CCTs for both models were extended and the faults were damped quicker and smoother. For the generic model, especially, the CCT boost was even higher, as apart from the reactive support, the torsional oscillations of the two-mass mechanical model were also assuaged.

Changing the pitch controller reference from active power to WTG rotational speed gave the pitch controller an active role in the fault damping process. The coordinated control of this pitch controller and the STATCOM significantly boosted the wind farm's LVRT capability, making it able to satisfy the grid code requirements of many European

countries. However, the fact the in this case, an alternative aerodynamic model was used for the generic model may raise a reservation for its validity, at least for the specific model.

The additional fault studies completed the wind farm's fault behavior profile. It was shown that the LVRT capability of the system is highly influenced by the grid connection line length, which renders the wind generation requirements in remote locations, even stricter. Different fault-occurring system points or alternative STATCOM connection point displayed which system parts were more sensitive than the others, with the Point of Common Connection being the most vulnerable.

Overall, it was concluded that the generic models are fulfilling their purpose and probably very soon there will be official models, representing effectively any wind turbine's dynamic behavior. Furthermore, the nature of the fixed-speed wind turbine and its susceptibility in mechanical strains, leads to the conclusion that the use of a STATCOM and/or the pitch controller with rotational speed as reference, is deemed necessary, especially if the farm is located in a weak system point.

As future work, a similar study of the dynamic behavior of the other wind turbine types could be performed, with the parallel corresponding generic model implementation, especially for the types 3 and 4, which constitute the more commercial types today. Moreover, the contribution of the STATCOM could be further examined by comparing the results with alternative control systems. Section 5.3.4 can serve as a guideline for this kind of work. Finally, to complete the system's fault behavior profile, different fault types could be simulated, e.g. two-phase faults.

Appendix

A. Space Phasors and Two-Dimensional Frames

1. Space-Phasor Representation of a Balanced Three-Phase Function

Consider the following balanced, three-phase, sinusoidal function:

$$f_a(t) = \hat{f}\cos(\omega t + \theta_0)$$
$$f_b(t) = \hat{f}\cos\left(\omega t + \theta_0 - \frac{2\pi}{3}\right) \quad \text{(A.1)}$$
$$f_c(t) = \hat{f}\cos\left(\omega t + \theta_0 - \frac{4\pi}{3}\right)$$

where $\hat{f}$, θ_0 and ω are the amplitude, the initial phase angle and the angular frequency of the function, respectively. For the sinusoidal function (A.1) the space vector is defined as

$$\overrightarrow{f(t)} = \frac{2}{3}\left[e^{j0}f_a(t) + e^{j\frac{2\pi}{3}}f_b(t) + e^{j\frac{4\pi}{3}}f_c(t)\right] \quad \text{(A.2)}$$

Substituting for f_{abc} from (A.1) in (A.2) and using the identities $\cos\theta = \frac{1}{2}\left(e^{j\theta} + e^{-j\theta}\right)$ and $e^{j0} + e^{j\frac{2\pi}{3}} + e^{j\frac{4\pi}{3}} \equiv 0$, one obtains:

$$\overrightarrow{f(t)} = \left(\hat{f}e^{j\theta_0}\right)e^{j\omega t} = \underline{f}e^{j\omega t} \quad \text{(A.3)}$$

where $\underline{f} = \hat{f}e^{j\theta_0}$. The complex quantity $\underline{f}$ can be represented by a vector in the complex plane. If $\underline{f}$ is a constant, the vector is analogous to the conventional phasor that is used to analyze linear circuits under steady-state sinusoidal conditions, and the tip of $\overrightarrow{f(t)}$ moves along the circumference of a circle centered at the complex plane origin (figure 123). Based on (A.3), the space phasor $\overrightarrow{f(t)}$ is the same phasor $\underline{f}$ that rotates counterclockwise with the angular speed ω. It should be noted that $\overrightarrow{f(t)}$ retains the form expressed by (A.3) even if $\hat{f}$ is not a constant; if $\hat{f}$ is a function of time, the corresponding phasor $\underline{f}$ is also a complex-valued function of time.

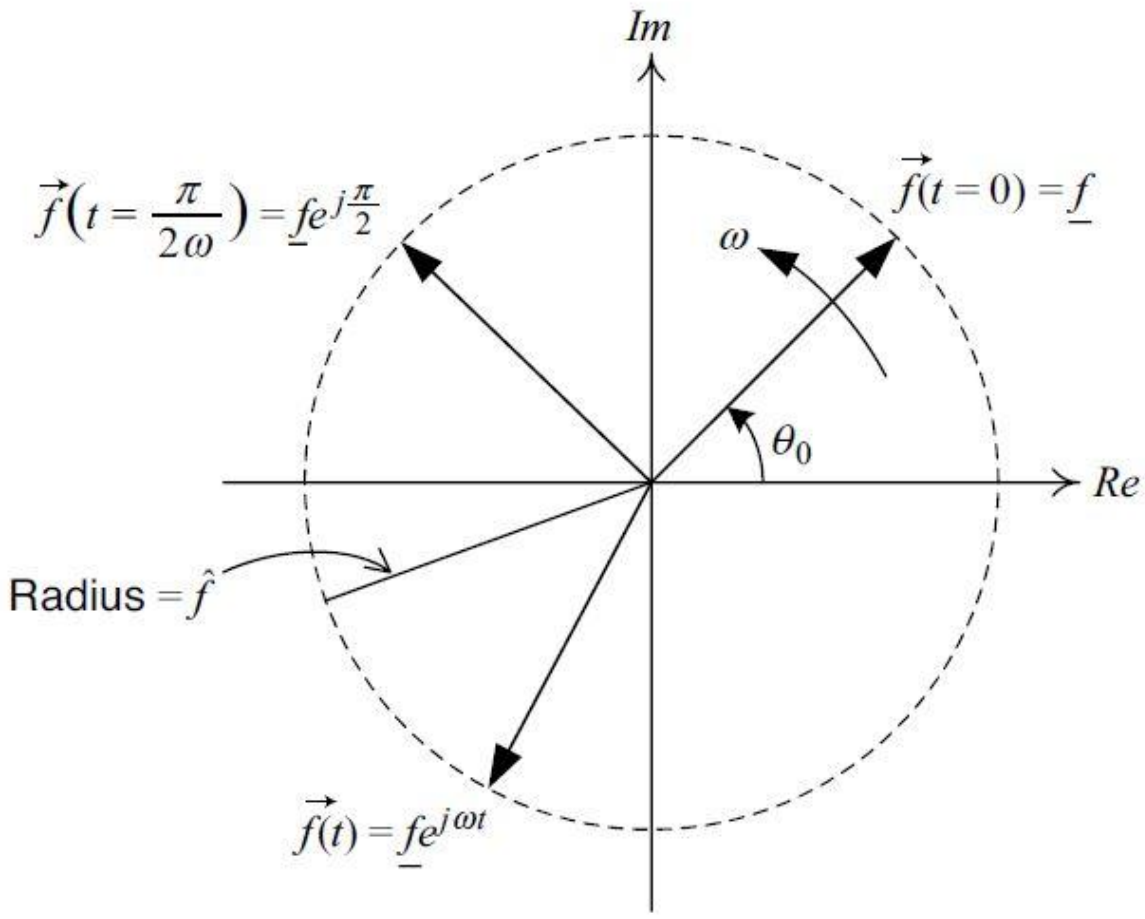

Figure 123: Space-phasor representation in the complex plane

2. dq0 transform

In Appendix A.1, it was demonstrated that every sinusoidal function of time can be represented by a vector in a stationary coordinate plane. The vector rotates counterclockwise with angular velocity ω. If we imagine, that the same vector is expressed in a coordinate system that is not stationary, but, instead, rotates itself counterclockwise with angular velocity ω, then vector $\overrightarrow{f(t)}$, would be stationary in reference to that coordinate system, in other words a DC quantity. This is idea behind the dq0 transform, which significantly simplifies the analysis of electrical variables, as they commonly have the same angular velocity. The rotating Real axis is the d-axis and the rotating imaginary axis the q-axis. A zero-axis component exists only in asymmetrical conditions.

The dq0 coordinates are calculated as follows:

$$\begin{bmatrix} f_d \\ f_q \\ f_0 \end{bmatrix} = [T] \begin{bmatrix} f_a \\ f_b \\ f_c \end{bmatrix} \tag{A.4}$$

where [T] is the transformation matrix and

$$[T] = \frac{2}{3} \begin{bmatrix} \cos\Theta & \cos\left(\Theta - \frac{2\pi}{3}\right) & \cos\left(\Theta + \frac{2\pi}{3}\right) \\ -\sin\Theta & -sin\left(\Theta - \frac{2\pi}{3}\right) & -sin\left(\Theta + \frac{2\pi}{3}\right) \\ \frac{1}{\sqrt{2}} & \frac{1}{\sqrt{2}} & \frac{1}{\sqrt{2}} \end{bmatrix} \tag{A.5}$$

where $\Theta = \omega t + \varphi_0$, ω the desired angular velocity and ϕ_0 is the angle between the d- and the a-axis. The inverse dq0 transform is expressed as:

$$\begin{bmatrix} f_a \\ f_b \\ f_c \end{bmatrix} = [T]^{-1} \begin{bmatrix} f_a \\ f_b \\ f_c \end{bmatrix} \tag{A.6}$$

where

$$[T]^{-1} = \begin{bmatrix} \cos\Theta & -\sin\Theta & \frac{1}{\sqrt{2}} \\ \cos\left(\Theta - \frac{2\pi}{3}\right) & -sin\left(\Theta - \frac{2\pi}{3}\right) & \frac{1}{\sqrt{2}} \\ \cos\left(\Theta + \frac{2\pi}{3}\right) & -sin\left(\Theta + \frac{2\pi}{3}\right) & \frac{1}{\sqrt{2}} \end{bmatrix} \tag{A.7}$$

Taking into account equation (A.1), we get:

$$f_d = \frac{2}{3} \hat{f} \left[\cos\Theta \quad \cos\left(\Theta - \frac{2\pi}{3}\right) \quad \cos\left(\Theta + \frac{2\pi}{3}\right)\right] \begin{bmatrix} \cos\theta \\ \cos\left(\theta - \frac{2\pi}{3}\right) \\ \cos\left(\theta - \frac{2\pi}{3}\right) \end{bmatrix} \tag{A.8}$$

In the latter equation, $\theta = \omega t + \theta_0$. With further manipulation and using the identities

$$\cos\left(\theta - \frac{2\pi}{3}\right) = \frac{-\cos\theta + \sqrt{3}\sin\theta}{2}$$
$$\cos\left(\theta + \frac{2\pi}{3}\right) = \frac{-\cos\theta - \sqrt{3}\sin\theta}{2} \quad \text{(A.9)}$$

we get:

$$f_d = \frac{2}{3}\hat{f}\cdot\frac{3}{2}(\cos\Theta\cos\theta + \sin\Theta\sin\theta) = \hat{f}\cos(\Theta - \theta)$$
$$= \hat{f}\cos(\varphi_0 - \theta_0) \quad \text{(A.10)}$$

Similarly, for the q-component, we get:

$$f_q = \hat{f}\cos(\varphi_0 - \theta_0) \quad \text{(A.11)}$$

Thus, the idea behind the dq0 transformation that the transformed variables are reduced to time-invariant (DC) quantities, is also validated mathematically.

3. Power in the dq0 Coordinate System

Let us assume that $\tilde{V}_{dq}$ and $\tilde{I}_{dq}$ are the voltage and current vectors at a point of a symmetrical three-phase circuit, expressed in the dq0 components. Then:

$$\tilde{V}_{dq} = v_d + jv_q \quad \text{(A.12)}$$

$$\tilde{I}_{dq} = i_d + ji_q \quad \text{(A.13)}$$

The rms value of the complex power is therefore calculated as:

$$S = 3\frac{\tilde{V}_{dq}}{\sqrt{2}}\frac{\tilde{I}^*_{dq}}{\sqrt{2}} = \frac{3}{2}\tilde{V}_{dq}\tilde{I}^*_{dq}$$
$$= \frac{3}{2}(v_d i_d + v_q i_q) + j\frac{3}{2}(v_q i_d + v_d i_q) \quad \text{(A.14)}$$

which leads us to define real and reactive power in the dq0 coordinates as:

$$P = \frac{3}{2}\left(v_d i_d + v_q i_q\right) \tag{A.15}$$

$$Q = \frac{3}{2}\left(v_q i_d + v_d i_q\right) \tag{A.16}$$

4. Stationary Circuit Variables Transformed to the Arbitrary Reference Frame

4.1. Resistive Elements

The voltage and current relationship for the resistance in the dq frame is simply given by the following equations:

$$\begin{aligned} v_d(t) &= R \cdot i_d(t) \\ v_q(t) &= R \cdot i_q(t) \end{aligned} \tag{A.17}$$

4.2. Inductive Elements

The voltage and current relationship for the inductance in the dq frame is given by the following equations:

$$\begin{aligned} v_d(t) &= L\frac{di_d(t)}{dt} - \omega L i_q(t) \\ v_q(t) &= L\frac{di_q(t)}{dt} + \omega L i_d(t) \end{aligned} \tag{A.18}$$

where ω is the reference frame rotating speed.

4.3. Capacitive Elements

The voltage and current relationship for the capacitance in the dq frame is given by the following equations:

$$\begin{aligned} i_d(t) &= C\frac{dv_d(t)}{dt} - \omega C v_q(t) \\ i_q(t) &= C\frac{dv_q(t)}{dt} + \omega C v_d(t) \end{aligned} \tag{A.19}$$

where ω is the reference frame rotating speed.

B. Park's Transformation in Induction Machine Analysis

In the late 1920s, R. H. Park introduced a new approach to electric machine analysis, where the stator variables were referred to a frame of reference fixed in a synchronous machine rotor. Park's transformation eliminated time-varying inductances from the voltage equations of the synchronous machine, which in turn simplified synchronous machine analyses and calculations.

Park's transformation initiated a new way of dealing with time-varying variables and these were later introduced to induction machine analysis by H. C. Stanley. Today, general transformation techniques based on the Park's transformation are being used for different types of power system studies.

Let us consider the windings of a three-phase, 3-pole, wye-connected induction machine, as depicted in figure 124.

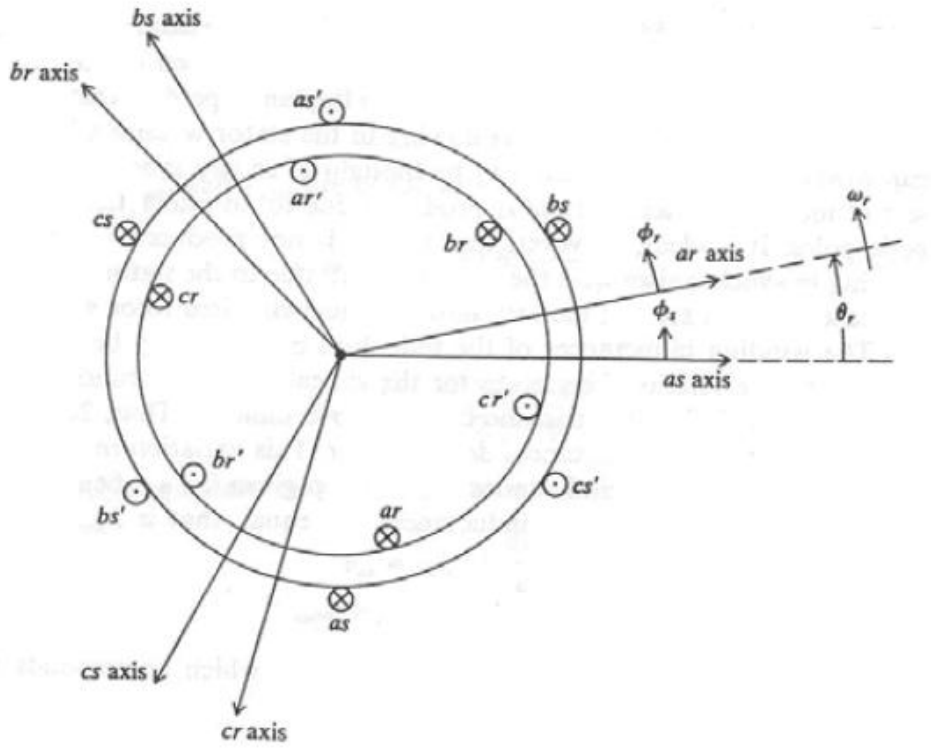

Figure 124: Three-phase, three-pole, wye-connected induction machine

The stator windings are identical with N_s turns and resistance r_s. With the same convention, the rotor winding can also be described by N_r identical turns and r_r resistance. The air gap is assumed to be uniform, so the stator self-inductances are equal:

$$L_{asas} = L_{bsbs} = L_{cscs} = L_{ls} + L_{ms} \tag{B.1}$$

The same applies for the stator mutual inductances and the rotor self-inductances.

The voltage equations for the machine of figure 124 are:

$$\begin{bmatrix} V_{as} \\ V_{bs} \\ V_{cs} \end{bmatrix} = r_s \begin{bmatrix} i_{as} \\ i_{bs} \\ i_{cs} \end{bmatrix} + \frac{d}{dt} \begin{bmatrix} \varphi_{as} \\ \varphi_{bs} \\ \varphi_{cs} \end{bmatrix}$$

$$\begin{bmatrix} V_{ar} \\ V_{br} \\ V_{cr} \end{bmatrix} = r_s \begin{bmatrix} i_{ar} \\ i_{br} \\ i_{cr} \end{bmatrix} + \frac{d}{dt} \begin{bmatrix} \varphi_{ar} \\ \varphi_{br} \\ \varphi_{cr} \end{bmatrix} \tag{B.2}$$

The linkage fluxes are expressed in forms similar to that of φ_{as}, namely:

$$\varphi_{as} = L_{asas} i_{as} + L_{asbs} i_{bs} + L_{ascs} i_{cs} + L_{asar} i_{ar} + L_{arbr} i_{br} + L_{arcr} i_{cr} \tag{B.3}$$

The complexity of equations B.2 because of the dependence of the mutual inductances between the stator and the rotor, which are in relative motion, makes the machine analysis a quite arduous task. By applying the Park transformation, this obstacle is surpassed.

During the analysis of an asynchronous machine, the following circuits appear:

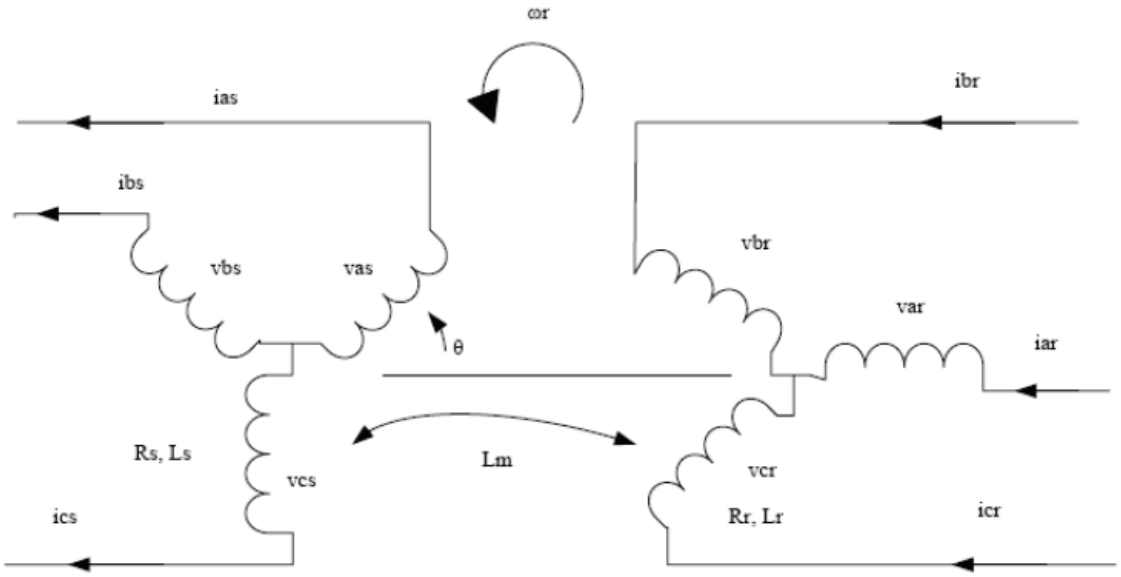

Figure 125: Stator and rotor circuit of an ansynchronous machine

The stator circuit is composed of the three-phase windings as, bs and cs, distributed by 120° of each other. Respectively, ar, br and cr are the rotor windings. θ is the angle by which the ar axis leads the as axis by the direction of the rotation. With constant angular velocity ω_r (rad/s), we have:

$$\theta = \omega_r t \tag{B.4}$$

Also, if s is the slip (constant) and ω_s is the angular velocity (rad/s) of the stator field, equation (B.4) is written as:

$$\theta = (1 - s)\omega_s t \tag{B.5}$$

The Park transformation is essentially the dq0 transformation described in Appendix A.2. Choosing the rotating angle to be θ, we manage to eliminate all the time-varying inductances in the machine voltage equations. The transformation matrix for the stator and the rotor equations respectively, are:

$$[T_s] = \sqrt{\frac{2}{3}}\begin{bmatrix} \cos\theta & \cos\left(\theta - \frac{2\pi}{3}\right) & \cos\left(\theta + \frac{2\pi}{3}\right) \\ \sin\theta & \sin\left(\theta - \frac{2\pi}{3}\right) & \sin\left(\theta + \frac{2\pi}{3}\right) \\ \frac{1}{\sqrt{2}} & \frac{1}{\sqrt{2}} & \frac{1}{\sqrt{2}} \end{bmatrix} \tag{B.6}$$

$$[T_r] = \sqrt{\frac{2}{3}}\begin{bmatrix} \cos s\theta & \cos\left(s\theta - \frac{2\pi}{3}\right) & \cos\left(s\theta + \frac{2\pi}{3}\right) \\ \sin s\theta & \sin\left(s\theta - \frac{2\pi}{3}\right) & \sin\left(s\theta + \frac{2\pi}{3}\right) \\ \frac{1}{\sqrt{2}} & \frac{1}{\sqrt{2}} & \frac{1}{\sqrt{2}} \end{bmatrix} \quad \text{(B.7)}$$

where $\theta = \omega_e t$ and ω_e is the electrical angular velocity ($\omega_e = 2\pi f$). The constant $\sqrt{\frac{2}{3}}$ has been chosen so that the expressions for the real and reactive power in the abc and dq frame are the same. In addition, the constant $\frac{1}{\sqrt{2}}$ has been chosen so that $T_s^{-1} = T_s^T$ and analysis is facilitated even more. Indeed:

$$T_s^{-1} = T_s^T = \sqrt{\frac{2}{3}}\begin{bmatrix} \cos\theta & \sin\theta & \frac{1}{\sqrt{2}} \\ \cos\left(\theta - \frac{2\pi}{3}\right) & \sin\left(\theta - \frac{2\pi}{3}\right) & \frac{1}{\sqrt{2}} \\ \cos\left(\theta + \frac{2\pi}{3}\right) & \sin\left(\theta + \frac{2\pi}{3}\right) & \frac{1}{\sqrt{2}} \end{bmatrix} \quad \text{(B.8)}$$

Using the stator transformation matrix, the stator voltage equations are written as:

$$\begin{bmatrix} V_{qs} \\ V_{ds} \end{bmatrix} = [T_s]\begin{bmatrix} V_{as} \\ V_{bs} \\ V_{cs} \end{bmatrix} = R_s[T_s]\begin{bmatrix} i_{as} \\ i_{bs} \\ i_{cs} \end{bmatrix} + [T_s]\frac{d}{dt}\begin{bmatrix} \varphi_{as} \\ \varphi_{bs} \\ \varphi_{cs} \end{bmatrix}$$

$$= R_s[T_s]\begin{bmatrix} i_{as} \\ i_{bs} \\ i_{cs} \end{bmatrix} + [T_s]\frac{d}{dt}\left\{[T_s^{-1}]\begin{bmatrix} \varphi_{qs} \\ \varphi_{ds} \end{bmatrix}\right\}$$

$$= R_s\begin{bmatrix} i_{qs} \\ i_{ds} \end{bmatrix} + [T_s]\frac{d}{dt}\{[T_s^{-1}]\}\begin{bmatrix} \varphi_{qs} \\ \varphi_{ds} \end{bmatrix} + [T_s][T_s^{-1}]\frac{d}{dt}\begin{bmatrix} \varphi_{qs} \\ \varphi_{ds} \end{bmatrix}$$

$$\Rightarrow \begin{bmatrix} V_{qs} \\ V_{ds} \end{bmatrix} = R_s\begin{bmatrix} i_{qs} \\ i_{ds} \end{bmatrix} + [T_s]\frac{d}{dt}\{[T_s^{-1}]\}\begin{bmatrix} \varphi_{qs} \\ \varphi_{ds} \end{bmatrix} + \frac{d}{dt}\begin{bmatrix} \varphi_{qs} \\ \varphi_{ds} \end{bmatrix} \quad \text{(B.9)}$$

Differentiating equation (B.8) we get:

$$\frac{d}{dt}\{[T_s^{-1}]\} = \sqrt{\frac{2}{3}}\begin{bmatrix} -\omega_e \sin(\omega_e t) & \omega_e \cos(\omega_e t) \\ -\omega_e \sin\left(\omega_e t - \frac{2\pi}{3}\right) & \omega_e \cos\left(\omega_e t - \frac{2\pi}{3}\right) \\ -\omega_e \sin\left(\omega_e t + \frac{2\pi}{3}\right) & \omega_e \cos\left(\omega_e t + \frac{2\pi}{3}\right) \end{bmatrix} \quad \text{(B.10)}$$

so,

$$[T_s]\frac{d}{dt}\{[T_s^{-1}]\}\begin{bmatrix}\varphi_{qs}\\ \varphi_{ds}\end{bmatrix} = \omega_e \begin{bmatrix}0 & 1\\ -1 & 0\end{bmatrix}\begin{bmatrix}\varphi_{qs}\\ \varphi_{ds}\end{bmatrix} = \omega_e \begin{bmatrix}\varphi_{ds}\\ -\varphi_{qs}\end{bmatrix} \quad \text{(B.11)}$$

Substituting equation (B.11) to equation (B.9), we get:

$$\begin{bmatrix}V_{ds}\\ V_{qs}\end{bmatrix} = R_s\begin{bmatrix}i_{ds}\\ i_{qs}\end{bmatrix} + \omega_e\begin{bmatrix}-\varphi_{qs}\\ \varphi_{ds}\end{bmatrix} + \frac{d}{dt}\begin{bmatrix}\varphi_{ds}\\ \varphi_{qs}\end{bmatrix} \quad \text{(B.12)}$$

Following the same procedure, the rotor voltage equations are written:

$$\begin{bmatrix}V_{dr}\\ V_{qr}\end{bmatrix} = R_r\begin{bmatrix}i_{dr}\\ i_{qr}\end{bmatrix} + (\omega_e - \omega_r)\begin{bmatrix}-\varphi_{qr}\\ \varphi_{dr}\end{bmatrix} \quad \text{(B.13)}$$

C. The Per-Unit System

1. Three-phase Base Values

In most applications, it is common practice to express the machine and other electrical components variables in the per-unit system. First, the base power and voltage levels are selected, and then all the other base values are determined according to these. Usually, for the abc frame variables, the RMS value of the nominal phase or line-to-line voltage is selected as base value, while for the dq frame variables, the maximum voltage value is selected. If, for example, $V_{B(abc)}$ is the RMS value of the phase voltage and constitutes the base voltage for the abc quantities, the base voltage for the dq0 quantities would be:

$$V_{B\,(dq0)} = \sqrt{2}V_{B(abc)} \quad \text{(C.1)}$$

The base power is calculated as one of the following:

$$S_B = 3V_{B(abc)} \cdot I_{B(abc)} \quad \text{(C.2)}$$

$$S_B = \frac{3}{2}V_{B(dq0)} \cdot I_{B(dq0)} \quad \text{(C.3)}$$

The base value of the generator torque is defines as follows:

$$T_B = \frac{S_B}{\left(2/P\right)\omega_b} \tag{C.4}$$

where:

ω_b: base generator frequency

P: the number of generator poles

Since the base voltage and power have been determined, the base current is calculated from one of the previous equations. The base value of the resistance is calculated from the equations below:

$$Z_B = \frac{V_{B(abc)}}{I_{B(abc)}} = \frac{3{V_{B(abc)}}^2}{S_B} \tag{C.5}$$

$$Z_B = \frac{V_{B(dq0)}}{I_{B(dq0)}} = \left(\frac{3}{2}\right)\frac{{V_{B(dq0)}}^2}{S_B} \tag{C.6}$$

2. DC Base Values

If we work with DC variables in the per-unit system, the base values are selected as follows:

$$V_{B(DC)} = \sqrt{2}V_{B(abc)} \tag{C.7}$$

$$I_{B(DC)} = \sqrt{2}I_{B(abc)} \tag{C.8}$$

$$S_B = \frac{3}{2}V_{B(DC)}I_{B(DC)} \tag{C.9}$$

$$Z_B = \frac{V_{B(DC)}}{I_{B(DC)}} = Z_{B(abc)} \tag{C.10}$$

3. Mechanical System Base Values

Since the mechanical system variables for the generic model implementation were expressed in per-unit units, the base values for each of the variables used are documented in this section:

$$Base\ Inertia: \quad J_B = \frac{2S_B}{\omega_b^2} \tag{C.11}$$

$$Base\ Stiffness\ Coefficient: \quad k_B = \frac{T_B}{\omega_b} \tag{C.12}$$

$$Base\ Damping\ Factor: \quad c_B = \frac{T_B}{\omega_b} \tag{C.13}$$

To refer one of these variables to the low-speed side base quantities, the following equations are used:

$$\frac{n^1}{n^2} = \frac{\omega_b^1}{\omega_b^2} = \frac{T_B^2}{T_B^1} = \sqrt{\frac{J_B^2}{J_B^1}} = \sqrt{\frac{k_B^2}{k_B^1}} = \sqrt{\frac{c_B^2}{c_B^1}} \tag{C.14}$$

The superscripts 1 and 2 are associated with low- and high- speed variables, respectively.

Bibliography

[1] G. Kosmadakis, S. Karellas and E. Kakaras, "Renewable and Conventional Electricity Generation Systems: Technologies and Diversity of Energy Systems".

[2] PBL Netherlands Environmental Assessment Agency, "Trends in Global CO2 Emissions: 2013 Report".

[3] U.S Energy Information Administration, "International Energy Outlook 2013".

[4] Renewable Energy Policy Network for the 21st Century, "Renewables 2013: Global Status Report".

[5] European Wind Energy Association (EWEA), "Wind in Power: 2013, European Statistics".

[6] Global Wind Energy Council (GWEC), "Global Wind Statistics 2013".

[7] "The World's 10 Biggest Wind Turbines," [Online]. Available: www.power-technology.com.

[8] S. Muyeen, J. Tamura and T. Murata, "Stability Augmentation of a Grid-Connected Wind Farm".

[9] Ι. Μάργαρης, "Μοντελοποίηση Ανεμογεννητριών για τη Μελέτη Δυναμικών Φαινομένων σε Συνθήκες Αυξημένης Αιολικής Διείσδυσης," 2011.

[10] C. Sourkounis and P. Tourou, "Grid Code Requirements for Wind Power Integration in Europe," 2013.

[11] M. Tsili, C. Patsiouras and S. Papathanassiou, "Grid Code Requirements for Large Wind Farms: A Review of Technical Regulations and Available Wind Turbine Technologies".

[12] H. Zhao, Q. Wu, I. Margaris, J. Bech, P. Sørensen and B. Andresen, "Implementation and Validation of IEC Generic Type 1 Wind Turbine Generator Model".

[13] Y. Coughlan, P. Smith, A. Mullane and M. O'Malley, "Wind Turbine Modelling for Power System Stability Analysis—A System Operator Perspective," *IEEE TRANSACTIONS ON POWER SYSTEMS, VOL. 22, NO. 3,* 2007.

[14] NERC, "Standard models for variable generation," 2010.

[15] WECC Working Group on Dynamic Performance of Wind Power Generation and the IEEE Working Group on Dynamic Performance of Wind Power Generation, "Description and Technical Specifications for Generic WTG Models - A Status Report," 2011.

[16] I. Margaris, A. Hansen, J. Bech, B. Andresen and P. Sørensen, "Implementation of IEC Standard Models for Power System Stability Studies".

[17] P. Sørensen, B. Andresen, J. Fortmann, K. Johansen and P. Pourbeik, "Overview, Status and Outline of the New IEC 61400 -27 – Electrical Simulation Models for Wind Power Generation," 2011.

[18] M. Behnke, A. Ellis, Y. Kazachkov, T. McCoy, E. Muljadi, W. Price and J. Sanchez-Gasca, "Development and Validation of WECC Variable Speed Wind Turbine Dynamic Models for Grid Integration Studies," in *AWEA's 2007 Wind Power Conference Los Angeles, California*, 2007.

[19] W. W. Price and J. J. Sanchez-Gasca, "Simplified Wind Turbine Generator Aerodynamic Models for Transient Stability Studies," 2006.

[20] K. Clark, N. W. Miller and J. J. Sanchez-Gasca, "Modeling of GE Wind Turbine Generators for Grid Studies," 2010.

[21] Ad Hoc Task Force on Wind Generation Model Validation of the IEEE PES Working Group on Dynamic Performance of Wind Power Generation of the IEEE PES Power System Stability Controls Subcommittee, "Model Validation for Wind Turbine Generator Models," *IEEE Transactions on Power Systems,* vol. 26, no. 3, 2011.

[22] E. Uzunovic, "EMPT, Transient Stability and Power Flow Models and Controls of VSC-Based FACTS Controllers," 2001.

[23] A. Yazdani and R. Iravani, Voltage-Sourced Converters in Power Systems: Modeling, Control and Applications.

[24] C. Schauder and H. Mehta, "Vector Analysis and Control of Advanced Static VAR Compensators".

[25] L. Qi, J. Langston and M. Steurer, " Applying a STATCOM for Stability Improvement to an Existing Wind Farm with Fixed-Speed Induction Generators".

[26] S. W. Mohod and M. V. Aware, "A STATCOM-Control Scheme for Grid Connected Wind Energy System for Power Quality Improvement".

[27] L. Xu, L. Yao and C. Sasse, "Comparison of Using SVC and STATCOM for Wind Farm Integration," *International Conference on Power System Technology,* 2006.

[28] M. Molinas, J. A. Suul and T. Undeland, "Low Voltage Ride Through of Wind Farms With Cage Generators: STATCOM Versus SVC".

[29] M. El-Moursi, B. Bak-Jensen and M. Abdel-Rahman, "Novel STATCOM Controller for Mitigating SSR and Damping Power System Oscillations in a Series-Compensated Wind Park," *IEEE Transactions on Power Electronics,* vol. 25, no. 2, 2010.

[30] H. Gaztañaga, I. Etxeberria-Otadui, D. Ocnasu and S. Bacha, "Real-Time Analysis of the Transient Response Improvement of Fixed-Speed Wind Farms by Using a Reduced-Scale STATCOM Prototype," 2007.

[31] M. Molinas, J. A. Suul and T. Undeland, "Torque Transient Alleviation in Fixed Speed Wind Generators by Indirect Torque Control with STATCOM," *Norwegian University of Science and Technology, Department of Electrical Power Engineering, Trondheim, Norway,.*

[32] C. Wessels, N. Hoffmann, M. Molinas and F. W. Fuchs, "StatCom Control at Wind Farms With Fixed-Speed Induction Generators Under Asymmetrical Grid Faults," 2012.

[33] A. Ortiz, T. Østrem and W. Sulkowski, "Indirect negative sequence voltage control for STATCOM supporting wind farms directly connected to the grid," 2011.

[34] X. Sun and W. Wu, "A New Sliding Mode Control of STATCOM and its Effects on Wind Farm," *International Conference on Electronic & Mechanical Engineering and Information Technology,* 2011.

[35] A. Demiroren and M. Guleryuz, "PSO Algorithm-Based Optimal Tuning of STATCOM for Voltage

Control in a Wind Farm Integrated System," *Istanbul Technical University, Istanbul, Turkey.*

[36] C. Sintamarean, A. Cantarellas, H. Miranda, P. Rodriguez and R. Teodorescu, "Smart-STATCOM Control Strategy Implementation in Wind Power Plants," *IEEE International Symposium on Power Electronics for Distributed Generation Systems (PEDG),* 2012.

[37] S. Muyeen, M. A. Mannan, M. H. Ali, R. Takahashi, T. Murata and J. Tamura, "Stabilization of Grid Connected Wind Generator by STATCOM," *Dept. of Electrical & Electronic Engineering, Kitami Institute of Technology, Hokkaido, Kitami, Japan,* 2005.

[38] M. Hossain, H. Pota, V. Ugrinovskii and R. Ramos, "Robust STATCOM Control for the Enhancement of Fault-Ride-Through Capability of Fixed Speed Wind Generators," *18th IEEE International Conference on Control Applications, Saint Petersburg, Russia,* 2009.

[39] S. George and F. M. Chacko, "Comparison of Different Control Strategies of STATCOM for Power Quality Improvement of Grid Connected Wind Energy System," 2013.

[40] R. Rezaeipour and B. Kiani, "Review of Novel Control Techniques for STATCOM and its Effects on a Wind Farm".

[41] S. Heier, "Grid Integration of Wind Energy Conversion Systems," 1998.

[42] H. Zhao, Q. Wu, P. Sørensen, J. Bech and B. Andresen, "Implementation of Draft IEC Generic Model of Type 1 Wind Turbine Generator in PowerFactory and Simulink".

[43] L. Dusonchet, F. Massaro and E. Telaretti, "Wind Turbine Mechanical Characteristics and Grid Parameters Influence on the Transient Voltage Stability of a Fixed-Speed Wind Turbine".

[44] P. Giroux, G. Sybille and H. Le-Huy, "Modeling and Simulation of a Distribution STATCOM Using Simulink's Power System Blockset," *The 27th Annual Conference of the IEEE Industrial Electronics Society,* 2001.

[45] J. G. Slootweg, Wind Power Modelling and Impact on Power System Dynamics, 2003.

[46] Z. Wu and C. Rui-fa, "Improved Low Voltage Ride-Through of Wind Farm Using STATCOM and Pitch Control," *Shanghai University of Electric power Shanghai, China,* 2009.

[47] S. K. Salma and A. L. Teo, "Windmill Modeling Consideration and Factors Influencing the Stability of a Grid-Connected Wind Power-Based Embedded Generator," *IEEE Transactions on Power Systems,* vol. 18, no. 2, 2003.